論文 / 著書情報
Article / Book Information

題目(和文)	
Title(English)	Application of PP-ECC on Rigid-Framed Bridges for Improving Structural Performance
著者(和文)	張鋭
Author(English)	Rui Zhang
出典(和文)	学位:博士（工学）, 学位授与機関:東京工業大学, 報告番号:甲第9789号, 授与年月日:2015年3月26日, 学位の種別:課程博士, 審査員:二羽　淳一郎,廣瀬　壮一,岩波　光保,竹村　次朗,佐々木　栄一
Citation(English)	Degree:, Conferring organization: Tokyo Institute of Technology, Report number:甲第9789号, Conferred date:2015/3/26, Degree Type:Course doctor, Examiner:,,,,
学位種別(和文)	博士論文
Type(English)	Doctoral Thesis

APPLICATION OF PP-ECC ON RIGID-FRAMED BRIDGES FOR IMPROVING STRUCTURAL PERFORMANCE

By

Rui Zhang

Supervisor: **Professor Junichiro Niwa**

A thesis submitted in partial fulfillment of the requirements for the degree of Doctor of Philosophy

Department of Civil Engineering
Tokyo Institute of Technology
Tokyo, Japan

December 2014

Acknowledgements

I would like to express my appreciation and gratitude to my advisor, Prof. Junichiro Niwa for his invaluable guidance, encouragement and support throughout this study. His knowledge, dedication, and work ethics have always been a constant source of inspiration.

The author also would like to take this opportunity to express my sincere appreciation and obligation towards the review committee: Prof. Hirose, Prof. Iwanami, Prof. Takemura and Prof. Sasaki for reviewing my dissertation and providing valuable advices and helpful comments to improve the quality of my work.

I also sincerely thank Assistant Prof. Koji Matsumoto for his invaluable support and sharing of his knowledge wherever in experiments or completing this thesis. For handling the administrative matters and creating homely environment in the Niwa Laboratory, I would like to thank the secretary Ms. Osami Kumagai and pre-secretary Ms. Noriko Nakajima.

Special acknowledge Prof. emeritus Kazuhiko Kawashima, for leading me into my graduate study in Japan. Without his acceptance, my graduate study at Tokyo Institute of Technology would not have been possible. I also acknowledge all the members in Concrete Laboratory, Niwa Laboratory, Otsuki Laboratory and Iwanami Laboratory for their kind support and friendly environment throughout the study period.

My graduate study in Japan would not have been possible without the financial support from G-COE Program, Asahi Corporation Scholarship and Honor Scholarship. I sincerely thank the Center for Urban Earthquake Engineering (CUEE) in Tokyo Institute of Technology, Asahi Corporation and Japan Student Services Organization (JASSO).

Last, but not the least, the author gratefully acknowledges the continuous encouragement, support and sacrifices of his family and friends, most especially to his family, to whom this dissertation is dedicated.

ABSTRACT

Bridges are vital components of transportation that requires a high degree of protection to ensure their safety during a strong earthquake. The extensive damages of RC bridges observed in the past earthquakes such as Northridge, Kobe and 2011 Great East Japan earthquakes triggered extensive researches on the behavior of beam-column joint connections for designing and constructing a safer infrastructure, which further resulted in the improvements of design codes focusing on providing sufficient ductility in the vulnerable structural member to prevent its brittle failure during a major seismic event. Accordingly, for reinforced concrete (RC) structures, a considerable amount of steel reinforcements are required to be provided in these vulnerable regions, such as the plastic hinge in the beam end adjacent to the column face in a beam-column joint connection in the rigid-framed railway bridges, to confine the concrete to realize the formation of ductile inelastic behavior in the plastic hinge. However, the increased and elaborated reinforcement details bring the difficulties in fabricating this complicated steel reinforcement cage as well as placing and consolidating concrete in it during the construction phase. The contradiction between increased high cost for design and construction due to these complicated reinforcements with accordingly raised requirements on seismic performance becomes more and more apparent.

In this research, a cementitious composite combined with fabricated polypropylene fibers named Polypropylene Fiber Reinforced Engineered Cementitious Composites (PP-ECC) with improved bond properties exhibiting the pseudo strain hardening and multiple fine cracking of ECC was utilized to reduce the transverse reinforcements in beam-column joint connections of rigid-framed bridges. PP-ECC also has a higher strain at the compressive strength than that of normal strength concrete. PP-ECC exhibits the strain hardening behavior and its yield and ultimate tensile strength is greater than 2.5 N/mm^2 and 3.0 N/mm^2, respectively. The tensile strain capacity of PP-ECC is greater than 2.5%. All above described mechanical properties of PP-ECC makes PP-ECC an ideal material for enhancing the shear capacity of structural members. Compared to the widely used polymer fibers such as polyvinyl alcohol (PVA) fibers or polyethylene (PE) fibers, polypropylene (PP) fiber is softer, costs lower and disperses faster, which all results in better workability. In addition, because of the hydrophobic and non-polar nature of PP fiber, PP-ECC has better durability in an alkaline environment.

Since this research mainly focused on the shear reinforcing effect of PP-ECC in the beam and the beam-column joint connection, the shear reinforcing effect of PP-ECC was confirmed by the beam tests with a total of seven beams including two conventional steel reinforced concrete (RC) beams with and without stirrups and five PP-ECC beams with various stirrup ratios ranging from the level of RC control beam to zero. Having confirmed that the PP-ECC could be an alternative to replacing stirrups, the T-shape one-sixth scaled beam-column joints of existing structure following Japanese railway design standards, "Design Standards for Railway Structures and Commentary (Concrete Structure)" (Railway Technical Research Institute, 2004) were prepared and tested under a lateral cyclic load. This kind of T-shape joint consists of an intermediate beam and columns above and below the beam. The dimensions of the beam and the column and the quantity of rebars including arrangement and detailing of the specimens resembled with the as built configuration of the rigid-framed bridge. Based on the findings in beam tests, the transverse reinforcements were reduced by replacing with PP-ECC in the joint, the beam and the column, one after another.

The experimental results reveal that PP-ECC is effective to enhance the shear capacities of beam when the matrix is replaced from normal strength concrete to PP-ECC. Based on the beam test results, the shear capacities of the beams with stirrups and without stirrups increased 20.6% and 107.6%, respectively, by replacing concrete with PP-ECC. In the experiments of beam-column joints, the specimens with the reduction of transverse reinforcements by using PP-ECC exhibits comparable structural performance, in terms of load capacity, energy dissipation and stiffness degradation with that without reduction of transverse reinforcements. It indicates that the PP-ECC could be a replacement of the transverse reinforcement in beam-column joint connection specimens to reduce the congestion in the beam-column joint connection.

TABLE OF CONTENTS

LIST OF TABLES

LIST OF FIGURES

LIST OF PHOTOS

Chapter 1

INTRODUCTION

1.1 Background

Bridges are vital components of transportation networks that require a high degree of protection to ensure their functionality even under a significant earthquake. However, the extensive damage to bridges resulting from the recent earthquakes with larger and larger magnitude in Tangshan, China (1976), Loma Prieta, US (1989), Northridge, US (1994), Kobe, Japan (1995), Kocaeli and Duzce, Turkey (1999), Wenchuan, China (2008), Chile (2010) and Tohoku, Japan (2011), revealed the vulnerability of bridges under extreme ground motion.

In Japan, a large portion of Shinkansen railway bridges covered by the rigid-framed structures (**Photo 1.1.1**). In this type of structures, a portion of a column within the

Photo 1.1.1 Rigid-framed railway bridge.

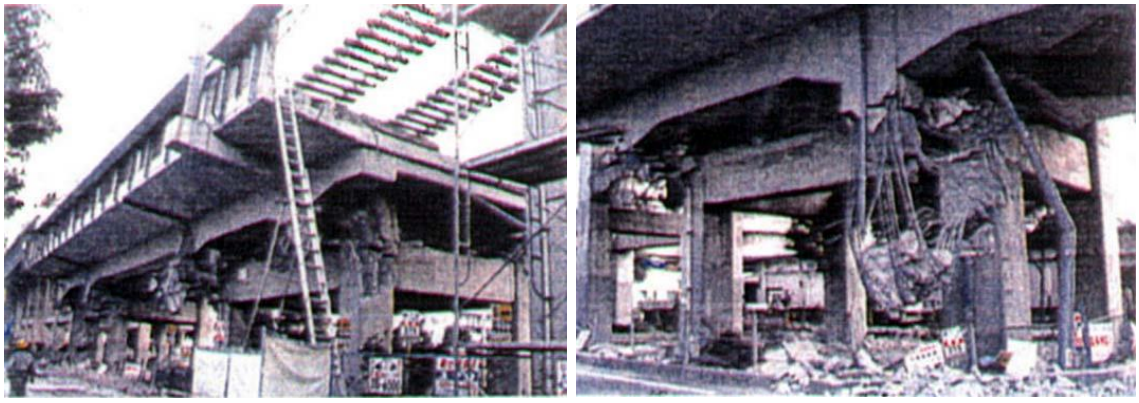

Photo 1.1.2 Shear failure of beam-column joints and columns.

(a) Flexural shear failure of columns.

(b) Shear cracking.

Photo 1.1.3 Damage to rigid-framed railway bridge in 2011 off the Pacific Coast of Tohoku Earthquake.

depth of the deepest beam that frames into the column is considered as the beam-column joint. The beam-column joint is one of the most important structural members which significantly govern the whole performance of the frame structures. Beam-column joints transfer the loads between the connecting structural members, beams and columns, in the structures. The design of beam-column joints may not be crucial to resist only the gravity loads, however, the joints subjected to earthquake can undergo heavy stress due to shear.

Through **Photo 1.1.2** to **1.1.3**, many catastrophic failures during earthquakes have indicated the vulnerability of beam-column joints in these damaged bridges which typically have the following deficiencies in the joint region: (1) strong beams, weak columns, (2) little or no joint transverse reinforcement, (3) beam bottom reinforcements with short embedment length, (4) wide spacing of column ties (Beres *et al.* 1996).

Photo 1.1.2 shows one of the examples of a total collapse of Tokimoto Viaduct during 1995 Kobe earthquake caused by shear failure of beam-column joints and columns. The observed extensive damages to these rigid-framed bridges triggered the urgent necessity of retrofitting and rehabilitation of existing structures and development of improved seismic analysis and design method for new constructed rigid-framed bridges. Accordingly, numerous retrofitting and rehabilitation techniques were exploited and implemented to the existing railway bridges (Matsumoto et al. (2000), Ishibashi and Tsukishima (2009)). Studying the performance and failure mechanism of rigid-framed railway bridges, many issues that should be addressed by the new design standards were highlighted by different researchers such as Ishibashi and Okamura (1997), Matsumoto et al. (2000) and Nishimura (2004). The design standards were revised incorporating the suggestions from numerous researchers and drastic improvements were done in the new railway design standards (Design standards for railway structures and commentary (Concrete Structures) (2004)) to design and construct new rigid-framed railway bridges.

The rigid-framed railway bridges, which were retrofitted, survived the recent devastating earthquake "The 2011 off the Pacific Coast of Tohoku Earthquake" whereas the bridges which were not retrofitted suffered heavy damages. The heavy damage on one of the rigid-framed railway bridges (Nakasone No.1 Viaduct, Kitakami Station, Iwate Prefecture) which was constructed in 1977-78 is shown in **Photo 1.1.3**(a). In this bridge, the columns were failed in shear in the post-yield range of longitudinal rebars. Such type of failure is common in the columns with comparatively smaller shear span-to-depth ratio, larger sections, small main reinforcement ratios and much small web reinforcement ratios. All of these examples of damages indicated that the

Photo 1.1.4 Large amount of longitudinal and shear rebars in bridge column.

rigid-framed bridges constructed prior to 1995 Kobe earthquake contain insufficient longitudinal and shear rebars to withstand huge seismic loads. In addition, flexural cracks were also observed in some of the intermediate link beams of rigid-framed railway bridge (Yachi No.2 Viaduct, Iwate Prefecture) as shown in **Photo 1.1.3**(b) during "The 2011 off the Pacific Coast of Tohoku Earthquake". On subjecting such a huge seismic load, the flexural cracks may become evident in a beam even if large amount of longitudinal rebars following the current design standards are provided in a beam.

Based on all these lessons learnt from the past earthquakes, the seismic design specification was extensively revised to require large amount of steel reinforcements with elaborated details, as shown in **Photo 1.1.4**. The purpose is to confine the concrete especially in the vulnerable regions, such as the plastic hinges in the columns and the beam-column joints to realize the formation of ductile inelastic behavior in the plastic hinge. However, the increased and elaborated reinforcement details bring the difficulties in fabricating this complicated steel reinforcement cage as well as placing and consolidating concrete in it during the construction phase. The contradiction between increased high cost for design and construction due to these complicated reinforcements with accordingly raised requirements on seismic performance becomes more and more apparent.

Previous researches (Tang *et al.*, 1992; Filiatrault *et al.*, 1994; Filiatrault *et al.*, 1995; Bayasi *et al.*, 2002; Shakya *et al.*, 2012) on steel fiber reinforced concrete (SFRC) have devoted significant effort studying the behavior of joints under reversed cyclic loadings, as well as on the development of design recommendations for ensuring sufficient ductile behavior in beam-column joint connections. SFRC, as one type of the fiber reinforced concretes (FRCs), is characterized by a tensile strain softening behavior after reaching its first cracking strength. However, a newly developed fiber-reinforced cement-based material named Engineered Cementitious Composites (ECC) exhibits multiple fine cracking, pseudo strain hardening behavior, large strain capacity between 1% and 5% and superior ductility. Its superior strain capacity makes it an ideal material for use in the plastic hinge of beam-column joint connections to undergo large inelastic deformation and reducing the quantity for transverse reinforcements. So far, various types of fibers have been utilized to produce ECCs, including steel, carbon and polymer fibers (Li, 1998), whereas most structural and retrofit applications of ECC reported in the literature use polymer fibers. The steel reinforced ECC (R/ECC) structural members

such as column with reduction of shear reinforcements (Li and Fischer, 2002) have been confirmed in previous studies. In addition, Parra-Montesinos *et al.* (2002) have revealed the feasibility of total elimination of transverse reinforcements in the joint and the increase in transverse reinforcement spacing in beam plastic hinge in beam-column joins constructed with Polyethylene Fiber Reinforced Engineered Cementitious Composites (PE-ECC). A cementitious composites combined with fibrillated polypropylene fibers having improved bond properties that exhibit the strain hardening and multiple cracking of ECC (refers to Hirata *et al.*, 2009) is referred herein as polypropylene fiber reinforced cementitious composites (PP-ECC). The research presented herein focused on the application of PP-ECC on rigid-framed railway bridges to reduce the shear reinforcements.

1.2 Objectives of the Study

This study is attempts to reduce the shear reinforcements in rigid-framed bridges to avoid over congestion in the beam-column joint connections based on the experimental investigation on the effects of stirrup ratios in PP-ECC beams.

This study mainly focused on the shear reinforcing effect of PP-ECC in the beam and the beam-column joint connection. The shear reinforcing effect of PP-ECC was confirmed by beam tests with a total of seven beams including two conventional steel reinforced concrete (RC) beams with and without stirrups and five PP-ECC beams with various stirrup ratios ranging from the level of RC control beam to zero. Having confirmed that the PP-ECC could be an alternative to replacing stirrups, the T-shape 1/6 scale beam-column joints of existing structure following Japanese railway design standards, "Design Standards for Railway Structures and Commentary (Concrete Structure)" (Railway Technical Research Institute, 2004) were prepared. This kind of T-shape joint consists of an intermediate beam and columns above and below the beam. The dimensions of the beam and the column and the quantity of rebars including arrangement and detailing of the specimens resembled with the as built configuration of the rigid-framed bridge. Based on the findings in beam tests, the transverse reinforcements were reduced by replacing with PP-ECC in the joint, the beam and the column, one after another.

Since the rigid-framed bridges are subjected to relatively smaller vertical load and are more vulnerable to seismic loads compared to the vertical static loads, the vertical loads

were not considered in this study. The horizontal load was applied using displacement controlled hydraulic actuator at the column of the T-shape joints. In the existing substructure of rigid-framed bridges (**Figure 1.2.1**(a)), the beams are connected to two or more faces of columns in two orthogonal horizontal directions at the intermediate level **Figure 1.2.1**(b). For simplicity and due to constrains in the available space and testing facility, the T-shape joint formed by connecting a column and an intermediate beam (**Figure 1.2.1**(c)) was considered only in this study.

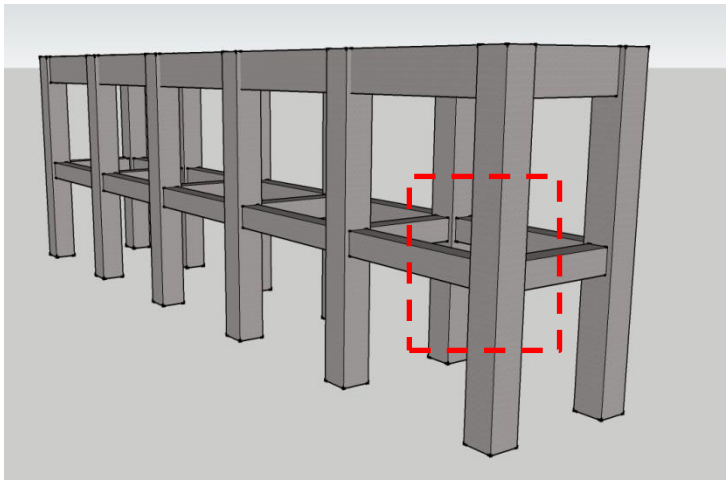

(a) Substructure of rigid-framed railway bridge.

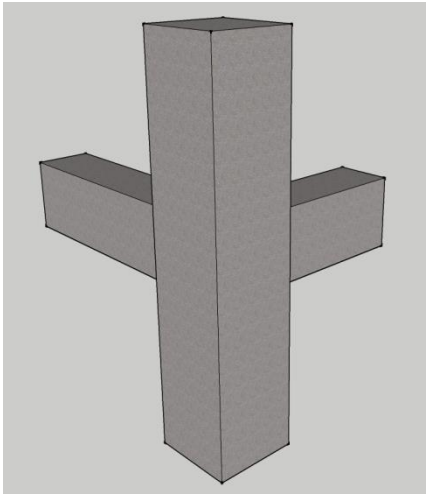

(b) Prototype.

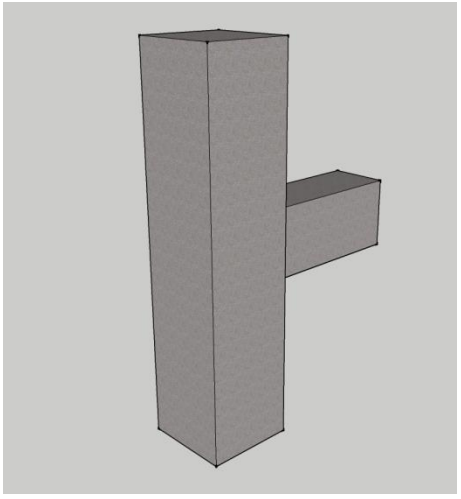

(c) This study.

Figure 1.2.1 Beam and column arrangement in T-shape joint.

1.3 Description of Prototype Bridge

One existing rigid-framed railway bridge is considered as the prototype bridge. The plan and elevation including the dimensions of the bridge are shown in **Figure 1.3.1**. The prototype bridge consists of 5 bays in longitudinal direction and a single bay in transverse direction. The beam-column joints of frame (1) in **Figure 1.3.1**(a) are considered as the representative beam-column joints in this study. The cross-sectional size of columns, intermediate beams and top beams at the end frames and intermediate top beams are of 1500 mm × 1500 mm (width × depth), 1500 mm × 2000 mm, 1000 mm × 1800 mm and 1000 mm × 1200 mm, respectively. Due to some constraints related to the confidentiality, the detailed dimensions and structural detailing including steel rebar arrangement in concrete sections of the prototype structure are not shown. However, to get some ideas about the steel rebar arrangements and its details in rigid-framed railway bridge, some drawings were extracted from "Design standards and commentary for railway structures (Concrete structures): Verification examples – RC rigid-framed elevated bridges" (Railway Technical Research Institute (2005)) and presented in **Figure 1.3.2** and **Figure 1.3.3**. In these drawings, it can be seen that various types of hooks with varying extension of hooks at the end of beam rebars can be seen.

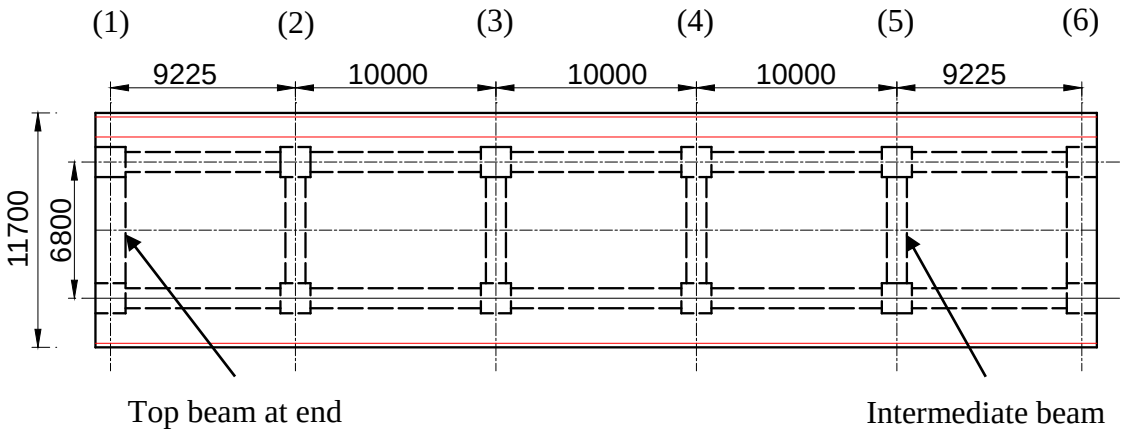

(a) Plan.

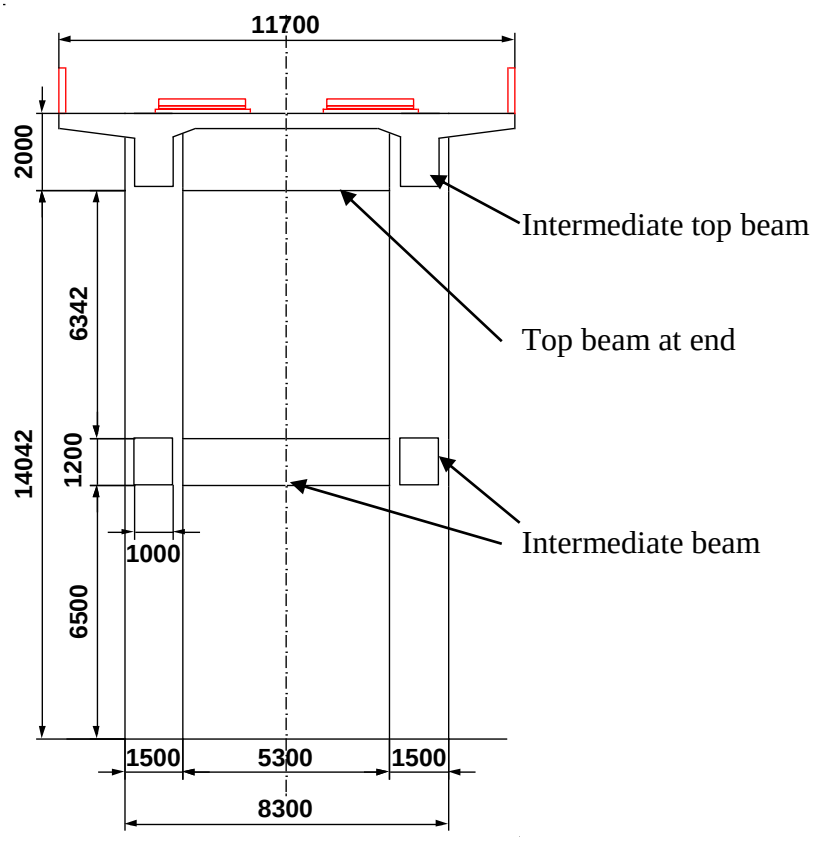

(b) Elevation.

Figure 1.3.1 Schematic drawing of the prototype rigid-framed railway bridge.

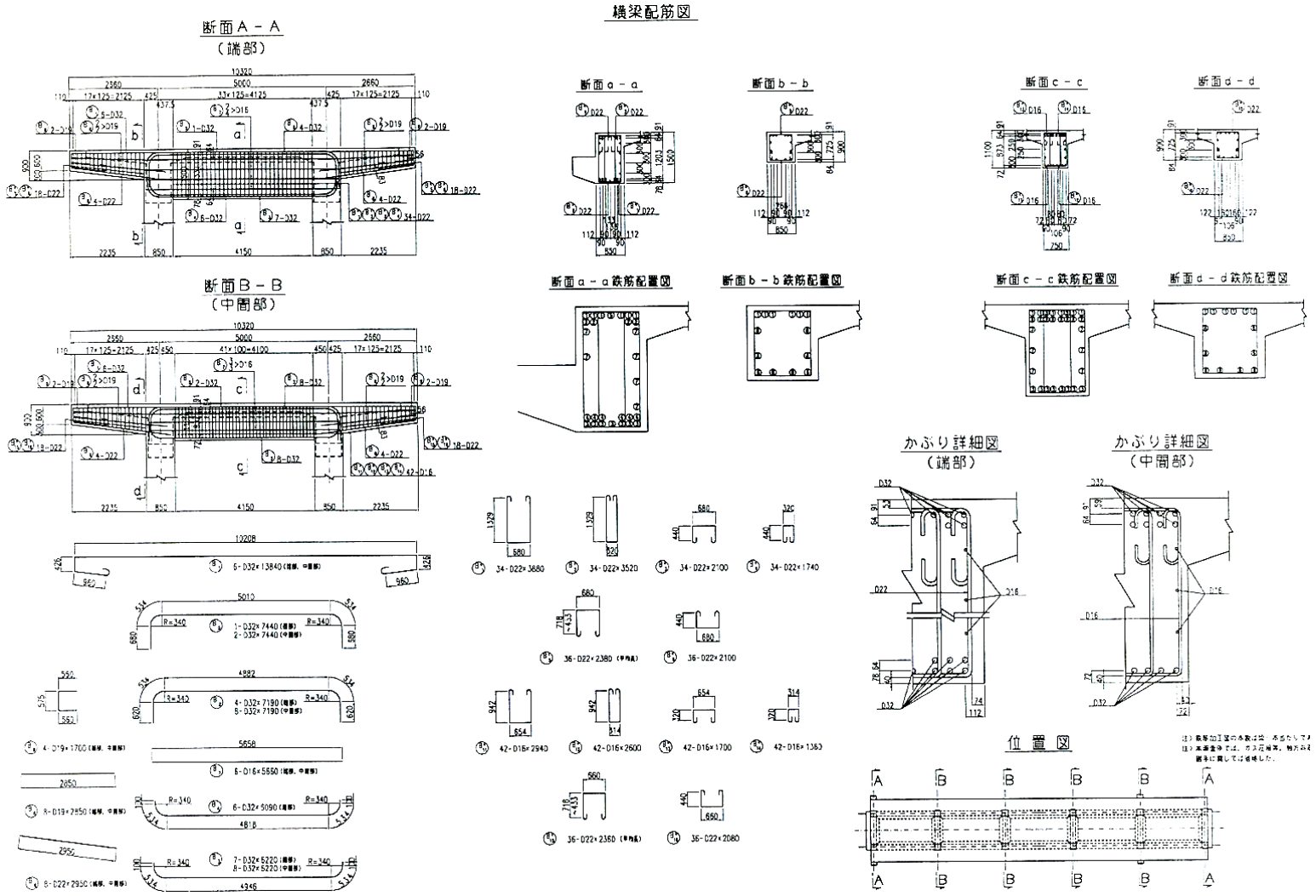

Figure 1.3.2 Steel rebar arrangement in beam of rigid-framed railway bridge.

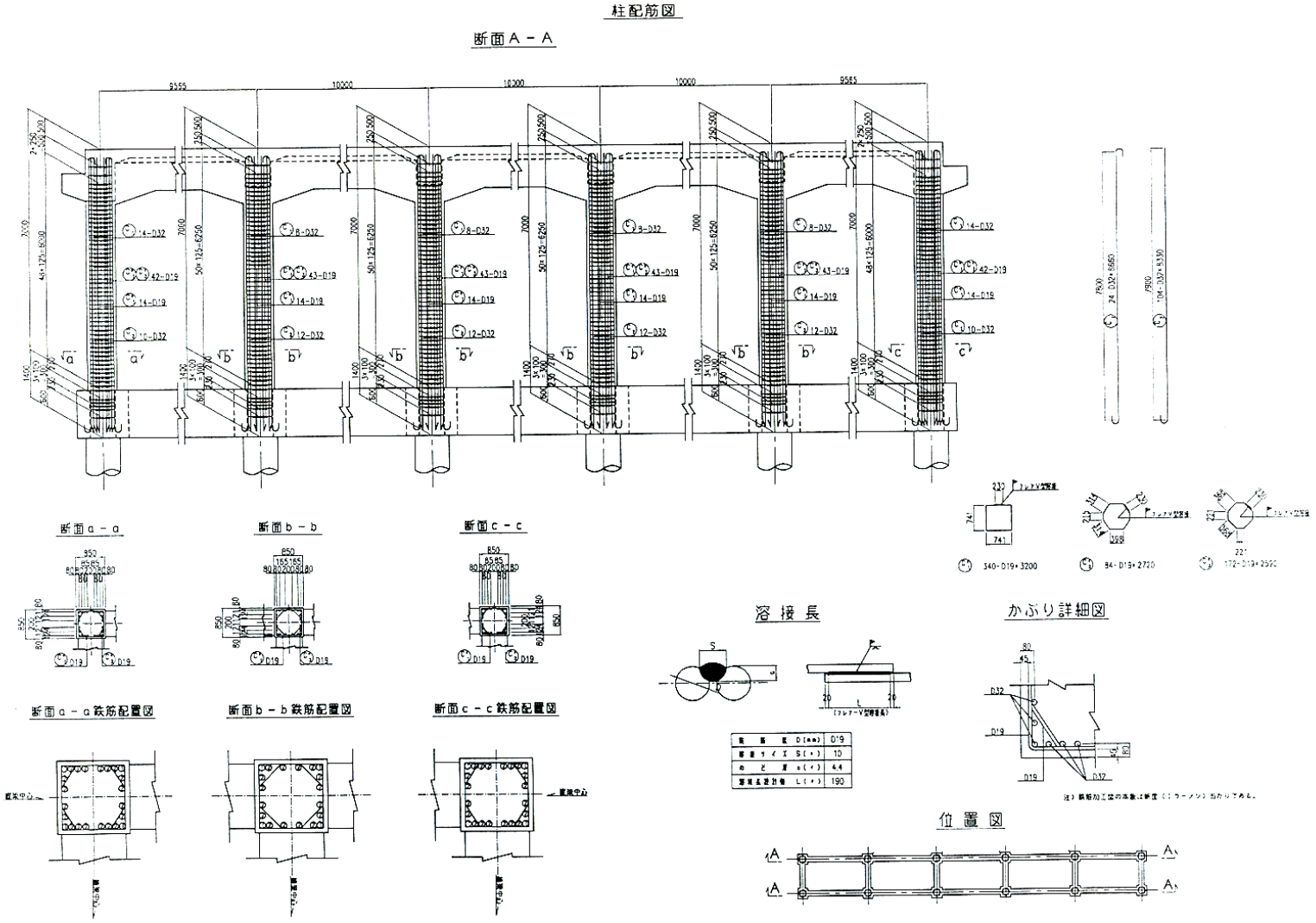

Figure 1.3.3 Steel rebar arrangement in column of rigid-framed railway bridge.

1.4 Contents Structure of the Thesis

The dissertation contains five chapters and the flow of this dissertation is summarized and shown in **Figure 1.4.1**.

Chapter 1 provides the information related to the background of beam-column joints including the problem of over congestion at the beam-column joints after implementation of new design standards. The objective of this study and brief description of the prototype structure are also included.

Chapter 2 summarizes the previous studies conducted to investigate the Engineered Cementitious Composites (ECC) and their application to beams and columns. Code provisions recommended in various design codes to design of beams are included. Damages in beam-column joints during past earthquakes and adopted various measures to retrofit and rehabilitate including different techniques adopted by different researchers to enhance the performance of beam-column joints are also illustrated.

Chapter 3 introduces the basic mechanical properties of PP-ECC, including compressive behavior and tensile behavior. As one of the most notable mechanical characteristics differing from the other building materials, strain-hardening behavior under tension was confirmed in this chapter.

In order to investigate the shear reinforcing effectiveness of PP-ECC, the beam monotonic loading tests presented in Chapter 4 were conducted. The experimental program of PP-ECC beam in detail is explained in **Chapter 4**. The contents in this chapter consist of design of specimen, experimental setup and experimental results. The effects of stirrup ratio in PP-ECC beams are investigated to compare with RC beams.

Based on the investigation in Chapter 4 which verified the feasibility for reducing transverse rebars, the response of T-joint specimens before and after reduction of transverse reinforcements in the joint, the beam and the column are presented in **Chapter 5**. The specimens after the reduction of transverse reinforcements are provided with PP-ECC. The performance of the specimen and the other specimens are compared in terms of crack patterns, load-displacement relationship, moment-curvature relationship, energy dissipation capacity and stiffness degradation. It is found that the PP-ECC is effective in replacing the transverse reinforcements in T-joints to improve

the workability and avoid congestion of rebars.

Finally, in **Chapter 6** the conclusions of the study are presented with some recommendations for future research.

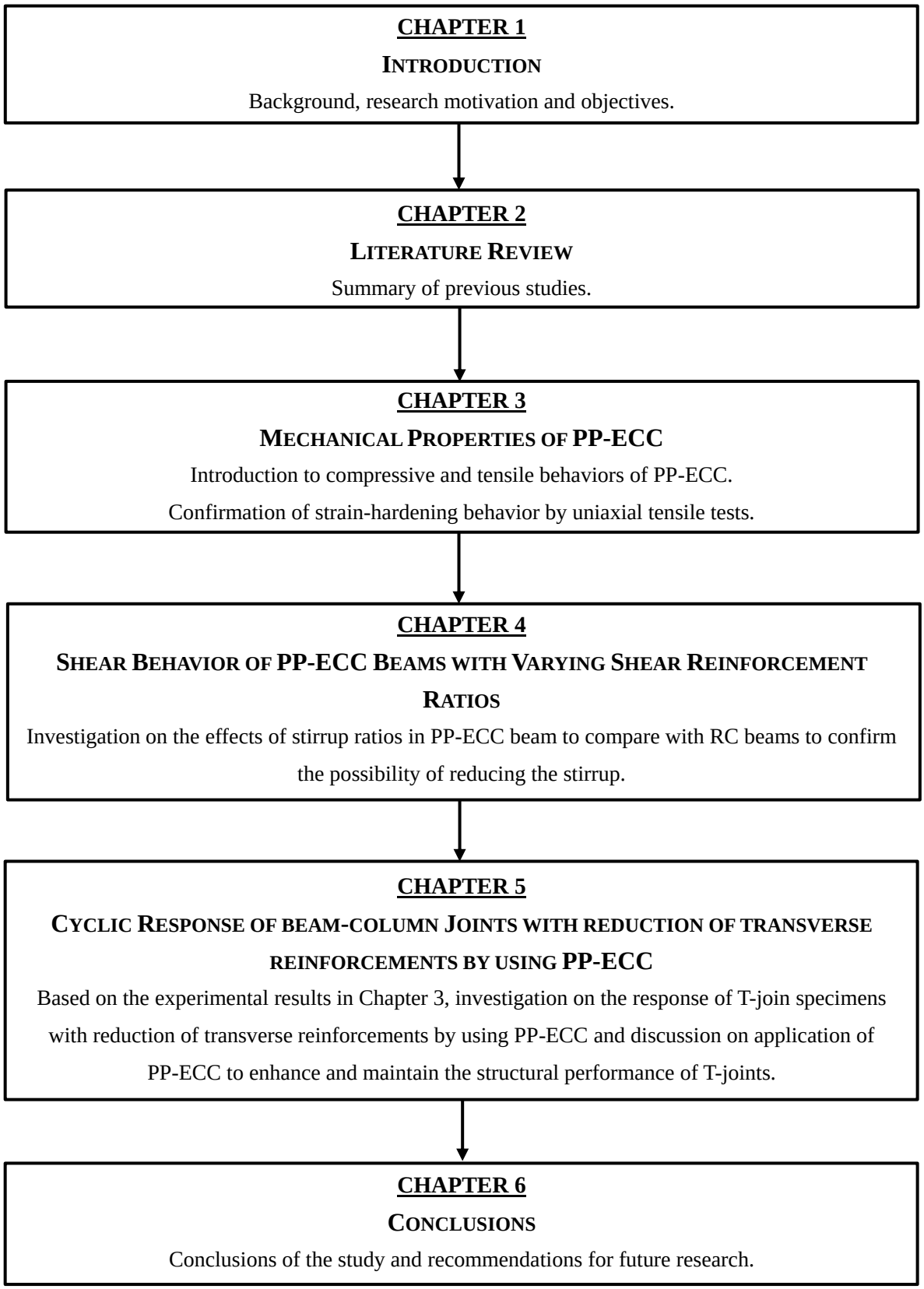

Figure 1.4.1 Outline of the dissertation.

References

Bayasi, Z. and Gebman, M.: Reduction of Lateral Reinforcement in Seismic Beam-Column Connection via Application of Steel Fibers, *ACI Structural Journal*, Vol. 99, No. 6, pp. 772-778, 2002.

Beres, A., Pessiki, S., White, R. N., and Gergely, P.: Implications of Experiments on the Seismic Behavior of Gravity Load Designed RC Beam-to-Column Connections, *Earthquake Spectra*, V. 12, No. 2, pp. 185-195, 1996.

Filiatrault, A., Ladicani, K. and Massicotte, B.: Seismic Performance of Code-Designed Fiber-Reinforced Concrete Joints, *ACI Structutrual Journal*, Vol. 91, No.5, pp. 564-570, 1994.

Filiatrault, A., Pineau, S. and Houde, J.: Seismic Behavior of Steel-Fiber Reinforced Concrete Interior Beam-Column Joints, *ACI Structural Journal*, Vol. 92, No.5, pp. 1-10, 1995.

Hirata, T., Kawanishi, T., Okano, M. and Watanabe, S.: Study on Material Properties and Structural Performance of High-Performance Cement Composites Using Polypropylene Fiber, *Proceeding of Japan Concrete Institute*, Vol. 31, No.1, pp. 289-294, 2009. (in Japanese)

Ishibashi, T. and Okamura, H.: Study on the design earthquake resistance and degree of earthquake damage of reinforced concrete viaducts, *Cement and Concrete Composites*, Vol. 19, pp. 193-201, 1997.

Ishibashi, T. and Tsukishima, D.: Seismic Damage of and Seismic Rehabilitation Techniques for Railway Reinforced Concrete Structures, *Journal of Advanced Concrete Technology*, Vol. 7, No. 3, pp. 287-296, 2009.

Li, V.: Engineered Cementitious Composites (ECC) – Tailored Composites through Micromechanical Modeling, Fiber Reinforced Concrete, Present and the Future, eds. N. Banthia, and A. Mufti, Canadian Society of Civil Engineers, pp. 64-97, 1998.

Li, V. and Fischer, G.: Effect of Matrix Ductility on Deformation Behavior of Steel Reinforced ECC Flexural Members under Reversed Cyclic Loading Conditions, *ACI Structural Journal*, Vol. 99, No. 6, pp. 781-790, 2002.

Matsumoto, N., Kitago, Y. and Sato, T.: Restoration, Seismic Strengthening and Seismic Design for Railway Viaducts after Hyogoken-Nanbu Earthquake, *Cement and Concrete Composites*, Vol. 22, No. 1, pp. 47-57, 2000.

Nishimura, A.: Damage Analysis and Seismic Design of Railway Structures for Hyogoken-Nanbu (Kobe) Earthquake, *Journal of Japan Association of Earthquake Engineering*, Vol. 4, No. 3, pp. 184-194, 2004.

Parra-Montesinos, G., Peterfreund, S. and Chao, S.: Highly Damage-Tolerant Beam-Column Joints Through Use of High-Performance Fiber-Reinforced Cement Composites, *ACI Structural Journal*, Vol. 102, No. 3, pp. 487-495, 2005.

Railway Technical Research Institute: Design Standards for Railway Structures and Commentary (Concrete Structures), 2004.

Railway Technical Research Institute: Design Standards for Railway Structures and Commentary (Concrete Structures) – Verification Examples – RC Rigid-Framed Elevated Bridges, No. 421, 2005.

Shakya, K., Watanabe, K., Matsumoto K. and Niwa J.: Application of Steel Fibers in Beam-Column Joints of Rigid-Framed Railway Bridges to Reduce Longitudinal and Shear Rebars, *Construction and Building Materials*, Vol. 27, No. 1, pp. 482-489, 2012.

Tang, J., Hu, C., Yang, K., and Yan, Y.: Seismic Behavior and Shear Strength of Framed Joint Using Steel-Fiber Reinforced Concrete, *ASCE Journal of Structural Engineering*, Vol. 118, No. 2, pp. 341-358, 1992.

Chapter 2

LITERATURE REVIEW

2.1 Introduction

Engineered Cementitious Composites (ECC) is a newly developed building material consists of two main components, the fiber and the matrix. The matrix can be a paste or mortar, is assumed to contain additives specified and fine aggregate or even no aggregates. The fiber is assumed to be discontinuous and distributed within the volume of the composite. Both the fiber and the matrix are assumed to work together resulting from surface bonding of fibers.

Before the emergence of ECC, Romauldi and co-workers (1963, 1964) first introduced an effective way to reduce the brittleness of concrete by adding short steel fibers. This development triggered the extensive research to various types of fibers, such as synthetics, glass, carbon and natural fibers in recent decades. According to the classification by tensile behavior (Naaman, 1987; Naaman and Reinhardt, 1996), this kind of fiber reinforced concrete (FRC) is characterized by a tensile strain softening

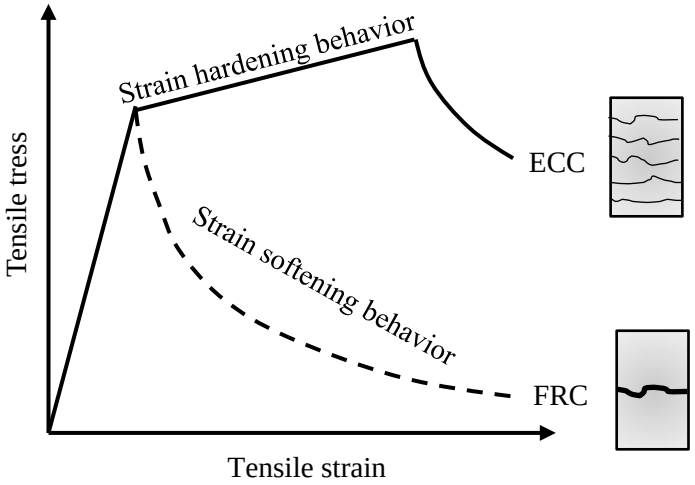

Figure 2.1.1 Tensile behavior of FRC and ECC.

behavior after reaching the first crack strength with a localized crack, while a new category of building material, referred to as ECC is characterized by a tensile strain-hardening behavior with multiple fine cracking. **Figure 2.1.1** illustrates schematically the differences between the tensile behaviors of FRC and ECC. The larger strain capacity and ductility of ECC compared to traditional FRC makes it suitable for use in member where subjected to large inelastic deformations. Matsumoto et al. have confirmed that the use of ECC leads to improvement in ductility, fatigue resistance and deformation capacity of member (Matsumoto and Mihashi, 2003).

Except the multiple fine cracking, pseudo strain hardening behavior and high ductility under uniaxial tensile loading are exhibited by ECC as mentioned above. It also has higher tensile strength compared to normal concrete and can reach ultimate tensile strain between 1% and 5% under monotonic tensile loading. Its pseudo strain-hardening behavior results from its unique multiple fine cracking mechanisms, in which closely spaced fine cracks form because of the bridging action of fibers (Maalej and Li, 1994; Li, 1998). Different from the normal concrete in mixture, ECC generally uses fine aggregates or even no aggregates and relatively low volume fractions of short and random fibers (approximately 2% to 3%). The compressive strength of ECC is similar to that of mortar (Li, 1998; Kesner, Billington and Douglas, 2003; Kesner and Billington, 2004). Due to the absence of coarse aggregate, the elastic modulus of ECC is comparatively lower than that of normal concrete (Li, Mishra and Wu, 1995; Li, 1998; Kesner and Billington, 2004).

Various types of fibers have been used to produces ECCs, including steel, carbon and polymer fibers (Li, 1998). So far, most structural and retrofit applications of ECC reported in the literature use Polyvinyl Alcohol (PVA) and Polyethylene (PE) fibers. Compared with widely used PVA fibers, polypropylene (PP) fiber is softer, costs lower and disperses faster, which all results in better workability. In addition, because of the hydrophobic and non-polar nature of PP fiber, PP-ECC has better durability in an alkaline environment (Brown, Shukla and Natarajan, 2002). A cementitious composite combined with fabricated polypropylene fibers with improved bond properties that exhibits the pseudo strain hardening and multiple fine cracking of ECCs (Hirata *et al*., 2009) is referred herein as Polypropylene Fiber Reinforced Engineered Cementitious Composites (PP-ECC).

2.2 ECC Material Literature Review

2.2.1 ECC material behavior

It is now well-known that composite properties depend on three groups of constituent properties – the fiber, matrix and interface properties (Li, 1998). Micromechanics relate macroscopic properties to the microstructures of a composite, and form the backbone of material design theory. Based on the principles of fracture mechanics and deformation mechanisms, micromechanics allow the systematic microstructure tailoring to control the failure mode, the tensile strength, and the ultimate tensile strain of composite as well as materials optimization (Li, 1998; Li, 2003).

2.2.2 Fiber pullout behavior

The development of ECC is based upon evaluating the pullout behavior of the fibers from the cement matrix (Marshall, 1985). In ECC materials, the fibers are used as a traction force (force acting across the crack faces), bridging the cracks, with the load carried by the fibers increasing with crack extension. Increasing crack extension results in the formation of multiple tensile cracks as the fibers continue to pullout of the matrix. During pullout the fibers remain elastic and may eventually completely pullout from the matrix.

In ECC materials, the formation of multiple tensile cracks results in a tensile stress-strain response that is similar to that of strain hardening metals. This type of response has been termed “pseudo-strain hardening” (Li, 1998). Multiple cracking arises as a result of the balance between the increase in composite toughness and the stress-intensity factor increase at the crack tips, due to applied load during crack extension (Li and Leung, 1992). The balance can be represented for a single crack by:

$$K_{tip} = K_l + K_b \tag{2.2.1}$$

where, K_{tip} is the stress intensity factor at the crack tips during crack propagation; K_b is the stress intensity factor due to fibers bridging behind the crack tips and K_l is the stress intensity factor across the crack flanks due to remote loading.

In the absence of fibers, Eq. (2.2.1) will reduce to the basic equation from fracture mechanics in which the stress intensity at the crack tip (K_{tip}) is equivalent to the stress intensity due to the applied load (K_I) (Anderson, 1995). When the stress intensity at the crack tip reaches a critical value (KIC), the cracks in the specimen will propagate in an uncontrolled manner resulting in fracture of the specimen. **Figure 2.2.1** shows a schematic of the condition represented in Eq. (2.2.1).

The bridging stress-crack opening is based upon a simple model of fiber pullout. It is assumed that the fibers are short enough (or with low enough interfacial friction) that all fibers will be pulled out without rupture (Li and Leung, 1992).

Figure 2.2.2 shows a single fiber with an embedded length l, the fiber bridging load P as function of crack opening δ, can be obtained as (Li and Leung, 1992)

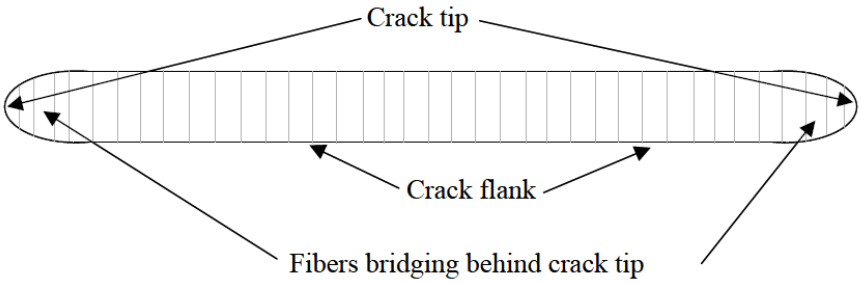

Figure 2.2.1 Schematic of fibers bridging crack.

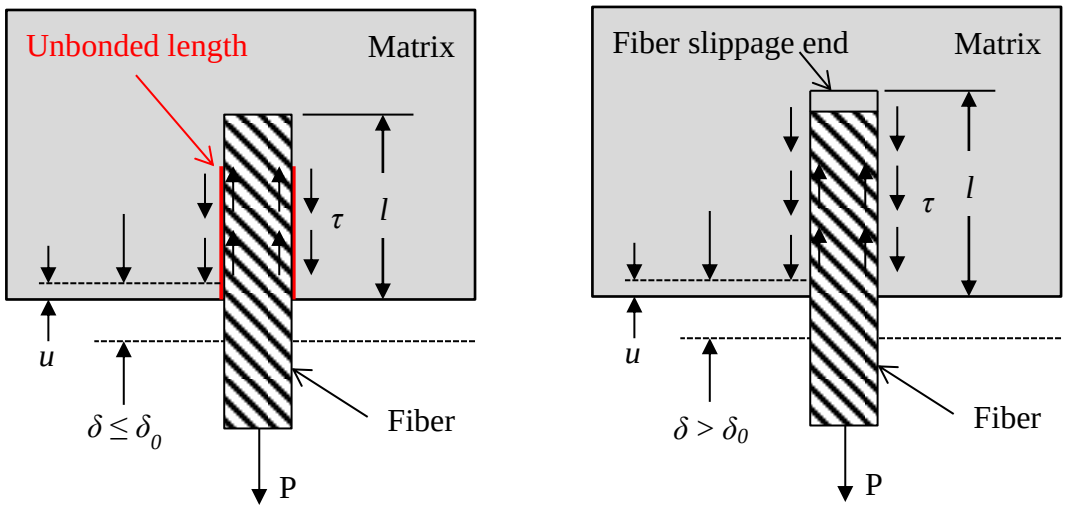

(a) Prior to full bonding of fiber.

(b) After full bonding of fiber.

Figure 2.2.2 Shear lag analysis of fiber pullout from matrix (Li and Leung, 1992, based upon original derivation by Marshall and Cox., 1985).

$$P(\delta) = \frac{\pi}{2}\sqrt{(1+\eta)\cdot E_f \cdot d_f^3 \cdot \tau \cdot \delta}\cdot e^{f\phi} \quad (\text{for } \delta \le \delta_0) \tag{2.2.2}$$

$$\delta_0 = \frac{4l^2\tau}{(1+\eta)\cdot E_f \cdot d_f^3} \tag{2.2.3}$$

$$\eta = \frac{V_f E_f}{V_m E_m} \tag{2.2.4}$$

where corresponds to the crack opening at which frictional debonding is completed for a fiber with embedment length of l, diameter d_f, elastic modulus E_f, and with an interfacial frictional bond strength τ. V_f is the fiber volume fraction in the composite, V_m is the matrix volume fraction in the composite and E_m is the matrix modulus of elasticity. $e^{f\phi}$ accounts for the snubbing as they are pulled out of the matrix. It accounts for the increase in fiber pull out force for fibers inclined at an angle ϕ to the loading axis. The snubbing coefficient f is an experimentally determined coefficient that is specific to a matrix and fiber combination (Li, Wang and Backer, 1990).

When the fiber is fully debonded ($\delta \ge \delta_0$), the load-displacement is mainly due to fiber slippage. If the end stretching of the fiber is neglected for simplicity (consider the end of the fiber to be unbonded), the pullout load is a function of the displacement given by (Li and Leung, 1992)

$$P(\delta) = \pi \cdot \tau \cdot L \cdot d_f \left(1 - \frac{\delta}{l}\right)\cdot e^{f\phi} \quad \left(\text{for } \delta_0 \le \delta \le \frac{L_f}{2}\right) \tag{2.2.5}$$

The stress of the composite as a function of the crack opening displacement can be predicted by integrating the contribution of the individual fibers over the probability distribution function of the fiber orientation angle ϕ and the centroidal distance of the fibers from the crack plane as (Li and Leung, 1992)

$$\sigma_B(\delta) = \frac{4V_f}{\pi d_f^2}\int_{\phi=0}^{\pi/2}\int_{z=0}^{L_f/2\cos\phi} P(\delta)\cdot p(\phi)\cdot p(z)\cdot dz\cdot d\phi \tag{2.2.6}$$

where $p(\phi)$ and $p(z)$ are the probability distribution function of the orientation angle

and the centroidal distance of fibers from the crack plane, respectively. For a uniform, three dimensional, random fiber distribution, $p(\phi) = \sin\phi$ evaluated from 0 to $\pi/2$ and $p(z) = 2/L_f$ evaluated from 0 to $L_f/2\cos\phi$ is the result obtained from Eq. (2.2.2) or (2.2.5) depending on the displacement range being considered.

At small crack opening, some fibers will undergo debonding governed by Eq. (2.2.2), while other fibers with short embedment length will undergo slippage governed by Eq. (2.2.5). Eq. (2.2.6) can be used to evaluate the load or stress versus displacement relation for fiber reinforced cement composite. The maximum value of Eq. (2.2.6) is referred to as the maximum bridging stress. It is given by (Li and Leung, 1992 based upon original derivation by Marshall and Cox., 1985)

$$\sigma_{br} = \frac{g \cdot \tau \cdot V_f}{2} \cdot \left(\frac{L_f}{d_f} \right) \tag{2.2.7}$$

where σ_{br} is the maximum bridging stress and g is the snubbing factor which is related to the snubbing coefficient, f.

2.2.3 Steady-state cracking

Steady-state cracking is essential for ductility in ECC. Steady-state cracking occurs under two conditions: (1) the stress at the midpoint of the crack must equal the first crack strength; and (2) the crack-opening displacement at the midpoint of the crack must be less than the displacement corresponding to the maximum bridging stress (Li and Leung, 1992). These two conditions place limits on the stress and opening size of cracks. When the first requirement is satisfied, the continued pullout of fibers will result in the formation of new cracks without an increase in applied load. When the second requirement is satisfied, the crack will have a parabolic shape with the cracks tips flattened out (Marshall and Cox, 1987). The flattened shape of the crack tips (crack flanks) allows the fibers behind the crack tip to be effective in limiting the stress intensity at the crack tips. If condition 2 is not satisfied, the crack will have sufficient opening width to prevent the fibers across the crack faces from being effective in bridging the cracks. This will prevent (2-1) from being satisfied, resulting in uncontrolled propagation of the cracks and a failure of the material.

2.2.4 Critical fiber volume fraction

Using a fracture mechanics based derivation and assuming the cracks are pulled out without rupture, and assuming a penny-shaped crack with fibers bridging across the crack surfaces, the two conditions required for steady-state cracking can be satisfied in terms of a minimum required fiber volume fraction. The following equation is the result of the derivation (Li and Leung,1992):

2.2.5 Fiber materials

Table 2.2.1 shows the physical properties of some widely used fibers, such as steel, fiberglass, PVA, PE and PP fibers in the ECC materials. According to fiber types, these ECC materials were named again to indicate the fiber they used, such as ECC with PVA or PE fibers was referred to PVA-ECC or PE-ECC, respectively. As will be discussed later, most structural and retrofit applications of ECC reported in the literature used PE and PVA fibers. Although PP fiber has comparatively lower cost to PVA and PE fibers and high durability in alkaline environment, it is not suitable for use in ECC (Kesner and Billington, 2004) due to its hydrophobic and non-polar nature leads to poor bonding with cement paste (Brown, Shukla and Natarajan, 2002). Polypropylene's hydrophobic surface prevents it from being wetted by cement paste (Hannant, 1978). Since they are non-polar, the bundles of polypropylene fibers do not cling or ball together (Hannant, 1978). On the other hand, PP fiber in the form of fibrillated films and tapes or woven meshes provided better bond with the cement matrix than chopped monofilament fibers (Daniel, Roller and Anderson, 1998). The improved bond is direct result of cement matrix penetration into the network of individual fiber filaments created by fibrillation (Hannant, 1978). A cement composite in combination with the fibrillated polypropylene fibers that exhibits the strain hardening and multiple cracking of ECC (Hirata *et al.*,

Table 2.21 Physical properties of fibers.

Fiber	Length (mm)	Diameter (μm)	Strength (MPa)	Elastic modulus (GPa)	Density (g/cm^3)
Steel	30	600	1050	206	7.85
Fiberglass	13	20	2450	80	2.78
PVA	12	43	1600	40	1.30
PE	12	38	2700	120	0.98
PP	12	36	482	5	0.91

2009) was used in this study.

2.2.6 Fiber treatments and mechanical deformations

Interfacial bond strength is a key parameter in the response of ECC materials. To develop better bond between the fiber and the matrix, different fiber treatments have been utilized. Due to the lack of bond between PE fibers and the cement matrix, plasma treatment has been employed to PE fibers by Li *et al*. (1996) and Li and Netravali (1992). From the single fiber pullout tests, the pullout load of treated fibers was higher compared to that of untreated fibers. In contrast to PE fibers, PVA fibers possess significant chemical bond between the fiber and the matrix, thus its surface was treated with coated oil by Li (2001 and 2002) to reduce the chemical bond and allow pullout of fibers from the matrix. Bond of steel fiber and the matrix can be improved by modifying the fiber along tis length by roughening its surface or by inducing mechanical deformations. The steel fibers can be smooth, indented, deformed, crimped, coiled, twisted, with end hooks, end paddles and end buttons (Naaman, 2003).

2.3 Mechanical characteristics of ECC

2.3.1 Compressive characteristics

The compressive strength of ECC, without significantly difference from normal strength concrete, ranges from 30 MPa to 90 MPa (Li, 2007). Its elastic modulus usually is lower than normal concrete due to the absence of coarse aggregates (Li, 2007). This is because the coarse aggregate has higher elastic modulus than cement matrix (Mehta, 1986). The lower modulus of elasticity also results in higher strain at the compressive strength compared to normal concrete (Li, 1998).

The post-peak behavior of ECC under compression tends to descend more gently than high strength concrete, accompanied by a gradual expansion of the cylinder specimen rather than explosive crushing failure in high strength concrete (Li, 2007).

2.3.2 Tensile characteristics

The tensile characteristics of a PE-ECC with 2% fiber volume fraction was examined by Li (1998) using tensile coupons 76 mm wide by 205 mm long by 12.7 mm thick. The

first crack strength and strain were 2.5 MPa and 0.021%, respectively. The ultimate tensile strength is 4.6 MPa and the ultimate tensile strain is 5.6%. Multiple cracking occurred with many sub-parallel cracks along the transverse direction of specimen during strain hardening process. Beyond the peak stress, a localized crack was developed resulting stress softening.

2.4 Structural application of ECC

The substantial strain capacity and ductility of ECC make it an ideal material for use in structural members subjected to large inelastic deformations. Currently, the cost of ECC associates with addition of fibers and cement matrix, in spite of that, it is still much higher than normal concrete. Therefore, ECC is not meant as a replacement for regular concrete but employed in constructions, where controlled crack growth can enhance the resistance against spalling and corrosion of rebars and where the enhanced ductility can be utilized (Li, 1998). So far, a number of investigations have been conducted at the potential applicable structural members, as shown in **Figure 2.4.1** (Parra-Montesinos, 2005).

2.4.1 Columns

Fischer and Li (2002) investigated the flexural behavior of PE-ECC columns with 100 mm by 100 mm square section and 500 mm height subjected to lateral cyclic loading.

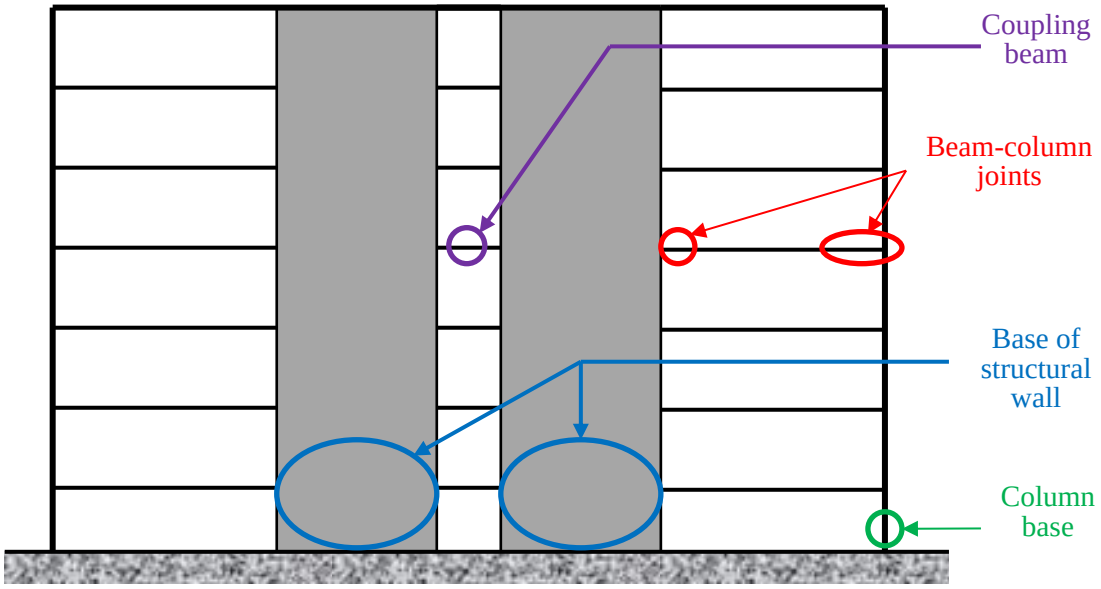

Figure 2.4.1 Potential applications of ECC in structure (Parra-Montesinos, 2005).

The columns were investigated were a control RC column with shear reinforcement, ECC column with shear reinforcement, ECC column without shear reinforcement and an ECC column with shear reinforcement and 10% axial load. Longitudinal steel reinforcement ratio was identical in all columns. PE-ECC was utilized in the footing and the full height of the column. Results show that ECC has higher damage tolerance than concrete preventing spalling during cyclic loading. Moreover, ECC serves as lateral confinement for the longitudinal reinforcing bars and prevent premature failure by reinforcement buckling.

2.4.2 Beams

Parra-Montesinos and Chompedra (2009) evaluated the deformation capacity and shear strength of flexural member using ECCs. Two types of fibers were used: PE fibers and steel hooked fibers. The volume of the fibers was varied: 1.5 and 2.0% volume fraction for PE fibers, and 1.0%, 1.5% and 2.0% volume fraction for the steel fibers. Seven beams with rectangular section of 100 mm × 250 mm and length of 1520 mm were cyclically loaded at the midspan. The specimens constructed with ECCs, with or without transverse reinforcement, exhibited stable shear-drift response until 4.0%. Buckling of longitudinal reinforcement in members with ECCs without web reinforcement was not observed up to plastic rotations of 4%. Results show that depending on the expected rotation demands, the use of transverse reinforcement can be reduced compared to that required by building codes.

Hirata *et al.* (2009) conducted five beams using PP-ECC including two beams designed to be flexural failure and the rest three beams designed to be shear failure. Four point loading tests were performed in all beams. Experimental results show that the flexural capacity of PP-ECC beams increases approximately 10% compared to RC beam while shear capacity of PP-ECC beam increases approximately 135% compared to RC beam.

Shimizu *et al.* (2004) evaluated the shear behaviors of PVA-ECC. A total of nine beams constructed with varied volume fraction of PVA fiber from 1.0% to 2.0%. The stirrup ratio was ranging from 0.00% to 0.30%. All beams were tested under Ohno-shear beam tests. The tensile behaviors of PVA-ECC with varied fiber volume fractions were also investigated to predict the shear strength of PVA-ECC beams. Then the tensile and compressive characteristics were incorporated into a modified truss-and-arch model (AIJ, 1990) to correlate the predictive value with experimental values. It shows good

agreement with both values.

However, by using FEM method comparing with experimental values in the previous studies, Kabele and Kanakubo (2007) revealed that only a fraction of ECC's tensile strength and strain capacity might be utilized in shear elements due to possible damage in the bridging fibers on the sliding crack surfaces.

2.4.3 Beam-column connections

PE-ECC with fiber volume fraction of 1.5% was used in hybrid reinforced concrete column-steel beams (RCS) connections by Parra-Montesinos and Wight (2000). One approximately 3/4 scale exterior beam-column subassembly was tested under large displacement reversals to evaluated the potential of ECC materials as a replacement of joint transverse reinforcements. Even without use of transverse reinforcements in the joint zone, the connection sustained peak shear distortion of 2% with little damage indicating the outstanding damage tolerance of ECC. Moreover, the ECC connection was 50% stronger than a companion standard RCS connection constructed with overlapping U-shaped stirrups and regular concrete.

Parra-Montesinos et al. (2005) similarly evaluated the effect of using PE-ECC on two large-scale interior beam-column joints. A transverse reinforcement at the joint region was totally eliminated and PE-ECC with fiber volume fraction of 1.5% was used. The connections were able to sustain shear stress demands comparable to the maximum limit allowed in the ACI 318-02 code with minor damage. PE-ECC was also found to be effective in reducing slip of rebars passing through beam-column joints.

2.4.4 Structural walls

Reinforced concrete squat walls exhibit limited drift capacities, typically below 1.0%. In addition, proper steel reinforcement detailing is required to avoid premature diagonal tension or compression failures, sliding shear failure, and crushing of the wall boundary regions. To improve the displacement capacity of low-rise walls, Kim and Parra-Montesinos (2003) investigated two ECC walls with a height-to-length ratio of 1.3 subjected to displacement reversals. The main experimental parameter was the influence of the ECC material. One wall used 1.5% volume fraction of PE fibers while the other wall used 2.0% volume fraction of steel hooked fibers. Both walls exhibited

stable hysteretic response with displacement capacities exceeding 2.0%. Test results showed that the use of fiber reinforced cementitious composites in low-rise walls could lead to a relaxation of distributed vertical and horizontal reinforcement requirements and, more important, to a substantial enhancement in drift capacity, which is limited for the case of reinforced concrete low-rise walls.

2.4.5 Coupling beams

As an alternative to the traditional diagonally reinforced concrete coupling beams, the use of ECC was studied by Canbolat, Parra-Montesinos, and Wight (2005) to eliminate the need for transverse reinforcement around the main diagonal bars. Two ECC materials were investigated: one with PE fibers in a 2.0% volume fraction, and the other with twisted steel fibers in a 1.5% volume fraction. Even though reinforcement requirements are simplified, the use of cast-in-place ECC coupling beams would impose additional challenges from a construction viewpoint. Therefore, the use of precast ECC beams, in combination with regular reinforced concrete structural walls, was proposed to facilitate construction and ensure adequate material quality control. Results demonstrated the superior damage tolerance of the ECC coupling beams. Transverse reinforcement around the diagonal bars was successfully eliminated due to the confinement of the ECC. In addition, the ECC material was effective in preventing buckling of the diagonal bars, even after damage localization occurred.

2.5 Current Design Guidelines for Steel reinforced ECC Members

The previous studies conducted to investigate the mechanical properties of ECC structural member have illustrated that the use of ECC can increase the flexural strength and shear strength. So far, some researchers have attempted to develop models to evaluate the flexural and shear strength of ECC structural members. Overall, the flexural capacity of steel reinforced ECC structural members can be predicted with satisfaction while the shear capacity cannot be well predicted.

2.5.1 Flexural behavior of steel reinforced ECC members

In JSCE *Recommendations for Design and Construction of High Performance Fiber Reinforced Cement Composites with Multiple Fine Cracks (HPFRCC)* (2008), since ECC is a highly ductile material exhibiting pseudo-strain hardening characteristics

under uniaxial tensile stress, it can bear part of the tensile forces in a stable manner. The contribution of tensile stress of ECC to the capacity of member cross section is taken account in the verification of safety. However, when the tensile yield strength of ECC is small, the contribution to the capacity of member cross section is found to be small by experiment. Thus, the tensile stress of ECC is defined to be considered only in the case that the design tensile yield strength is greater than 1.5 N/mm^2. The strain and stress distributions are schematically represented by **Figure 2.5.1**.

The tensile stress-strain curve of ECC in JSCE code for ECC (JSCE, 2008) is determined based on the uniaxial tensile tests and schematically shown in **Figure 2.5.2**.

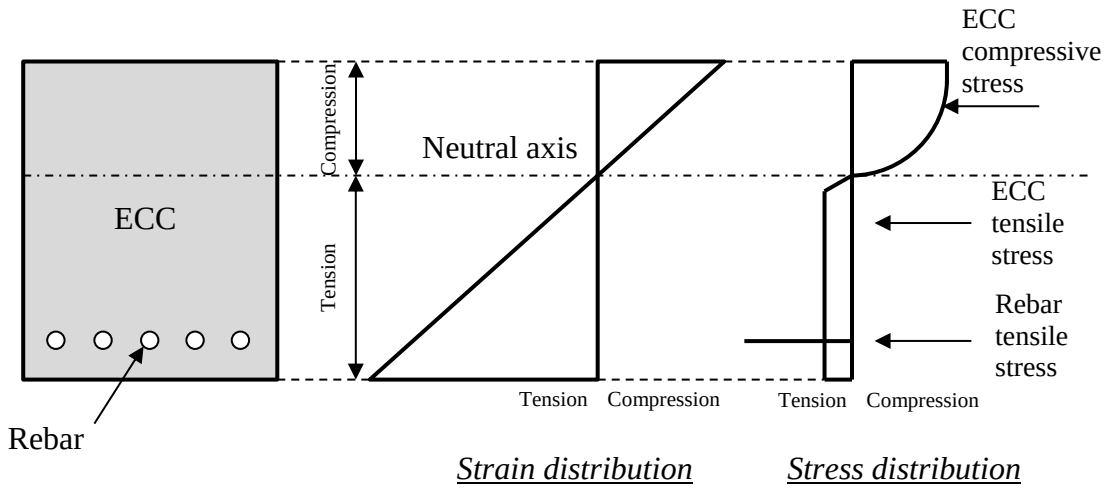

Figure 2.5.1 Schematic representations of strain and stress distributions.

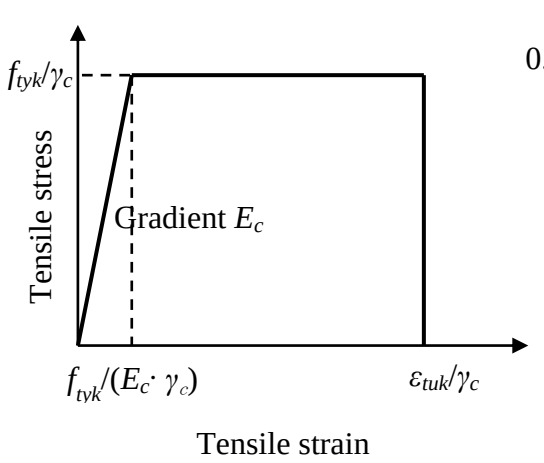

Figure 2.5.2 Tensile stress-strain curve of ECC (JSCE, 2008).

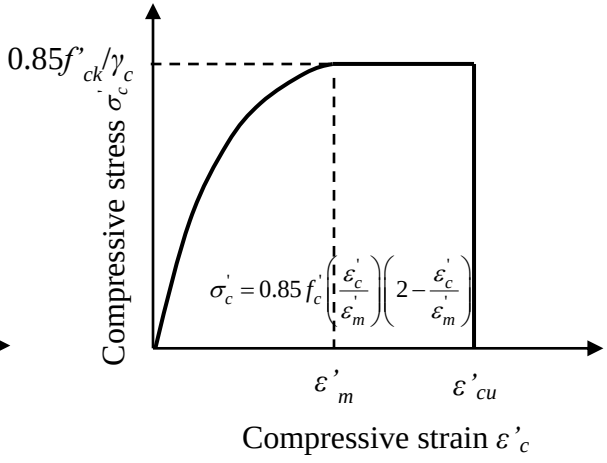

Figure 2.5.3 Compressive stress-strain curve of ECC (JSCE, 2008).

The tensile stress-strain curve shown in **Figure 2.5.2** is used when studying the ultimate limit state of section for members subjected to a bending moment or a bending moment and axial forces. The code adopts a perfect elastoplastic model that uses the characteristic values of tensile yield strength divided by the material safety factor, as denoted by a solid line in the figure. The ultimate strain of ECC is normally greater than the yield strain of the reinforcing bar and the strain of the tensile steel bar reaches yield strain before ECC reaches its ultimate strain. Thus, the effect of the ultimate strain value of ECC on the cross-sectional strength is estimated negligible.

The compressive stress-strain curve defined by JSCE code for ECC (JSCE, 2008) is derived from the results of tests on cylinder specimens of 100 mm in diameter and 200 mm in height, as shown in **Figure 3.5.3**. The strain ε'_m at the peak stress is greater than 0.002, i.e. that of ordinary concrete. Because the compressive characteristics of ECCs are varied to the type of ECC, JSCE code specifies that the determination of the stress-strain relation should be based on the basis of flexural tests of ECC. However, when appropriate test data are not available, ε'_m can be the strain at the maximum compressive stress, and ε'_{cu} can be set equal to ε'_m.

2.5.2 Shear behavior of steel reinforced ECC member

So far, some attempts have been made to develop models to evaluate the shear strength of ECC structural members. The currently available simplified models are the truss-and-arch model based on that proposed in AIJ *Design Guidelines for Earthquake Resistant Reinforced Concrete Buildings Based on Ultimate Strength Concept* (AIJ, 1990), and the modified truss model recommended by JSCE *Recommendations for Design and Construction of High Performance Fiber Reinforced Cement Composites with Multiple Fine Cracks (HPFRCC)* (JSCE, 2008), which incorporated an equation accounting for the shear carried by fibers (V_f). Both models mentioned above incorporated the shear carried by fibers independently by employing an equation.

Kanakubo *et al.* (2007) assumed that principle tensile stress of ECC keeps tensile strength (σ_t) at shear failure. The average of tensile stress on beam is expressed by with σ_t a reduction factor ν_t. They considered that beam specimen exhibits the maximum load when compressive strut is failed by principle compressive stress as shown in **Figure 2.5.4**. Because the compressive strut has some angles with main shear crack, local compressive failure takes place at the crack surface. This approach has same way to

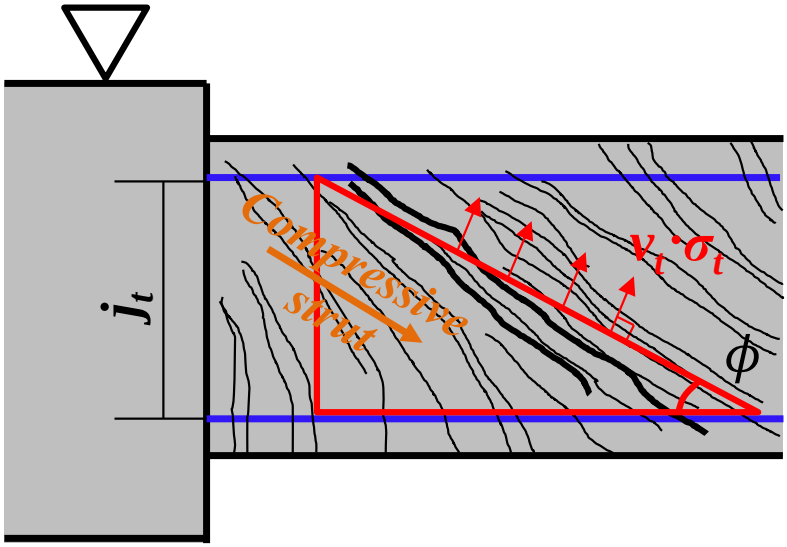

Figure 2.5.4 Model for shear strength (Kanakubo, *et al.*, 2007).

ordinary RC beams. In case of RC, shear transmitting force at the crack surface is carried by mainly bearing of coarse aggregate. In case of R/ECC, the force is carried by bridging of fibers. AIJ A-Method (AIJ, 1990) was utilized as a basic formula to express shear strength, shear strength of R/ECC beam is calculated as follows:

$$V = V_t + V_a + V_{ECC} \tag{2.5.1}$$

$$V_t = b \cdot j_t \cdot p_w \cdot \sigma_{wy} \cdot \cot\phi \tag{2.5.2}$$

$$V_a = \tan\theta \cdot (1-\beta) \cdot \nu \cdot \sigma_B \cdot b \cdot \frac{D}{2} \tag{2.5.3}$$

$$\tan\theta = \sqrt{(L/D)^2 + 1} - (L/D) \tag{2.5.4}$$

$$\beta = (1 + \cot^2\phi) \cdot p_w \cdot \sigma_{wy} / \nu \cdot \sigma_B \tag{2.5.5}$$

$$\nu = 1.70\sigma_B^{-0.333} \tag{2.5.6}$$

$$\cot\phi = \min \begin{cases} 2.0 \\ j_t / (D \cdot \tan\theta) \\ \sqrt{\nu \cdot \sigma_B / (p_w \cdot \sigma_{wy}) - 1} \end{cases} \tag{2.5.7}$$

$$V_{ECC} = b \cdot j_t \cdot \nu_t \cdot \sigma_t \cdot \cot\phi \tag{2.5.8}$$

where,

V : shear strength;
V_t : shear strength by truss mechanism;
V_a : shear strength by arch mechanism;
b : width of member;
j_t : distance between compression and tension bars;
p_w : stirrup ratio;
σ_{wy} : yield strength of stirrup;
σ_B : compressive strength of ECC;
ϕ : angle of compressive strut;
θ : angle of arch mechanism;
v : effective coefficient of compressive strength of ECC;
D : depth of member;
L : clear span length;
v_t : reduction factor for tensile strength of ECC;
σ_t : tensile strength of ECC.

In above formulas, effective coefficient of compressive strength of ECC (v) is treated as same as case of ordinary concrete proposed by *fib*. So far, reduction factor (v_t) for tensile strength of ECC (σ_t) is still unknown, even the attempts, such as reverse calculation using experimental data were used to derive the value of reduction factor. The tendency by any structural factor such as shear span ratio, stirrup ratio and fiber volume fraction cannot be found.

In *JSCE Standard Specification for Concrete Structures-2007 [Structural Performance and Verification]* (JSCE, 2007), the shear capacity of RC beam is evaluated based on modified truss model. The equation accounting for the shear carried by concrete is modified to be more conservative base on the equation proposed by Niwa (1986):

$$V_c = 0.20 \cdot f_c'^{1/3} \cdot \left(d/1000\right)^{-1/4} \cdot p_w^{1/3} \left[0.75 + \frac{1.4}{a/d} \right] \cdot b_w \cdot d \qquad (2.5.9)$$

where, V_c is the shear force carried by concrete (N); f'_c is compressive strength of concrete (N/mm^2); d is effective depth (m); p_w is longitudinal reinforcement ratio; b_w is

the web thickness (mm); *a* is the shear span (mm). Eq. 2.5.9 is an empirical equation obtained by analyzing 265 beams failed in shear.

The consideration of the shear strength of fiber reinforced cementitious composites, (UFC) with compressive strength more than 150 N/mm^2 and tensile strength more than 5 kN/mm^2 was taken into JSCE *Recommendations for Design and Construction of Ultra High Strength Fiber Reinforced Concrete Structures*, (JSCE, 2006). The shear capacity of UFC is defined by following equations:

$$V = V_{rpc} + V_f \tag{2.5.10}$$

$$V_{rpc} = 0.18 \cdot f_c'^{1/2} \cdot b_w \cdot d \tag{2.5.11}$$

$$V_f = \left(f_v / \tan \beta_u \right) \cdot b_w \cdot d \tag{2.5.12}$$

where, V is the shear capacity of UFC member; V_{rpc} is the shear carried by matrix; V_f is the shear carried by fibers; f_v is the average tensile strength of UFC; β_u is the angle of the diagonal crack (40° when there is no axial force). The shear capacity of UFC member is divided into the shear carried by matrix and fibers, respectively. Because it is required that steel rebars cannot be used in UFC, the equation for the shear carried by shear rebars is not included. Hence, the shear carried by matrix is not affected by the longitudinal reinforcement ratios.

The tensile strength of ECC was also considered in JSCE *Recommendations for Design and Construction of High Performance Fiber Reinforced Cement Composites with Multiple Fine Cracks (HPFRCC)* (JSCE, 2008). Meanwhile, the steel reinforcements are allowed to be used in ECC similar to RC structural member. Therefore, JSCE specification for ECC (JSCE, 2008) propose evaluated equation for shear capacity of R/ECC structural members based on that for RC and UFC structural members as following equations:

$$V = 0.7V_c + V_s + V_f \tag{2.5.13}$$

$$V = V_{rpc} + V_f + V_s \tag{2.5.14}$$

$$V_c = 0.7 \times 0.2 \sqrt[2]{f_c'} \cdot \sqrt[4]{1/d} \cdot \sqrt[3]{100 p_w} \cdot b_w \cdot d \quad (2.5.15)$$

$$V_s = A_w \cdot f_{wy} \cdot (\sin \alpha_s + \cos \alpha_s) \cdot z / s_s \quad (2.5.16)$$

where, Eq. 2.5.13 is the modified equation by adding the shear carried by fibers as that used for UFC. However, due to the absence of coarse aggregate in ECCs, the shear carried by matrix in ECC adopted the equation used for evaluating the shear carried by light-weight concrete with a reduction factor of 70%, as shown in Eq. 2.5.15. The accuracy of the shear capacity predictive equation provided by JSCE code (JSCE, 2008) is going to be examined in the **Chapter 4** based on the experimental results.

2.5.3 Code provisions for design of beam-column joints

Significant shear stresses induced in the beam-column joint from the connecting beams can cause the development of diagonal cracks in the joint and yielding of lateral reinforcement forming plastic hinge at the joint. Generally, the design codes do not allow to form plastic hinge at the joints mainly because:

1) The beam-column joint is a part of column which must sustain the gravity load;
2) It is difficult to obtain large hysteretic energy dissipation and deformation capacity in the joint;
3) The joint are difficult to repair internal damage occurs during seismic events.

Hence, all codes were revised to avoid the shear failure at the joint based on the experience in the past earthquakes.

AIJ codes (AIJ, 1991) has classified the beam-column joints into four types of joints which are commonly existed in the buildings as shown in **Figure 2.5.5**. The code emphasizes that the shear strength should be greater than the design shear. The shear strength of the beam-column joints is expressed by following equation,

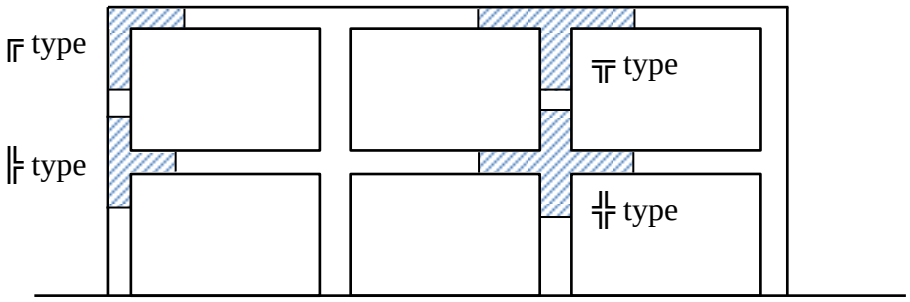

Figure 2.5.5 Type of beam-column joints classified by AIJ code.

$$V_{ju} = \kappa \phi F_j b_j D_j \tag{2.5.17}$$

where, κ = 1.0 for ╬ type, κ = 0.7 for ╦ or ╠ type and κ = 0.4 for ╔ type.
ϕ = 1 if both sides of joint provided with perpendicular beams
ϕ = 0.85 otherwise.

$$F_j = 0.8 \times f_c^{'} \tag{2.5.18}$$

b_j is effective width of joint; D_j is effective depth of joint; f'_c is compressive strength of the concrete.

In ╬ type and ╦ type joints, the beam longitudinal rebars continues through the joint, $D_j = D$ (for ╬ type and ╦ type).

In ╠ type and ╔ type beam longitudinal rebars are terminated in the joint, $D_j = 0.75D$ (for ╠ type and ╔ type).

where, D is the depth of column. For the joints without beams in two perpendicular directions, the ultimate shear strength of each type of joint is given by

$$\tau_{ju} = 0.680 f_c^{'0.7} \quad \text{(for ╬ type)} \tag{2.5.19}$$

Table 2.5.1 Value of γ for beam-column connections.

Classification		Connection Type	
		I	II
Joint with a continuous column	Joints effectively confined on all four vertical faces.	24	20
	Joints effectively confined on three vertical faces or on opposite vertical faces.	20	15
	Other cases.	15	12
Joint with a discontinuous column	Joints effectively confined on all four vertical faces.	20	15
	Joints effectively confined on three vertical faces or on opposite vertical faces.	15	12
	Other cases.	12	8

$$\tau_{ju} = 0.476 f_c^{'0.7} \quad \text{(for } \overline{\top}\text{ type)} \tag{2.5.20}$$

$$\tau_{ju} = 0.357 f_c^{'0.7} \quad \text{(for } \vdash\text{ type)} \tag{2.5.21}$$

$$\tau_{ju} = 0.204 f_c^{'0.7} \quad \text{(for } \sqsubset\text{ type)} \tag{2.5.22}$$

ACI standards (ACI Committee 318, 2008) classifies the beam-column connections into two categories, Type I and Type II, according to the loading conditions and the anticipated deformations of connected frame members during resisting lateral loads. In Type I beam-column connections, members cannot undergo significant inelastic deformation whereas the member in Type II possess enough strength to sustain inelastic deformations during reversal loading. Moreover, the joints are sub-categorized as the joint with a continuous column and the joints with a discontinuous column based on the continuity of column. If the joint consists of beams framing in from two perpendicular directions, the horizontal shear in the joint is checked independently in each direction. According to ACI 352R-02 (2002), the nominal shear strength of joint:

$$V_n = 0.083\gamma\sqrt{f_c^{'}} \cdot b_j \cdot h_c \tag{2.5.23}$$

where, b_j is effective width of joint; hc is depth of column; f_c' is compressive strength of concrete and a constant γ is given in **Table 2.5.1**. Based on Eq. 2.5.23, ACI 318-08 has recommended the joint shear strength as follows:

$$V_n = 1.7\sqrt{f_c'} \cdot A_j \quad \text{(for joints confined on all four faces)} \tag{2.5.24}$$

$$V_n = 1.25\sqrt{f_c'} \cdot A_j \quad \text{(for joints confined on three faces or on two opposite faces)} \tag{2.5.25}$$

$$V_n = 1.0\sqrt{f_c'} \cdot A_j \quad \text{(for others)} \tag{2.5.26}$$

Eurocode 8 (EN1998-1:2003) classifies the joints into two types, interior joints and exterior joints. While dealing with shear strength of joints, the effect of axial load in the column is also taken into account. The nominal shear strength of the joints can be calculated using following equations.

a) Interior joints

$$V_{jhd} \le \eta f_{cd} \sqrt{1 - \nu_d / \eta} \cdot b_j \cdot h_{jc} \tag{2.5.27}$$

$$\eta = 0.6\left(1 - f_c'/250\right) \tag{2.5.28}$$

where, f_{cd} is design concrete compressive strength, b_j is effective width of joint; h_{jc} is the distance between extreme layers of column reinforcement; ν_d is the normalized axial force in the column above the joint and f_c' is the compressive strength of concrete.

b) Exterior joints

V_{jhd} shoule be less than 80% of the value given by the Eq. 2.5.27.

References

ACI Committee 318, 2002: Building Code Requirements for Structural Concrete (ACI 318-02) and Commentary (318R-02), American Concrete Institute, Farmington Hills, Mich., 443 pp.

Architectural Institute of Japan (AIJ): *AIJ Standards for Structural Calculation of Steel Reinforced Concrete Structures*, 1991.

Architectural Institute of Japan: Design Guidelines for Earthquake Resistant Reinforced Concrete Buildings Based on Ultimate Strength Concept, pp. 106-116, 1990.

Brown, R., Shukla, A. and Natarajan, K. R.: Fiber Reinforcement of Concrete Structures, University of Rhode Island Transportation Center (URITC) Project No. 536101, 2002.

Canbolat, B. A., Parra-Montesinos, G. J. and Wight, J. K.: Experimental Study on the Seismic Behavior of High-Performance Fiber-Reinforced Cement Composite Coupling Beams, ACI Structural Journal, Vol. 102, No. 1, pp. 159-166, 2005.

Daniel, J. I., Roller, J. J. and Anderson, E. D.: Fiber Reinforced Concrete, *Portland Cement Association*, Chapter 5, pp. 22-26.

Hannant, D. J.: Fibre Cements and Fibre Concretes, John Wiley and Sons, Ltd., New York, 1978.

Hirata, T., Kawanishi, T., Okano, M. and Watanabe, S. : Study on Material Properties and Structural Performance of High-Performance Cement Composites Using Polypropylene Fiber, *Proceeding of Japan Concrete Institute*, Vol. 31, No. 1, pp. 289-294, 2009. (in Japanese)

Japan Society of Civil Engineers (JSCE): Standard Specification for Concrete Structures-2007 [Structural Performance and Verification], 2010.

Japan Society of Civil Engineers (JSCE): *Recommendations for Design and Construction of Ultra High Strength Fiber Reinforced Concrete Structures*, 2006.

Japan Society of Civil Engineers (JSCE): *Recommendations for Design and Construction of High Performance Fiber Reinforced Cement Composites with Multiple Fine Cracks (HPFRCC)*, 2008.

Joint ACI-ASCE Committee 352: *ACI 352R-02, Recommendations for Design of Beam-Column Connections in Monolithic Reinforced Concrete Structures*, 2002.

Kabele, P. and Kanakubo, T.: Experiential and Numerical Investigation of Shear Behavior of PVA-ECC in Structural Elements, *Proc. of 5th International RILEM Workshop on High Performance Fiber Reinforced Cement Composites (HPFRCC5)*, Reinhardt and Naaman, eds., pp. 137-146, 2007.

Kanakubo, T., Shimizu, K., Kanda, T. and Nagai, S.: Evaluation of Bending and Shear Capacities of HPFRCC Members toward the Structural Application, *Proceeding of the Hokkaido University COE Workshop on High Performance Fiber Reinforced Composites for Sustainable Infrastructure System – Material Modeling, Structural Design and Application, Sapporo*, Japan, February, 2007.

Kesner, K.E., Billington, S.L., and Douglas K.S.: Cyclic response of Highly Ductile Cement-based Composites, *ACI Materials Journal*, Vol. 100, No. 5, pp. 381-390, 2003.

Kesner, K.E. and Billington S.L.: Investigation of Infill Panels made from Engineered Cementitious Composites for Seismic Strengthening and Retrofit, *ASCE Journal of Structural Engineering*, Vo. 131, No. 11, pp. 1712-1720, 2005.

Kesner, K.E. and Billington S.L.: Tension, Compression and Cyclic Testing of Engineered Cementitious Composite Materials, *Technical Report MCEER-04-0002*, 2004.

Kim, L. and Parra-Montesinos, G.: Behavior of HPFRCC Low-Rise Walls Subjected to Displacement Reversals, High Performance Fiber Reinforced Cement Composites (HPFRCC 4), *Proceedings of the Fourth RILEM Workshop*, A. E. Naaman and H. W. Reinhardt, eds., RILEM Publications S.A.R.L., Cachan Cedex, France, pp. 505-515, 2003.

Li, V.: Engineered Cementitous Composites (ECC) – Tailored Composites through Micromechanical Modeling, in *Fiber Reinforced Concrete: Present and the Future*, eds. Banthia N. and Mufti, A., Canadian Society of Civil Engineers, Montreal, Canada, pp. 64-97, 1998.

Li, V., Mishra, D. and Wu, H.: Matrix Design for Pseudo Strain-hardening Fiber Reinforced Cementitious Composites, *Journal of Materials and Structures, RILEM*, Vo. 28, No. 183, pp. 586-595, 1995.

Li, V. and Leung, C.: Strady-state and Multiple Cracking of Short Random Fiber Composites, Journal of Engineering Mechanics, ASCE, Vol. 118, No. 11, pp. 2246-2264, 1992.

Li, V.: Engineered Cementitious Composites (ECC) – Material, Structural, and Durability Performance, *Concrete Construction Engineering Handbook*, Ed. E.Nawy, CRC Press, 2007.

Maalej, M. and Li, V.: Flexural/tensile-strength Ratio in Engineered Cementitious Composites, *Journal of Materials in Civil Engineering, ASCE*, Vol. 6, No. 4, pp. 513-528, 1994.

Matsumoto, T. and Mihashi, H.: DFRCC Terminology and Application Concepts, *the Journal of Advanced Concrete Technology*, Vol. 1, No. 3, pp.335-340, 2003.

Naaman, A. E.: High-Performance Fiber-Reinforced Cement Composites, *Concrete Structures for the Future*, IABSE Symposium, Zurich, pp. 371-376, 1987.

Naaman, A. E. and Reinhardt, H.: Characterization of High Performance Reinforced Cement Composites – HPFRCC, *High Performance Fiber Reinforced Cement Composites 2 (HPFRCC 2)*, Proceedings of the Second International RILEM Workshop, eds. A. Naaman and H. Reinhardt, E&FN Spon, London, pp. 1-24, 1996.

Niwa, J.: Evaluation of the Equation for Shear Strength of Reinforced Concrete Beams without Web Reinforcement, *Proceedings of JSCE*, No.372/V-5, pp. 167-176, 1986.

(in Japanese)

Parra-Montesinos, G.: High-Performance Fiber-Reinforced Cement Composites: An Alternative for Seismic Design of Structures, *ACI Structural Journal*, Vol. 102, No. 5, pp. 668-675, 2005.

Parra-Montesinos, G. and Chompreda, P.: Deformation Capacity And Shear Strength of Fiber-Reinforced Cement Composite Flexural Members Subjected to Displacement Reversals, *ASCE Journal of Structural Engineering*, Vol. 133, No. 3, pp. 421-431, 2007.

Parra-Montesinos, G. and Wight, J.: Seismic Response of Exterior RC Column-to-Steel Beam Connections, *ASCE Journal of Structural Engineering*, Vol. 126, No. 10, pp. 1113-1121, 2000.

Parra-Montesinos, G., Peterfreund, S. and Chao, S.: Highly Damage-Tolerant Beam-Column Joints through Use of High-Performance Fiber-Reinforced Cement Composites. *ACI Structural Journal*, Vol. 102, No. 3, pp. 487-495, 2005.

Romualdi, J.P. and Baston, G.B.: Mechanics of Crack Arrest in Concrete, *Proceedings of the ASCE Journal of Engineering Mechanics Division*, 89, EM3, pp. 147-168, 1963.

Romualdi, J.P. and Mandel, J.A.: Tensile Strength of Concrete Affected by Uniformly Distributed and Closely Spaced Short Lengths of Wire Reinforcement, *ACI Journal Proceedings*, 61, pp. 657-670, 1964.

Shimizu, K, Kanakubo, T., Kanda, T. and Nagai, S.: Shear Behavior of PVA-ECC Beams, *Proceeding of Japan Concrete Institute*, Vol. 26, No. 2, pp. 1537-1542, 2004. (in Japanese)

Chapter 3

MECHANICAL PROPERTIES OF PP-ECC

3.1 Introduction

ECC exhibits strain hardening and multiple cracking upon loading in tension which leads to improvement in ductility, toughness, fatigue resistance and performance capacity (Matsumoto and Mihashi, 2003). The compressive strength of ECC, without significantly difference from normal strength concrete, ranges from 30 MPa to 90 MPa (Li, 2007). Its elastic modulus usually is lower than normal concrete due to the absence of coarse aggregates (Li, 2007). This is because the coarse aggregate has higher elastic modulus than cement matrix (Mehta, 1986).

In previous studies, the monotonic tension and compression behaviors of ECCs reported mostly regards to PVA-ECC or PE-ECC. Fukuyama et al. (1999) investigated tension-compression reversed experiments of PVA-ECC with 1.5% fiber volume fraction using cylinder specimen 100 mm diameter by 200 mm high. Slip behavior in the change of loading from tension to compression was observed. Kesner, Billington and Douglas (2003) and Kesner and Billington (2004) examined the uniaxial monotonic response of PVA-ECC and PE-ECC with 2% fiber volume fraction. The variables are mixture design, specimen geometry. Cylinders with 50 mm diameter by 100 mm high were used in monotonic compression experiments while the dogbone shaped specimens with central section of 25 mm × 25 mm were used for tension experiments.

In this chapter, the basic mechanical properties of PP-ECC, namely compressive and tensile characteristics are investigated. Strain hardening behavior, as one of the most notable characteristics of ECC, was investigated by employing uniaxial tensile tests. The compressive characteristics of PP-ECC were investigated by cylinder compression loading tests. The PP-ECC material used in this research is a class of short-fiber, randomly distributed cementitious composites with 3% fiber volume fraction.

3.2 Production of PP-ECC

3.2.1 Mix design

The target nominal compressive strength of the PP-ECC is 30 MPa. The material components and mixture proportion used in this investigation were based on a study by Hirata *et al.* (2009). Ordinary Portland Cement (OPC), fly ash (maximum grain size of 0.3 mm), water and 3% volume fraction of PP fibers were combined using mix proportion shown in **Table 3.2.1**. It should be noted that, different from normal concrete, the compressive strength of ECC is not only affected by water-to-cement ratio, but also other factors, such as tensile strength of fiber, compressive strength of matrix, bonding strength of fiber with matrix, the volume fraction of fibers, air content, etc. (Kawamata *et al.*). The air content of PP-ECC used in this study is around 10%. The PP fibers, as shown in **Photo 3.2.1**, are fibrillated fibers having diameter of 36 μm, length of 12 mm, tensile strength of 482 MPa and elastic modulus of 5 GPa, as summarized in **Table 3.2.2**. This fibrillated polypropylene fiber with rugged surface results in improvement of bond properties and exhibits the pseudo strain hardening and multiple fine cracking of ECC under tensile stress.

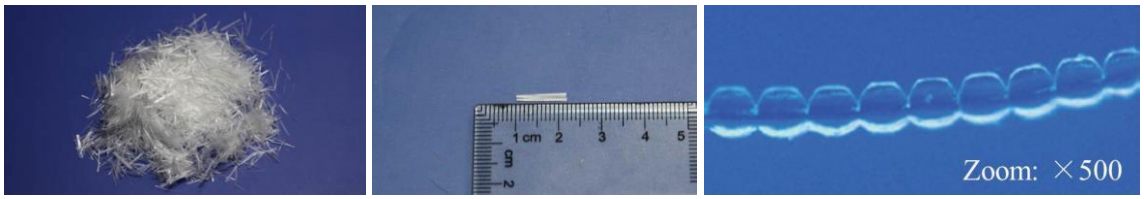

(a) A cluster of fiber. (b) A single fiber. (c) Cross section.

Photo 3.2.1 Polypropylene (PP) fibers.

Table 3.2.1 Mix proportion of PP-ECC.

Slump flow (mm)	W/B (%)	FA/B (%)	Unit weight (kg/m^3)			
			W	B	PP fiber	AE
Approx. 500	27	32.9	371	1400	27	7

W: water; B: binder; FA: fly ash; AE: air-entrainment.

Table 3.2.2 Properties of polypropylene fiber.

Fiber	Length (mm)	Diameter (μm)	Elastic modulus (×10^3 N/mm^2)	Tensile strength (N/mm^2)
Polypropylene	12	36	5	482

Photo 3.2.2 Biaxial mixer for mixing PP-ECC.

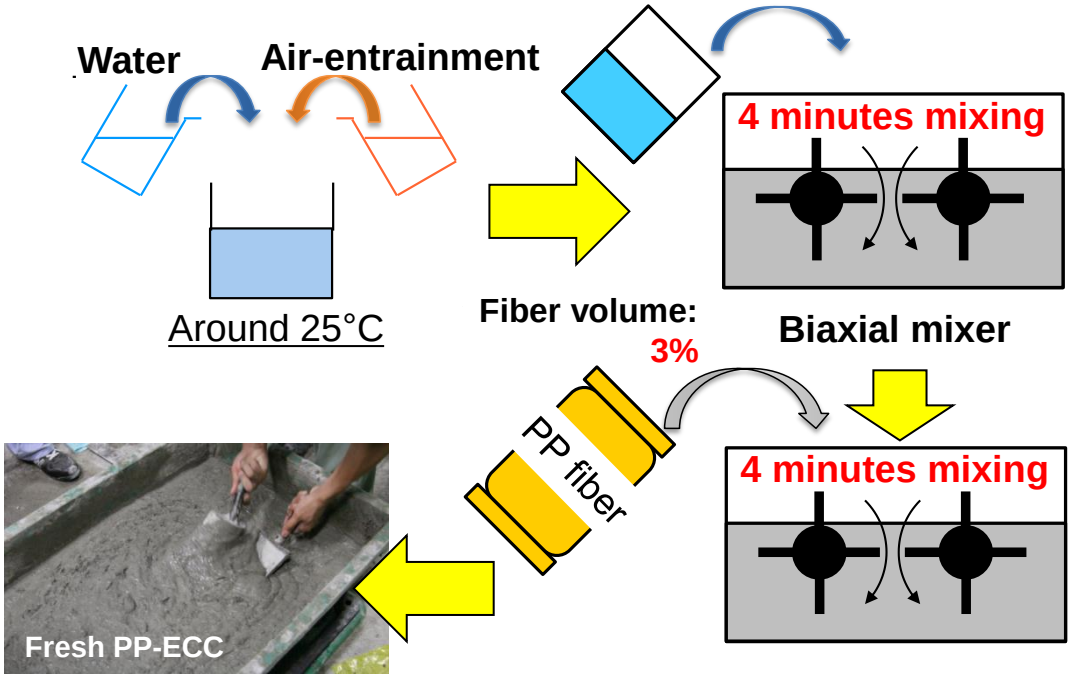

Figure 3.2.1 Mixing process of PP-ECC .

3.2.2 Production process

Photo 3.2.2 shows the biaxial mixer used for mixing PP-ECC. Such mixer is used due to the high viscosity of PP-ECC required. **Figure 3.2.1** shows the mixing process of PP-ECC. The cement and water mixed with air-entrainment was poured into the mixer firstly. The mixture was mixed together for four minutes. When the mixture of cement paste became flowable and uniform, the PP fibers were added into the mixer. Then PP

fiber and cement paste was mixed for four minutes. To total mixing time for one batch was approximately 10 minutes.

3.3 Compressive Characteristics

3.3.1 Specimen design

The compressive properties of PP-ECC were inspected by employing the cylinder compression test following the standard of JIS A 1108: *Method of test for compressive strength of concrete*. The PP-ECC cylinders with diameter of 100 mm and height of 200 mm were prepared.

3.3.2 Construction

According to the earlier described mix proportion of PP-ECC, PP-ECC was cast and placed into the standardized mold for compression cylinder loading tests. The formwork was demolded after 24 hours curing and then PP-ECC cylinders were submerged in the water with temperature around 20°C for curing. The curing of these cylinders takes 28 days before testing.

3.3.3 Compression loading tests and results

After the curing of PP-ECC cylinders, the sizes of PP-ECC cylinders were measured to obtain the average diameters:

$$d = \frac{d_1 + d_2}{2} \tag{3.3.1}$$

where, d is the average diameter (mm); d_1 and d_2 is the diameter in orthogonal direction (mm). After the measurement, the monotonic compression load was applied on these cylinders up to the failure. The compressive strength of PP-ECC can be derived by

$$f_c^{'} = \frac{P}{\pi\left(d/2\right)^2} \tag{3.3.2}$$

Table 3.3.1 Compressive properties of PP-ECC.

Material	Compressive strength (N/mm^2)	Compressive strain (%)	Elastic modulus (N/mm^2)
PP-ECC	33.6	0.4	1.5×10^4
Concrete	30.0	0.2	2.8×10^4

where, f'_c is the compressive strength of PP-ECC (N/mm^2); P is the maximum load applied during the compression tests. The results of compression loading tests of PP-ECC compared to that of normal strength concrete with compressive strength of 30 N/mm^2 are shown in **Table 3.3.1**. Even with equivalent compressive strength to normal strength concrete, the structural member utilizing ECC can lead to a higher structural performance in comparison to concrete or fiber reinforced concrete (Li, 2007).

3.4 Tensile Characteristics

3.4.1 Specimen design

The tensile characteristics of PP-ECC were investigated by employing uniaxial tensile

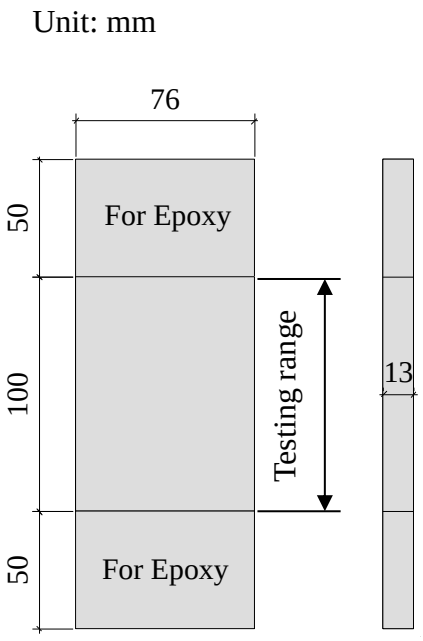

(a) Front view. (b) Side view.

Figure 3.4.1 Dimensions of plate.

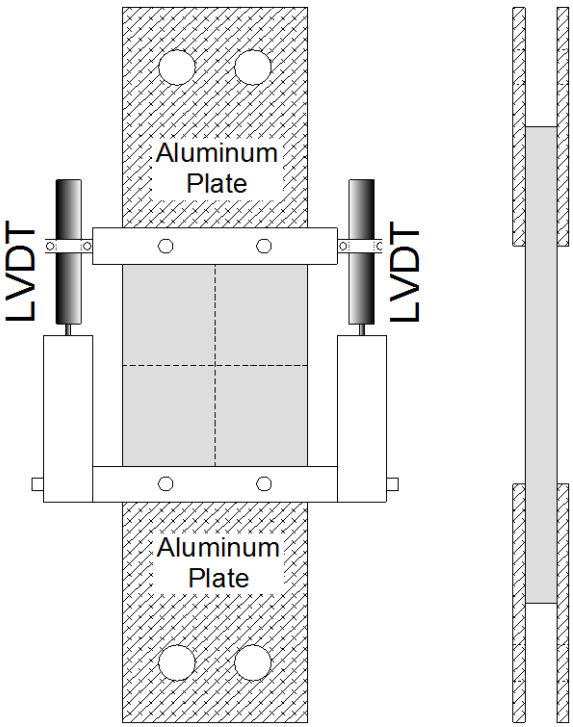

Figure 3.4.2 Connecting plates.

method. As shown in **Figure 3.4.1**, the PP-ECC plate specimens with rectangular cross section of 76 mm wide and 13 mm thick were designed. The length of plate specimen is 200 mm, including 50 mm attaching length with aluminum plates at both sides of plate. For each plate specimen, four aluminum plates with precast holes as shown in **Figure 3.4.2** were prepared for connecting the loading facility. The tensile span of the PP-ECC plate is 100 mm.

3.4.2 Construction

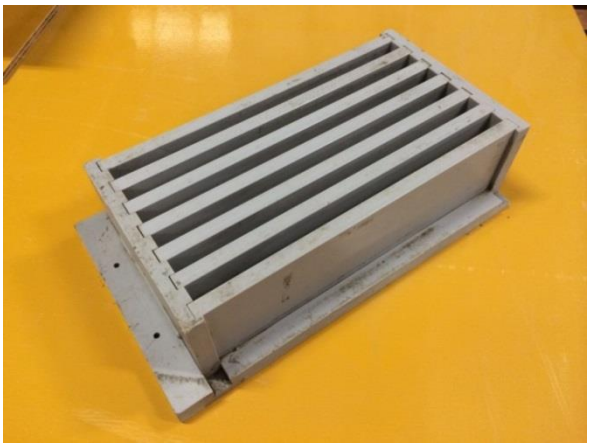

Photo 3.4.1 Formwork for uniaxial tensile tests.

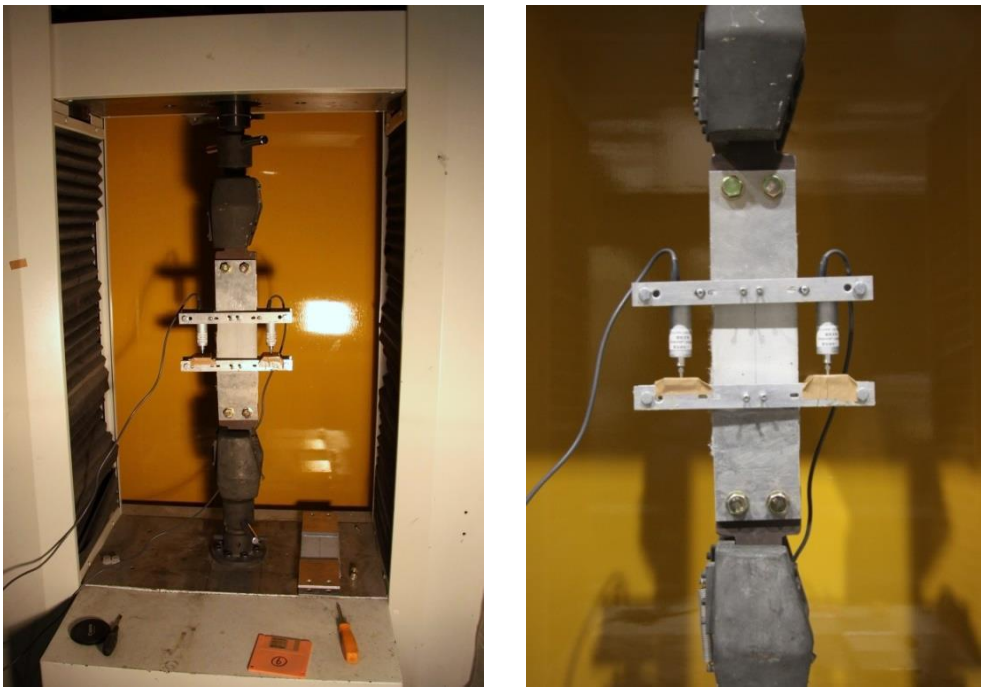

Photo 3.4.2 Experimental setup of the uniaxial loading tests.

According to the earlier described mix proportion of PP-ECC, PP-ECC was cast and placed into the formwork as shown in **Photo 3.4.1** with moving the pouring position continuously along the longitudinal direction of the plate. 24 hours after the casting, the formwork was removed and the plate specimens were coated by soaking cloths. The plastic sheet was used to coat the specimen along with moistened cloths to prevent evaporation. After the moist-curing for 28 days, all PP-ECC plate specimens were attached with aluminum plates by using epoxy for next experimental setup.

3.4.3 Loading setup

As shown in **Figure 3.4.2**, two Linear Variable Differential Transformers (LVDTs) set parallel to applied loading direction at both sides, were used to measure the axial deformation. For each plate, two steel plates with precast holes which are at the same location as aluminum plates were inserted into the gap between two aluminum plates and connected with specimen via four bolts penetrating two aluminum plates and one steel plate. Then the steel plates at both were griped by testing facility. The data-logger was used to record the load data from testing facility and the deformation data from two LVDTs. **Photo 3.4.2** shows the experimental setup before loading test.

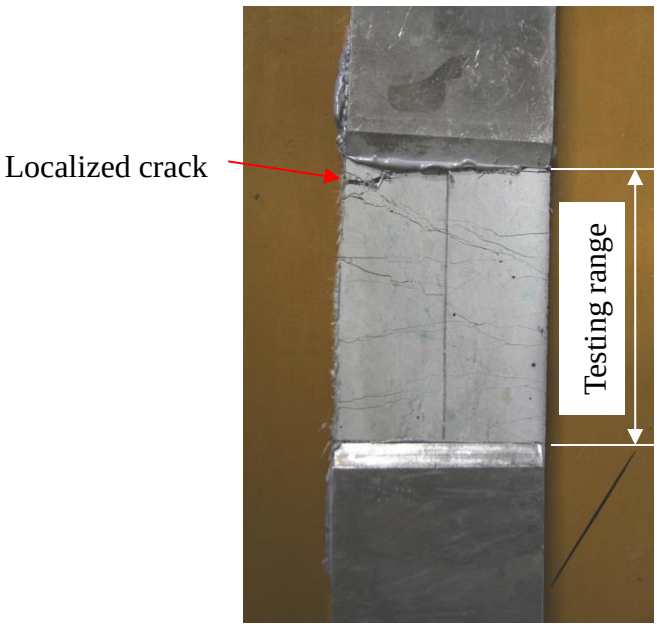

Photo 3.4.3 Crack pattern after the uniaxial loading tests.

3.4.4 Loading protocol

The monotonic tensile load was provided by a digital close-loop displacement controlled material test facility (**Photo 3.4.2**) with maximum load capacity of 50 kN. The speed of load head was selected as 0.1mm/min.

3.4.5 Results and discussions

Photo 3.4.3 shows the crack pattern of the PP-ECC plate specimen after uniaxial tension loading test. The obvious multiple fine cracks were distributed within the testing range and a localized crack was finally developed next to aluminum plate leading to the tensile failure of plate specimen.

According to the experimental data captured by the data-logger, the stress and strain could be derived by the following equations:

$$\sigma_{ECC} = \frac{P}{w \cdot t} \tag{3.3.3}$$

$$\varepsilon_{ECC} = \frac{\Delta L}{L} \tag{3.3.4}$$

where, σ_{ECC} is the tensile stress; ε_{ECC} is the tensile strain; P is the tensile load; w is the width of plate; t is the thickness of the plate; ΔL is the increased displacement due to tensile load; L is the testing length of the plate.

Then the stress-strain response of PP-ECC plates subjected to monotonic tensile load is as shown in **Figure 3.4.3**. The test result clearly shows typical pseudo strain hardening behavior of PP-ECC from the first cracking strain up to 2.5% strain. From the beginning of the tests, the stress continued to increase until the first crack occurred. At the moment of occurrence of the first crack, the stress then suddenly dropped slightly but then continued to increase afterword before the occurrence of the second crack. As the loading continued, the increase and drop of stress continued to take place. Meanwhile, more and more fine cracks were observed on the surface of the specimen. At around 3% strain, a localized crack gradually formed and the stress began to turn to softening. The tensile yield strength is determined as the lower value immediately after first cracking

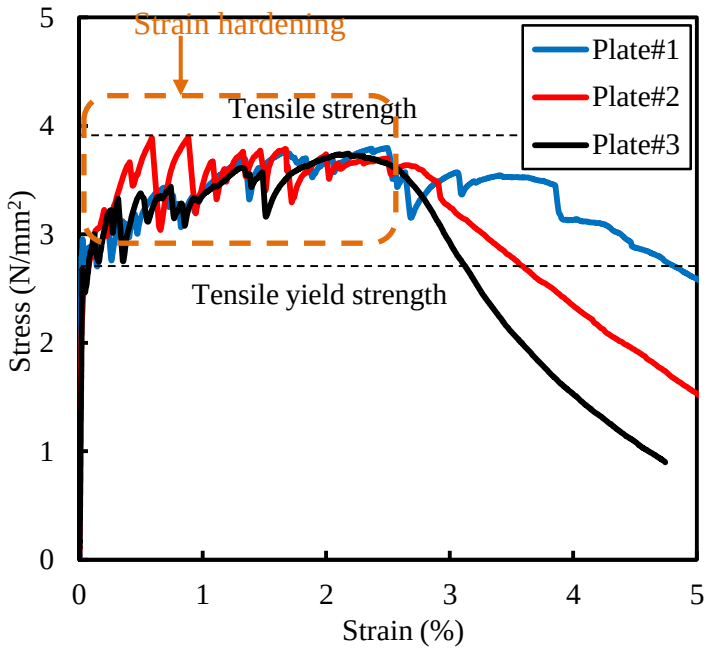

Figure 3.4.3 Results of uniaxial tensile tests.

based on the stress-strain relationship. The tensile strength is defined as the maximum stress in the tensile stress-strain curve obtained from uniaxial tensile tests. In this study, the strain capacity of PP-ECC is greater than 2.5%. The yield and tensile strength were greater than 2 and 3 N/mm^2, respectively.

3.5 Summary

The monotonic compression and tensile tests were performed to investigate the compressive and tensile behavior of PP-ECC. Based on the experimental results presented, the following findings were obtained:

1) In cylinder compression loading tests, PP-ECC has similar compressive strength to normal strength concrete while its elastic modulus is lower than normal strength concrete. PP-ECC also has a higher compressive strain than that of normal strength concrete.

2) In monotonic tensile tests, PP-ECC exhibits the strain hardening behavior and its yield and ultimate tensile strength is greater than 2.5 N/mm^2 and 3.0 N/mm^2, respectively. The strain capacity of PP-ECC is greater than 2.5%.

References

Fukuyama, H., Matsuzaki, Y., Nakano, K. and Sata, Y.: Structural Performance of Beam Elements with PVA-ECC, *Proc. Third International Workshop on High Performance Fiber Reinforced Cement Composites* (HPFRCC3) H.W. Reinhardt and A.E. Naaman (eds.), pp. 531-542, 1999.

Hirata, T., Kawanishi, T., Okano, M. and Watanabe, S. : Study on Material Properties and Structural Performance of High-Performance Cement Composites Using Polypropylene Fiber, *Proceeding of Japan Concrete Institute*, Vol. 31, No. 1, pp. 289-294, 2009. (in Japanese)

Japanese Standards Association (JSA): JIS A 1108: *Method of test for compressive strength of concrete*.

Kawamata, A., Mitsuhashi, H. and Kaneko, Y.: Study on Effect of Air Content and Water-to-Cement Ratio on Mechanic Characteristics of Fiber Reinforced Mortar, Proceeding of Japan Concrete Institute, Vol. 22, No. 2, pp. 301-306, 2000. (in Japanese)

Kesner, K.E., Billington, S.L., and Douglas K.S.: Cyclic response of Highly Ductile Cement-based Composites, *ACI Materials Journal*, Vol. 100, No. 5, pp. 381-390, 2003.

Kesner, K.E. and Billington S.L.: Tension, Compression and Cyclic Testing of Engineered Cementitious Composite Materials, *Technical Report MCEER-04-0002*, 2004.

Li, V.: Engineered Cementitious Composites (ECC) – Material, Structural, and Durability Performance, *Concrete Construction Engineering Handbook*, Ed. E.Nawy, CRC Press, 2007.

Matsumoto, T. and Mihashi, H.: DFRCC Terminology and Application Concepts, *the Journal of Advanced Concrete Technology*, Vol. 1, No. 3, pp.335-340, 2003.

Mehta, P. K. and Monteiro, P. J. M.: Effect of Aggregate, Cement, and Mineral Admixtures on the Microstructure of the Transition Zone, *MRS Proceedings*, Vol.

114, No. 65, 1987.

Chapter 4

SHEAR BEHAVIOR OF PP-ECC BEAMS WITH VARYING STIRRUP RATIOS

4.1 Introduction

With the objective of avoiding the over congestion at the T-joints, the transverse reinforcements was decided to be reduced. Therefore, it is the key to investigate the effect of stirrup ratio on the shear behavior of PP-ECC beams prior to beam-column joint tests.

Up to date, ECC has been proposed to be employed in constructions, where controlled crack growth can enhance the resistance against spalling and corrosion of rebars and where the enhanced ductility can be utilized. The steel reinforced ECC (R/ECC) structural members such as column and beam-column joints with reduction of stirrups have been confirmed in previous studies (Li and Fisher, 2002; Parra-Montesinos, 2005); however, the shear behavior of ECC beams with reduction in shear reinforcements has not been completely clarified yet. To further assess the shear behavior of R/ECC, several Ohno shear beams were tested and reported by RILEM. The shear strength of the tested beams was predicted by employing the truss-and-arch model with reduced tensile strength which was obtained from the uniaxial tensile tests. However, Kabele and Kanakubo revealed that only a fraction of ECC's tensile strength and strain capacity might be utilized in shear elements due to possible damage in the bridging fibers on sliding crack surfaces. Moreover, Suryanto *et al.* (2010) further investigated the shear capacity and failure mechanism of PVA-ECC and correlated them with existing experimental data by utilizing an explicit shear transfer model and anisotropic stress-strain fields. The study showed that the failure mechanism of R/ECC beams was not only due to the breakdown of tensile stress transfer at cracks, but also to shear transfer mechanisms, which indicated that the shear capacity of R/ECC member might have occurred prior to the tensile strength of ECC by inducing a reduction factor to

account for this mechanism.

This chapter is going to the investigation of shear performance of PP-ECC beams with varying shear reinforcement ratios with comparisons with reference beams which were constructed by the normal concrete. The shear behaviors of PP-ECC were clarified and the shear capacities of PP-ECC beams would be correlated with predictive equations provided by *JSCE Recommendations for Design and Construction of High Performance Fiber Reinforced Cement Composites with Multiple Fine Cracks (HPFRCC)*.

4.2 Design and Construction of Beam Specimens

4.2.1 Specimen design

In order to clarify the differences of shear behaviors between RC and PP-ECC beams, two different types of matrixes (concrete and PP-ECC), a total of seven beams were constructed and tested. Among these seven beams, two RC beams were prepared including one control beam by providing an amount of stirrups in the shear span named RC-Ref and another RC beam without stirrups within the shear span named RC-00. For the rest of five PP-ECC beams, the stirrup ratios of these specimens were decreasing from the level of the RC-Ref to zero. **Table 4.2.1** summarizes the layout of these specimens. The designations of these seven specimens were determined according to

Table 4.2.1 Layout of beam specimens.

Beam designation	Length L (mm)	Stirrups		Longitudinal rebar		Matrix type
		r_w (%)	s (mm)	A_s (mm^2)	p_w (%)	
RC-Ref	2100	0.42	100	1013.4	2.7	Concrete
RC-00		0.00	–			
RE-42		0.42	100			PP-ECC
RE-30		0.30	140			
RE-24		0.24	175			
RE-12		0.12	350			
RE-00		0.00	–			

r_w: stirrup ratio; s: the spacing of stirrups; A_s: the total cross-sectional area of longitudinal rebars in tension; p_w: the longitudinal reinforcement ratio.

Unit: mm

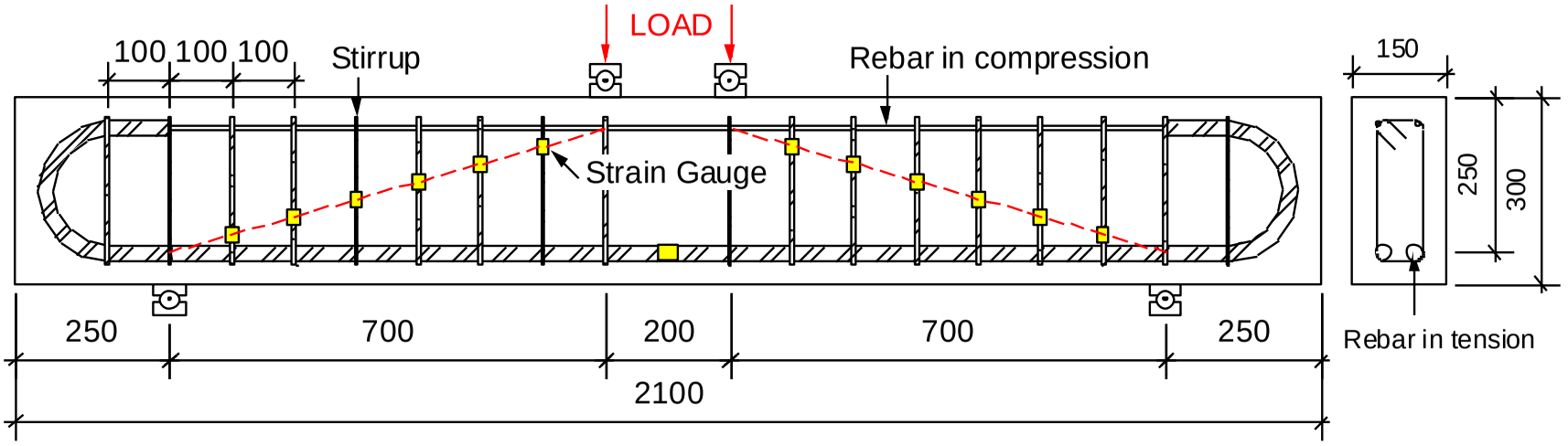

Figure 4.2.1 Dimensions and reinforcement details of RC-Ref. or RE-42.

Unit: mm

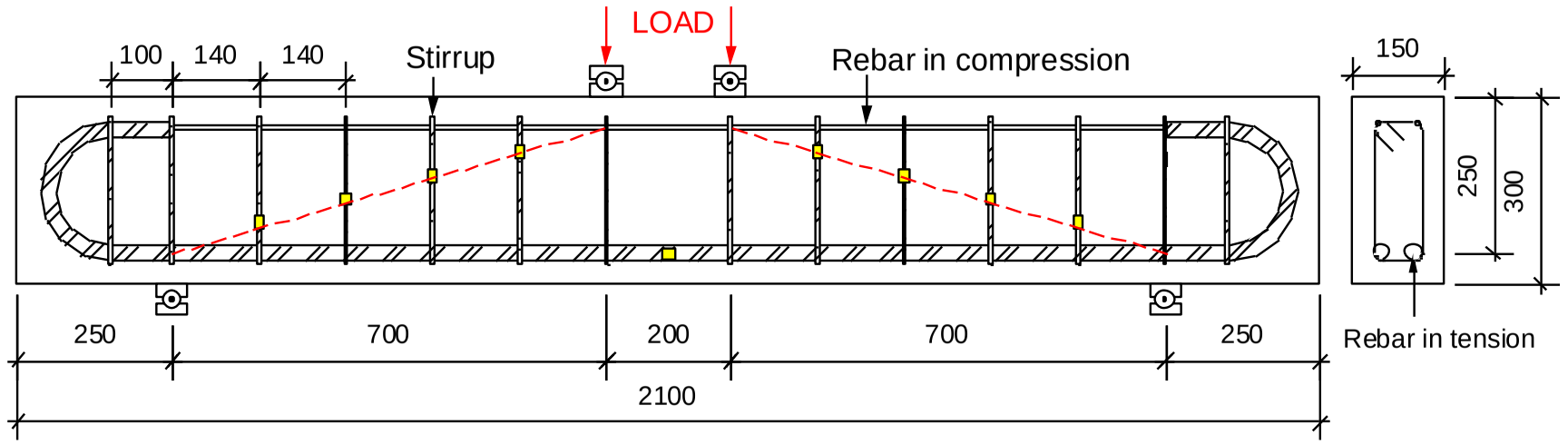

Figure 4.2.2 Dimensions and reinforcement details of RE-30.

Unit: mm

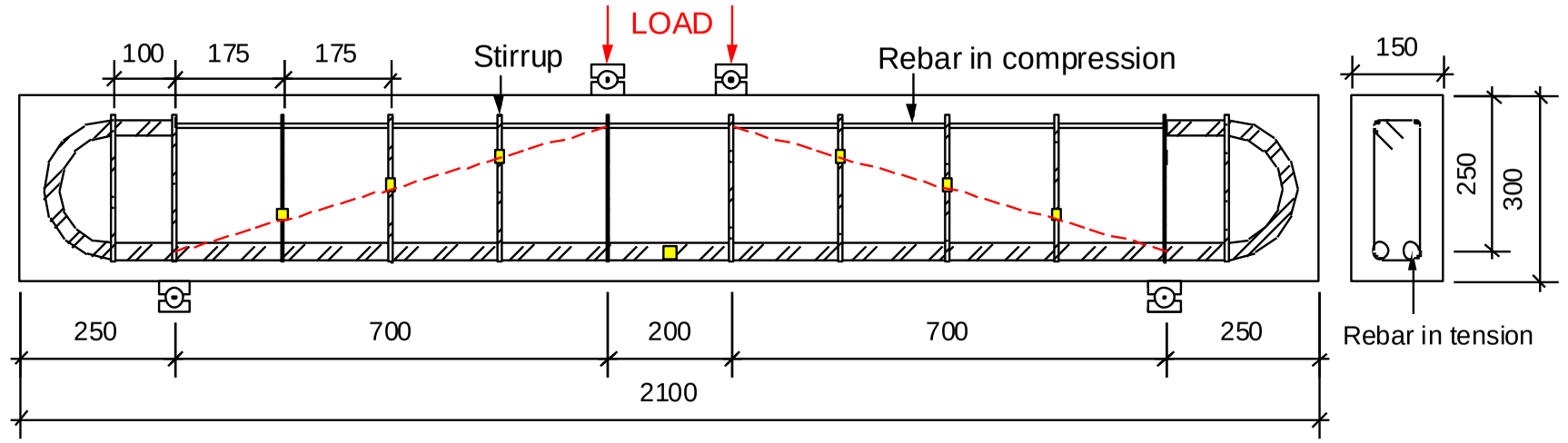

Figure 4.2.3 Dimensions and reinforcement details of RE-24.

Unit: mm

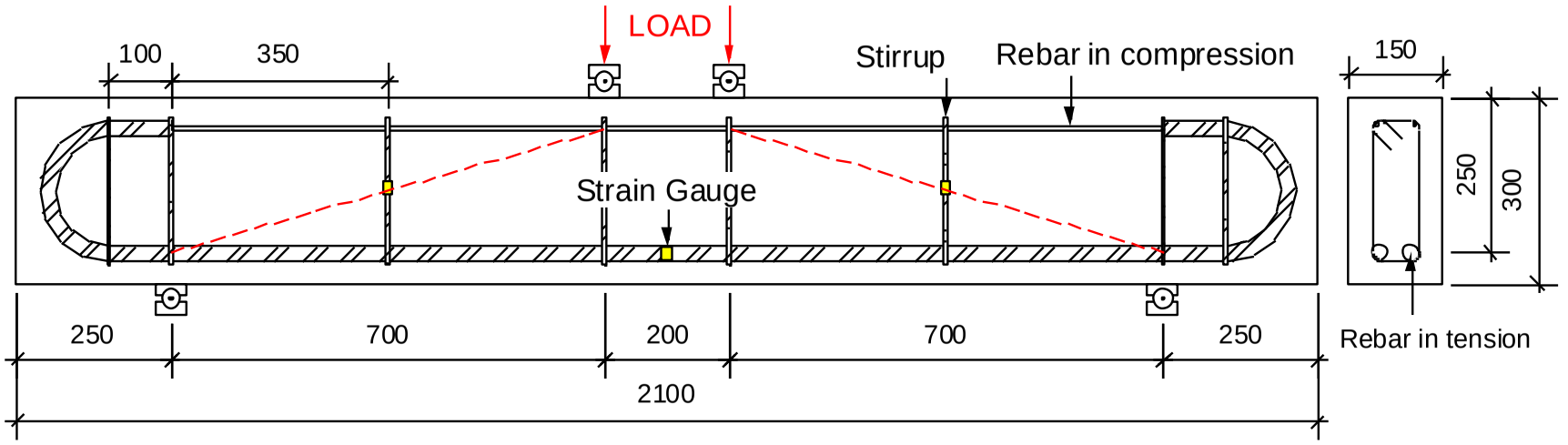

Figure 4.2.4 Dimensions and reinforcement details of RE-12.

Unit: mm

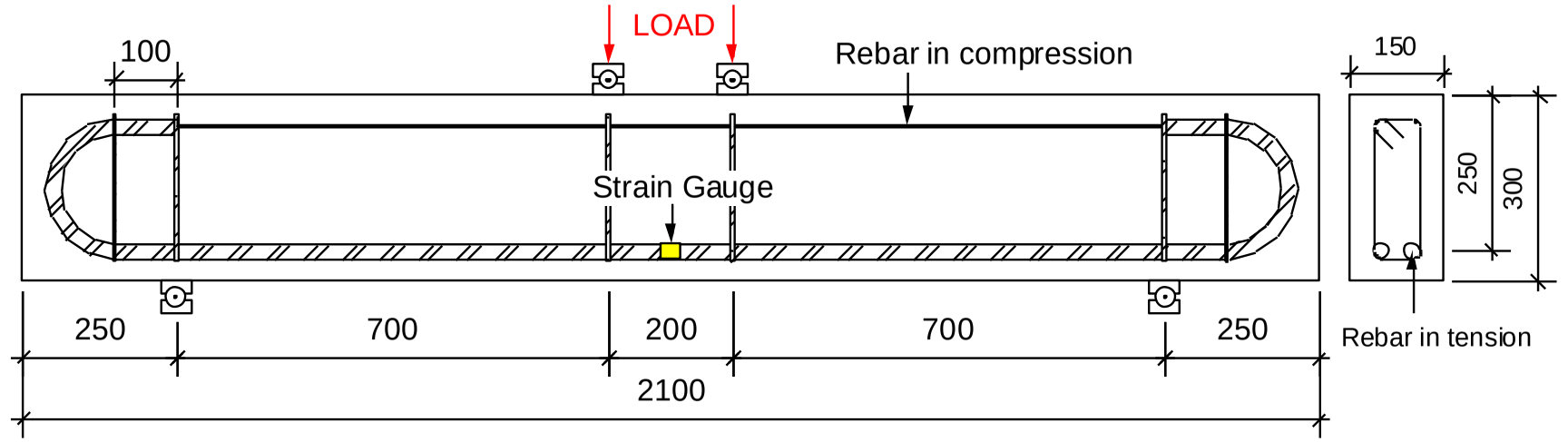

Figure 4.2.5 Dimensions and reinforcement details of RC-00 or RE-00.

their matrix type and stirrup ratio. ‘RC’ or ‘RE’ indicates that the matrix type of the specimen is ‘Reinforced Concrete’ or ‘Reinforced ECC’, respectively. Except in the case of control beam (RC-Ref), the latter digit in specimen designations indicates the stirrup ratio, e.g., RE-24 refers to a specimen with stirrup ratio of 0.24% using PP-ECC.

To investigate the shear capacity of beam specimens, as summarized in **Table 4.2.1**, all beam specimens had the same cross-sectional dimension (150mm×300mm), longitudinal rebars arrangement and shear span-effective depth ratio that is 2.8, which was designed to fail beams in shear prior to flexure (Macgregor, 2011). The only parameter was stirrup ratio. The stirrups were distributed symmetrically within both shear spans. The RC control beam, RC-Ref was designed to be failed in shear rather than the flexural failure following *JSCE Standard Specifications for Concrete Structures-2007 [Design]* (2010). The calculation of shear capacity in the JSCE specifications for RC structural members is based on the theory of modified truss analogy, in which the shear capacity of RC structural member is divided into two components, such as

a. the shear force carried by the stirrups
b. the shear force carried by another mechanism than stirrups (contribution from concrete)

and therefore the total shear capacity of a RC beam could be formulated by Eq.(4.2.1):

$$V = V_c + V_s \tag{4.2.1}$$

where, V is the shear capacity; V_s is the contribution from stirrups; and V_c is the contribution from the concrete, which is approximated to be the shear capacity of RC beam without stirrups. The shear capacity of RC beam without stirrups is evaluated by diagonal cracking capacity, in which, it is considered that the shear stress along the crack plane is considered to be resisted by the following effects (**Figure 4.2.6**):

a. direct shear resistance in the flexural compression zone
b. aggregate interlocking along the crack surface
c. dowel action of longitudinal steel

The specific equations to formulate these effects have not been developed while the

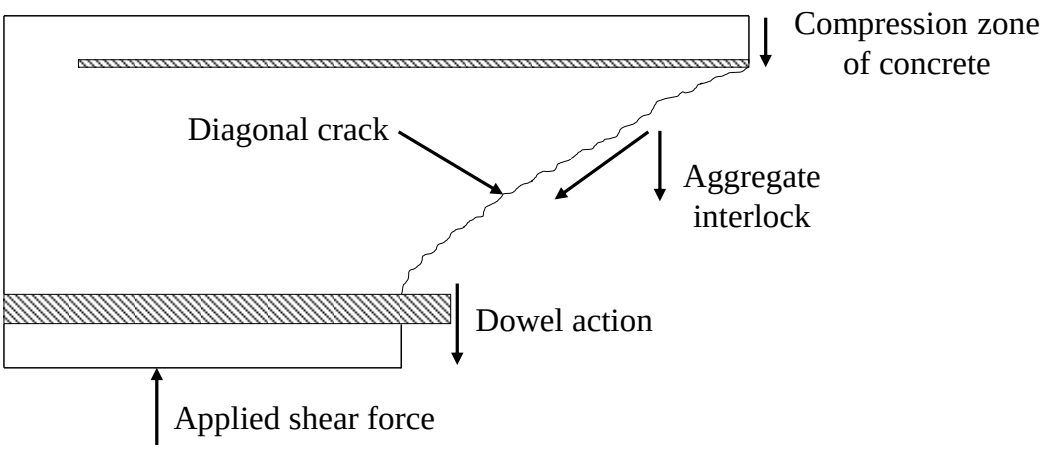

Figure 4.2.2 Internal forces to resist applied shear force.

empirical equation summing all effects has been developed. From numerous experimental data on the shear strength of RC beams without stirrups, the empirical equation was proposed by Okamura and Higai (Okamura and Higai, 1980). Based on this equation, the modification has been made to incorporate the size effect directly in 1986. This modification was proposed by Niwa and Okamura and the revised equation has been adopted into JSCE Shear Design Specifications.

The calculated shear force taken by the concrete and the stirrups is explicated by Eqs. (4.2.2) and (4.2.3), respectively:

$$V_c = 0.20\sqrt[3]{f_c'} \cdot \sqrt[4]{1/d} \cdot \sqrt[3]{100\,p_w} \cdot b_w \cdot d \tag{4.2.2}$$

$$V_s = A_w \cdot f_{wy} \cdot \left(\sin\alpha_s + \cos\alpha_s\right) \cdot z/s_s \tag{4.2.3}$$

where, V_c is the shear force carried by concrete (N); f'_c is compressive strength of concrete (N/mm^2); d is effective depth (m); p_w is longitudinal reinforcement ratio; b_w is the web thickness (mm); V_s is the shear force carried by stirrups (N); A_w is the total cross sectional area of the stirrups placed at spacing s_s; f_{wy} is the yield stress of stirrups; α_s is the angle of shear reinforcements to the member axis, which was taken as 90 degree in this study; s_s is the spacing of stirrups; and z is the distance from the location of compressive stress resultant to centroid of tensile steel, taken here as d/1.15.

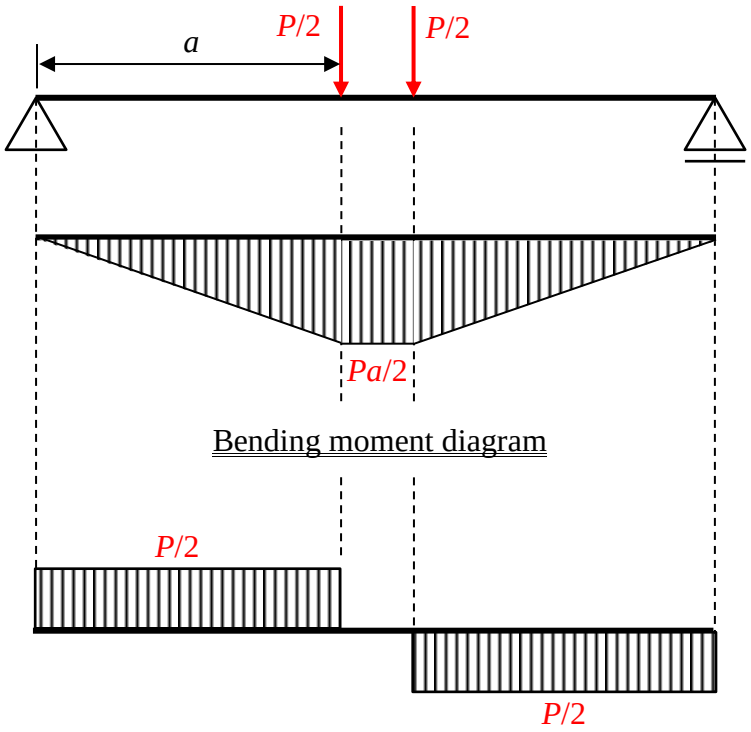

Figure 4.2.7 Bending moment and shear force distribution.

For RC control beam RC-Ref with target compressive strength of 30 MPa, the calculated shear force carried by concrete (V_c) and stirrups (V_s) are 45.9 kN and 44.5 kN, respectively. According to Eq.(4.2.1), the calculated shear capacity is 90.4 kN and therefore according to the four-point loading test as shown in **Figure 4.2.7**, the applied load at the calculated shear capacity was 180.8 kN.

The flexural capacity of RC control beam was also calculated following *JSCE Standard Specifications for Concrete Structures-2007 [Design]* (2010). The uniaxial stress-strain relationship of concrete and steel is specified by following equations:

$$\sigma_c^{'} = k_1 f_c^{'} \left[2\left(\frac{\varepsilon_c^{'}}{0.002} \right) - \left(\frac{\varepsilon_c^{'}}{0.002} \right)^2 \right] \quad \left(0 \le \varepsilon_c^{'} \le 0.002 \right) \tag{4.2.4}$$

$$\sigma_c^{'} = k_1 f_c^{'} \qquad \left(0.002 \le \varepsilon_c^{'} \le \varepsilon_{cu}^{'} \right) \tag{4.2.5}$$

$$\sigma_s = E_s \varepsilon_s \qquad \left(\varepsilon_s \le \varepsilon_y\right) \tag{4.2.6}$$

$$\sigma_s = f_y \qquad \left(\varepsilon_y < \varepsilon_s\right) \tag{4.2.7}$$

$$\sigma'_{sc} = E_s \varepsilon'_{sc} \qquad \left(\varepsilon'_{sc} \le \varepsilon'_y\right) \tag{4.2.8}$$

$$\sigma'_{sc} = f'_y \qquad \left(\varepsilon'_y < \varepsilon'_{sc}\right) \tag{4.2.9}$$

where, σ'_c is the compressive stress of the concrete; ε'_c is the compressive strain of concrete; k_1 is the reduction coefficient for compressive strength of concrete which is stipulated to be 0.85 in JSCE specifications; ε'_{cu} is the ultimate compressive strain of concrete which is stipulated to be 0.035 for normal strength concrete; f'_c is the compressive strength of concrete; σ_s is the tensile stress of the longitudinal steel; ε_s is the tensile strain of the longitudinal steel; E_s is the elastic modulus of the longitudinal steel; f_y and f'_y is the yield strength of longitudinal steel in tension and compression, respectively; σ'_{sc} is the compressive stress of longitudinal steel in compression; ε'_{sc} is the compressive strain of longitudinal steel in compression. The idealized stress-strain curve adopted in calculation is shown in **Figure 4.2.8**.

The stress-strain curve of concrete in flexural compression zone uses equivalent stress block as shown in **Figure 4.2.9** rather than the parabolic curve specified in **Figure**

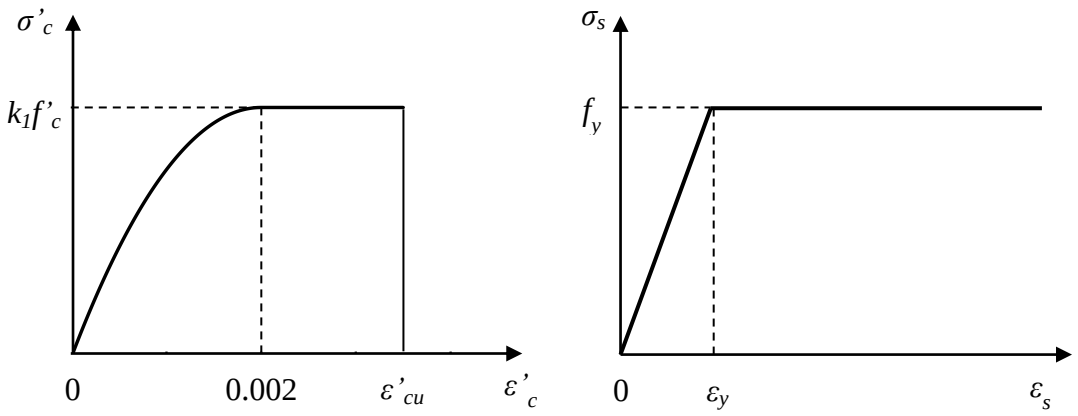

(a) Concrete. (b) Steel.

Figure 4.2.8 Stress-strain relationships for concrete and steel.

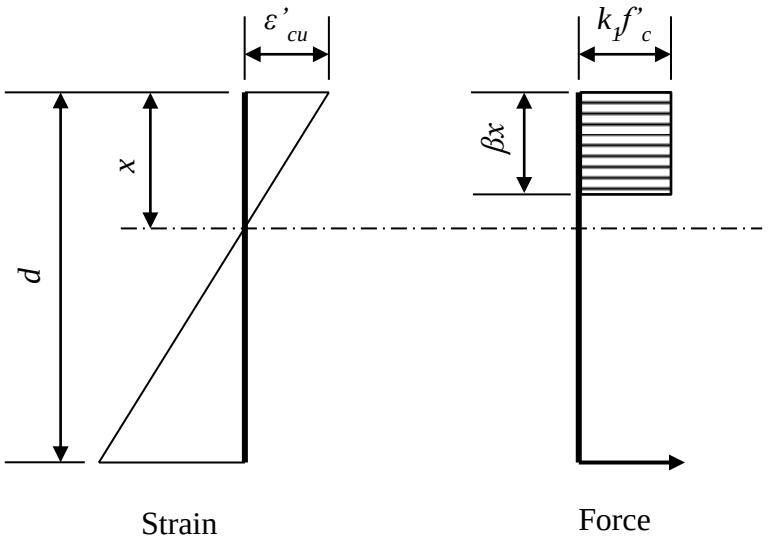

Figure 4.2.9 Equivalent stress block.

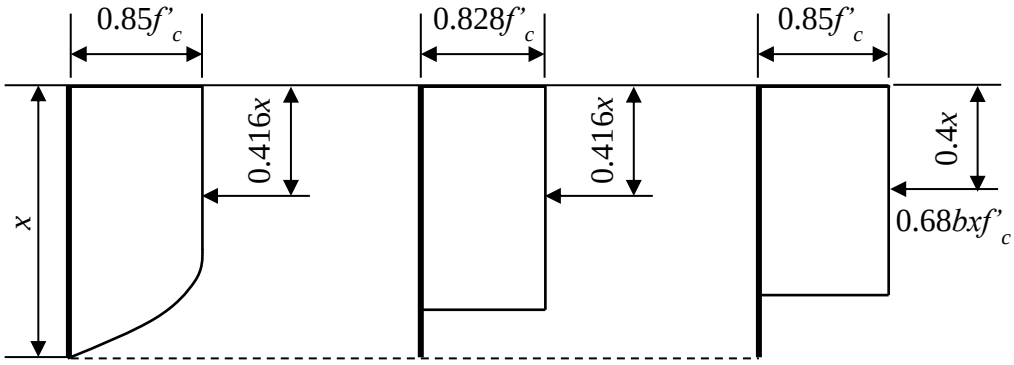

Figure 4.2.10 Equivalent stress block for flexural compression zone.

4.2.10 since the same resultant compressive force and its location can produce almost the same ultimate moment. The flexural capacity of RC control was calculated according earlier described and its value is 85.9 kN·m. According to the four-point loading tests as shown in **Figure 4.2.7**, the peak load at the flexural capacity can be derived by following equation:

$$P = \frac{2 \cdot M_u}{a} \tag{4.2.9}$$

where, P is the peak load at the flexural capacity; M_u is the ultimate flexural capacity of

the RC control beam; *a* is the shear span which is 0.7 m in this study. Hence, the applied load at the flexural capacity was 242.6 kN while the applied load at the calculated shear capacity is 180.8 kN, which indicates that the RC-Ref would be failed in shear prior to flexural failure.

The specimen corresponding to RC-Ref using PP-ECC, namely RE-42, having the same stirrup ratio as the RC control beam RC-Ref, was also prepared for comparisons. The dimension and rebar details of these two beams are shown in **Figure 4.2.1**. To evaluate the shear behavior without stirrups, another normal concrete beam specimen RC-00 without shear reinforcements was designed to compare the shear capacity with the specimen RE-00 with identical reinforcement arrangement but using matrix of PP-ECC. The dimension and reinforcement arrangement are shown in **Figure 4.2.5**. For the remaining three PP-ECC beam specimens, the stirrup ratios varied from 0.30% to 0.12%. All stirrups were uniformly arranged within the shear spans. The dimensions and configurations along with reinforcement arrangements of these three PP-ECC beams are shown through **Figures 4.2.2** to **4.2.4**.

4.2.2 Material properties

A regular deformed steel rebar with nominal diameter of 25.4 mm and yield strength of 400 N/mm^2 was used for longitudinal rebars in the tension side for all specimens while a round steel bar with diameter of 6 mm and yield strength of 277 N/mm^2 was used for longitudinal rebars in the compression side. All specimens used deformed bars with nominal diameter of 6.35 mm and yield strength of 323 N/mm^2 as the stirrups. The type and properties of all steel bars used in these seven beam specimens are summarized in **Table 4.2.2**.

The PP-ECC material used in this research is as described in **Chapter 3**. The mixture proportion of PP-ECC used in this study is shown in **Table 3.2.1**. After casting fresh PP-ECC, it was poured into the formwork by moving the pouring position continuously along the direction of the beam axis.

For normal concrete beams, concrete with a target compressive strength of 30 N/mm^2 was used. Mixture components include 20 mm maximum size coarse aggregate, fine aggregate and high-early strength cement. **Table 4.2.3** gives the mix proportion of normal concrete.

4.2.3 Specimen construction

The target nominal compressive strength f'_c of the PP-ECC is 30 MPa. The PP-ECC, with mixture proportion earlier shown in **Table 3.2.1** (**Chapter 3**), was used in the beam tests As mentioned in **Chapter 3**, the volume of PP fibers in PP-ECC was based on the study by Hirata *et al.* (2009) where by using fiber volume of 3%, the tensile strength and strain was improved compared to a composite without fibers.

Before the casting, the steel reinforcement cages were fabricated and attached with strain gauges as indicated through **Figures 4.2.1** to **4.2.5**. Then the steel reinforcement cages were set in the formwork as designed before casting PP-ECC. The mixing process of PP-ECC followed the exactly sequence as earlier described in **Section 3.2.2** (Chapter 3). Immediately after the accomplishment of mixing, the flowable PP-ECC was poured into the prepared formwork. In order to orient the fiber direction along the longitudinal direction of the beam specimen, the pouring position was continuously moving along the direction of beam axis as shown in **Figure 4.2.11**.

Table 4.2.2 Properties of steel rebars.

Steel rebars	Nominal diameter (mm)	f_y (N/mm^2)	f_y (N/mm^2)	ε_y	ε_u
Rebar intension	25.4	400	577	0.002000	0.22
Stirrups	6.35	323	499	0.001615	0.17
Rebar in compression	6	277	434	0.001385	0.33

f_y: the yield strength; f_u: the ultimate strength; ε_y: the yield strain; ε_u: the ultimate strain.

Table 4.2.3 Mix proportion of concrete.

G_{max} (mm)	W/C (%)	Unit weight (kg/m^3)				
		W	C	S	G	Superplasticizer
20	60	177	294	830	970	2.94

G_{max}: the maximum size of coarse aggregate; W: water; C: cement; S: fine aggregate; G: coarse aggregate.

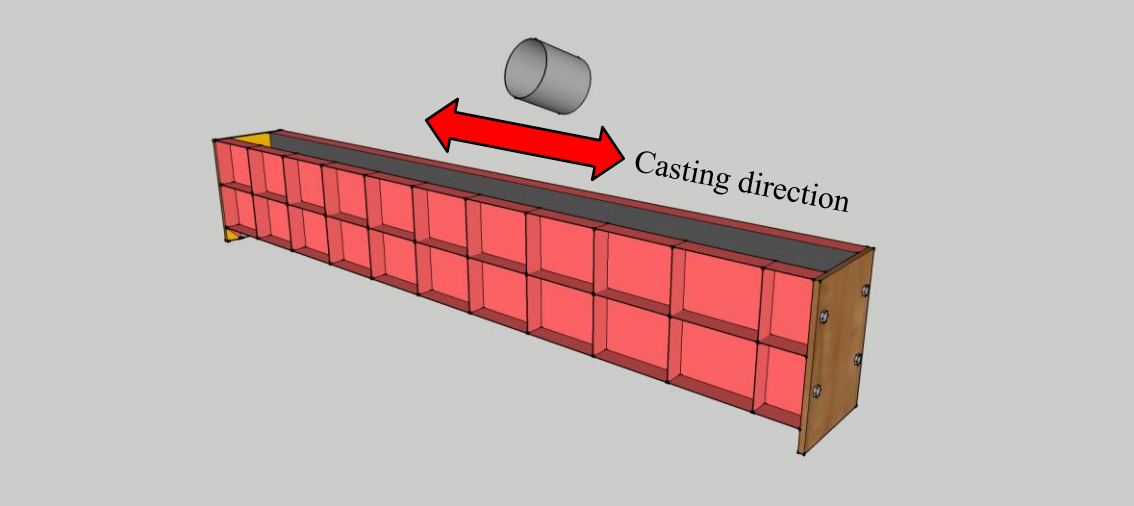

Figure 4.2.11 Casting the PP-ECC into the formworks.

All beam specimens including RC and PP-ECC were demolded 24 hours after casting. The clothes soaked by water were used to cover the beam specimens and provide moist-curing environment. Outside of the beam and clothes, the plastic sheets were used to wrap them to prevent the prevent evaporation. All PP-ECC beam specimens were tested after the moist-curing for 28 days while two RC beams specimens were tested after moist-curing for 7 days since the usage of high-early strength cement.

4.3 Experimental Program and Instrumentation

4.3.1 Experiment setup

The experimental setup for all specimens is shown in **Figure 4.3.1**(a). The beam was subjected to a four-point loading test and the distance between two loading points was 200 mm. In order to reduce the horizontal friction between supports and beam specimen, two layers of the Teflon sheets coated by lubricating oil were placed between the supports and beam specimen. The share span was 700 mm and the effective depth was 250 mm. The shear span-effective depth ratio *a/d* for all beam specimens was 2.8. As shown in **Figure 4.3.1**(b), two LVDTs were set vertically under the midspan to capture the data of the deflection in the midspan, and another two LVDTs were set vertically at the supporting positions to monitor the vertical displacement at the supporting positions. The precast grid with unit square size of 50 mm × 50 mm was drawn on the side surface of both shear spans to investigate the crack behavior which would be described in the

following sections. Two digital cameras were set at the side of the beam where the precast grid was drawn to take the pictures of the crack pattern at load levels with interval of 10 kN load. Before the loading tests, all instrumentation devices were connected to a data-logger to record the experimental data. A monotonic load was applied at the loading beam as shown in **Figure 4.3.1**(b) up to the failure of the specimen.

4.3.2 Loading protocol

The monotonic load was applied as the location indicated by **Figure 4.3.1**(b) monotonically. It should be noted that all PP-CC beam specimens were loaded to some extent after the post peak rather than termination after the peak load. For RC-beam,

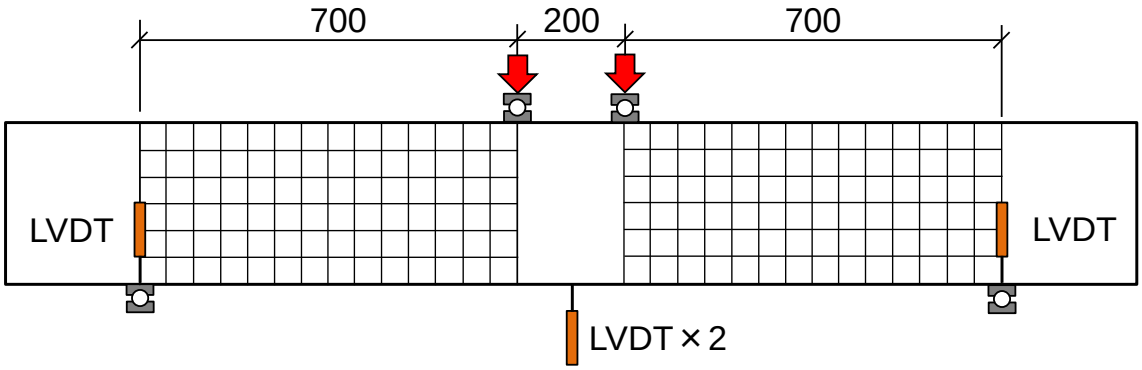

(a) Plan.

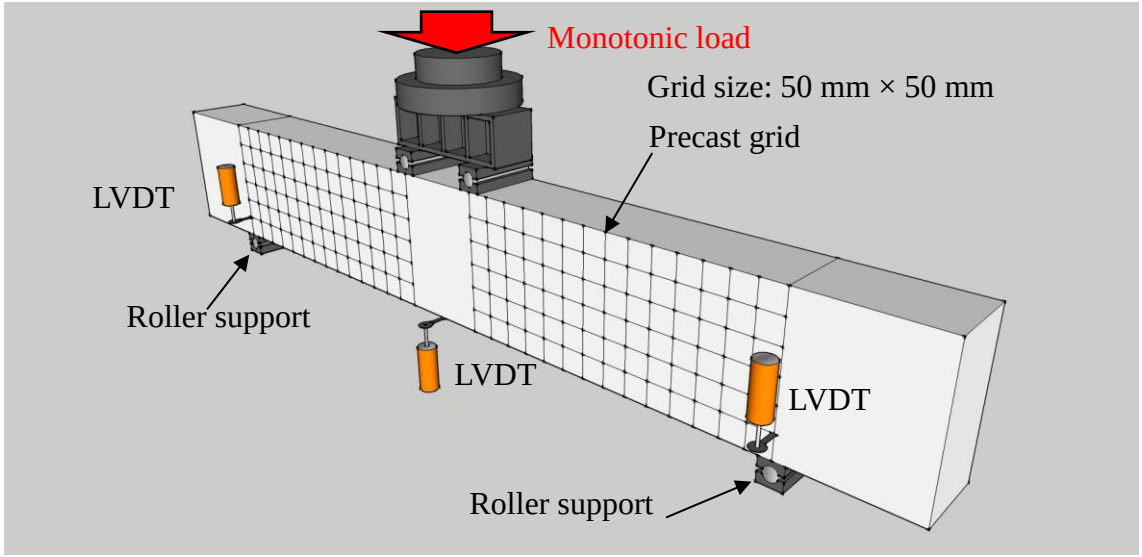

(b) Setup.

Figure 4.3.1 Experimental setup of beam tests.

especially the specimen of RC-00 which contains no stirrups in the shear span, the load was terminated after the sudden drop in carried load by beam.

4.3.3 Instrumentation

The load data (P) carried by beam specimen was output by the load cell embedded in the loading facility in electrical voltage and recorded by the data-logger. Two LVDTs under the midspan point were set at both side of beam specimen to record the midspan deflection (Δd_1 and Δd_2). Two LVDTs were set vertically at the supporting positions to monitor the vertical displacement at the supporting positions (Δd_3 and Δd_4). Therefore, the midspan deflection can be derived by

$$\Delta d = (\Delta d_1 + \Delta d_2)/2 + \Delta d_3 + \Delta d_4 \tag{4.3.1}$$

where, Δd is the midspan deflection; Δd_1 and Δd_2 are the midspan displacements recorded by two LVADs in the middle of the beam; Δd_3 and Δd_4 are the displacement at the supporting point.

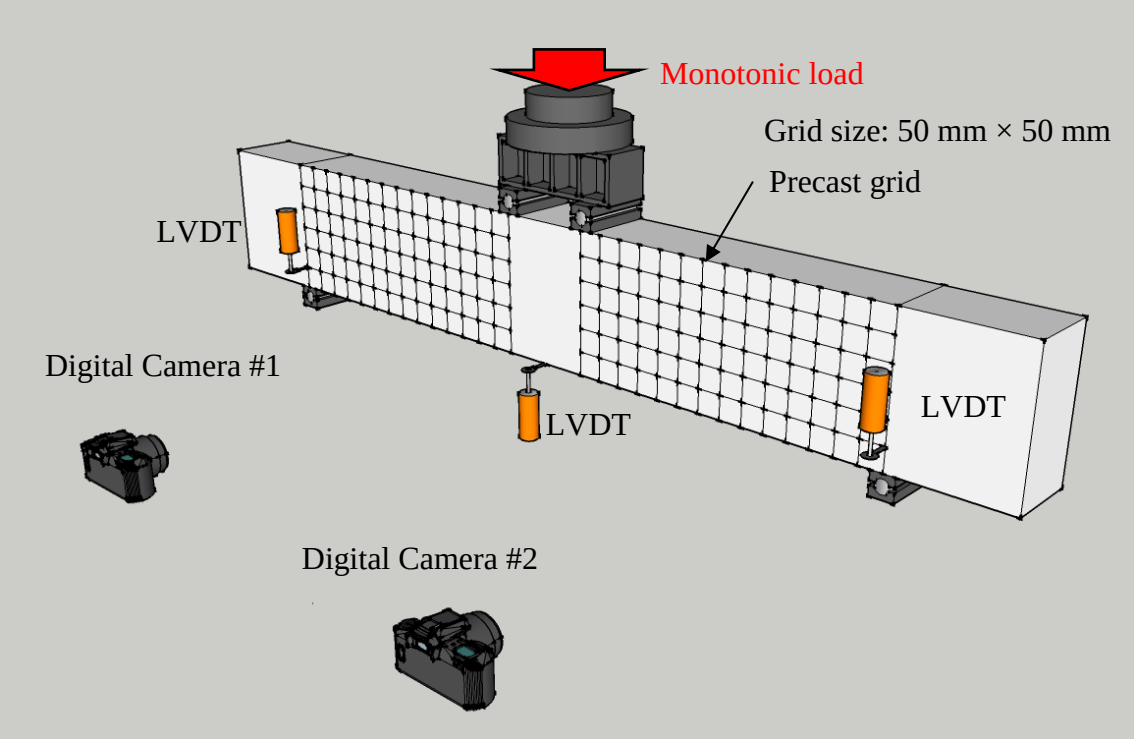

Figure 4.3.2 Image recording during loading tests.

The electrical strain gauges were attached to the longitudinal rebars at the midspan and the stirrups where a diagonal crack was expected to occur indicated by the red dashed line as shown through **Figure 4.2.1** to **4.2.5**.

In addition, to further investigate the behaviors of critical crack surfaces in PP-ECC beams, as shown in **Figure 4.3.2**, the grid with unit square size of 50mm×50mm was marked on the side surface of the beam specimens prior to the loading tests. Two digital images were utilized to take the digital images of development of crack pattern per 10 kN from the start of loading tests up to the unloading. After the loading tests, the digital images at the different load levels were imported into computer for further investigation on crack behavior.

4.4 Experimental Results and Discussions

4.4.1 Load-deflection behaviors and failure modes

The load versus midspan deflection curves for all beams are shown in **Figures 4.4.1**. The midspan deflection was the calculated value as described in Eq. 4.3.1.

As shown in **Figure 4.4.1**(a), all beams had a load drop immediate after the peak load, which indicates the shear failure occurred in all beam specimens. In addition, even with lower elastic modulus in PP-ECC compared to normal concrete as described in **Section 3.3.3**, **Figure 4.4.1**(a) reveals that PP-ECC beam has equivalent or even higher stiffness compared to RC beams. This phenomenon can be explained as mentioned by Li (2007), in structural elements loaded beyond the first crack, it is reasonable to expect equal or even higher structural stiffness in R/ECC elements compared to RC elements, despite the lower elastic modulus of ECC as compared to concrete. This is due to the capability of ECC to continue to carry load with reinforcements, long after the first crack appears. This concept was verified in an analytic study of cracked reinforced beams by Szerszen *et al.* (2006).

The experimental results of all specimens including material tests are summarized in **Table 4.4.1**. **Photo 4.4.1** shows the failed span of all beams after the loading tests. The

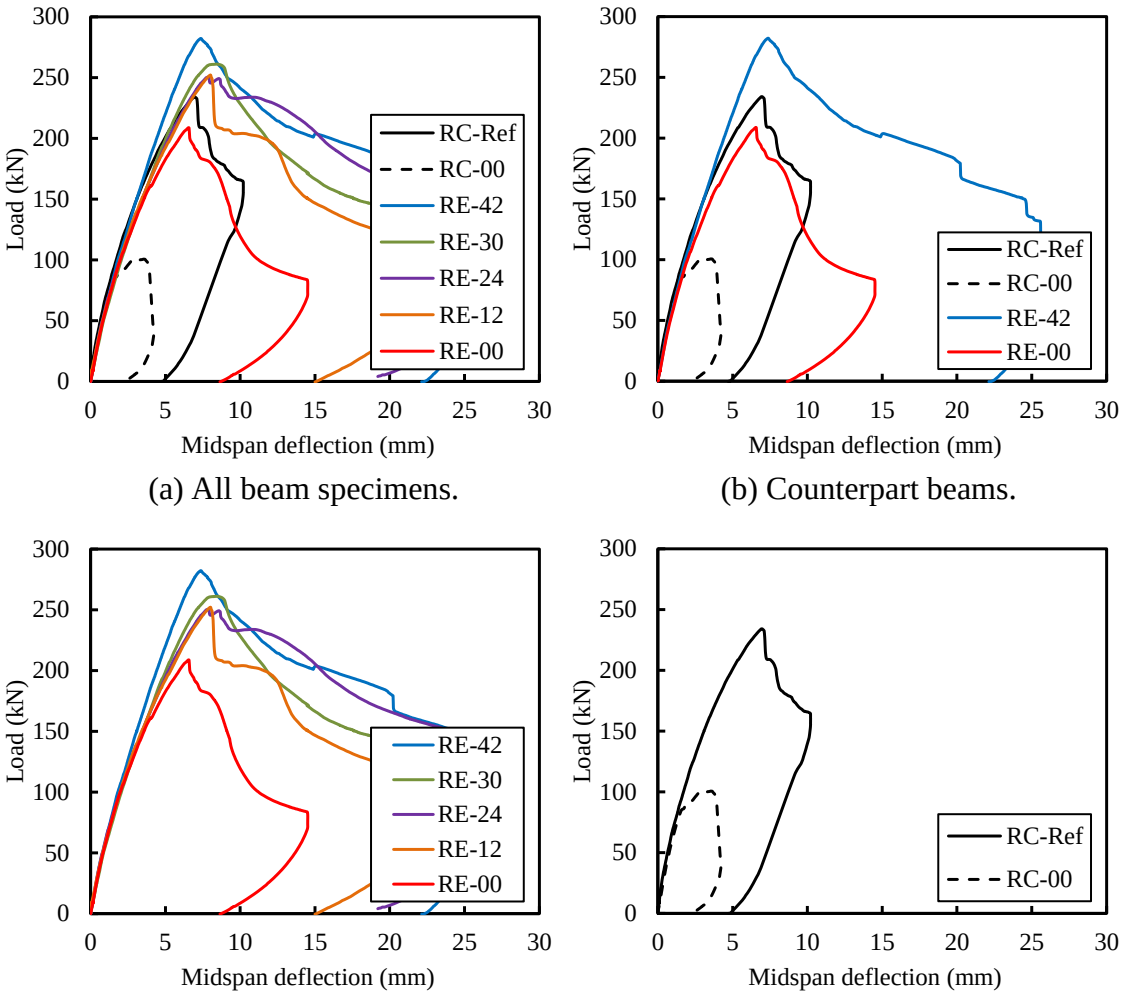

Figure 4.4.1 Load vs. deflection curves for all beam specimens.

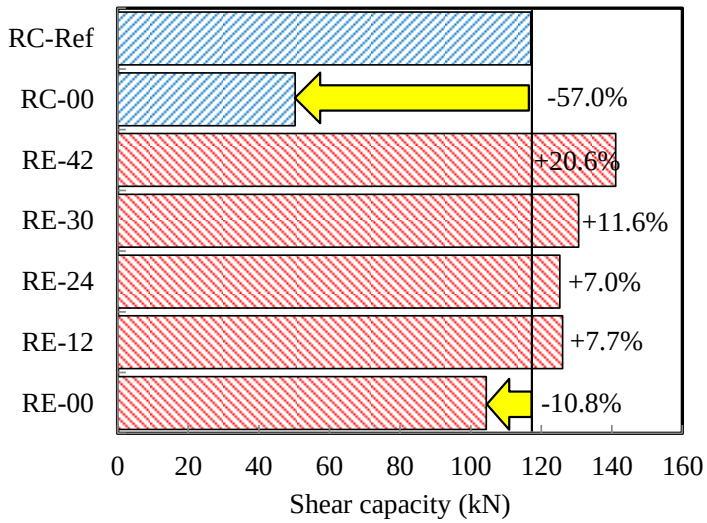

Figure 4.4.2 Comparisons of shear capacities.

steel tension rebars for six specimens with stirrups reached yielding strength at their peak loads but soon decreased with the increase in load as well as development of localization of a critical crack, also indicating the shear failure in all specimens. According to shear force diagram as shown in **Figure 4.4.2**, the shear capacities of all beams were calculated and compared by taking the shear capacity of RC control beam (RC-Ref) as standard. It shows that three PP-ECC beams (RE-30, RE-24 and RE-12) even with less stirrup ratios still show larger shear capacities than that of RC-Ref.

The shear capacities of two pairs of counterpart beams, namely RC-Ref and RE-42, RC-00 and RE-00, were compared in **Figure 4.4.1(b)**. As for RC-Ref, the first crack appeared in the constant moment region at a load of 54 kN, then inclined shear cracks were induced and propagated with increasing load. The ultimate load capacity of RC-Ref was 234.1 kN. After the peak load, the beam finally gave in as the concrete crushed and spalled in the compression zone of the shear span near the loading point. Beam RE-42 had the same reinforcement layout to that of RC-Ref, except a different matrix; however, the ultimate load capacity was 20.6% higher than that of RC-Ref, which was 282.2 kN. The first crack load of RE-42 was 86 kN, which was 32 kN greater than that of RC-Ref. Beyond the cracking load, the flexural stiffness decreased slightly but continued to be almost constant up to the failure. Several inclined cracks developed in the shear span, forming as extension of flexural cracks. These shear cracks bent following the compressive stress trajectory with the increase in load. Because of the lower shear span-depth ratio *a/d* (2.8 for all specimens), the beam flexural capacity

Table 4.4.1 Summary of beam tests.

Beam	V_{exp} (kN)	Midspan deflection (mm)	Compression strength (N/mm^2)	Tensile strength (N/mm^2)	Tensile yield strength (N/mm^2)
RC-Ref	117.03	8.72	29.1	2.53*	–
RC-00	50.27	4.42	34.9	2.88*	–
RE-42	141.09	9.23	30.4	3.67	2.51
RE-30	130.56	10.55	33.1	3.56	2.30
RE-24	125.24	9.87	31.5	3.39	2.38
RE-12	126.05	10.02	35.6	3.68	2.45
RE-00	104.38	8.19	32.8	3.71	2.50

* Tensile strength was obtained by split compression method. The rest were tested by direct tensile tests as described in **Chapter 3**. V_{exp} is the experimental shear capacities of beams.

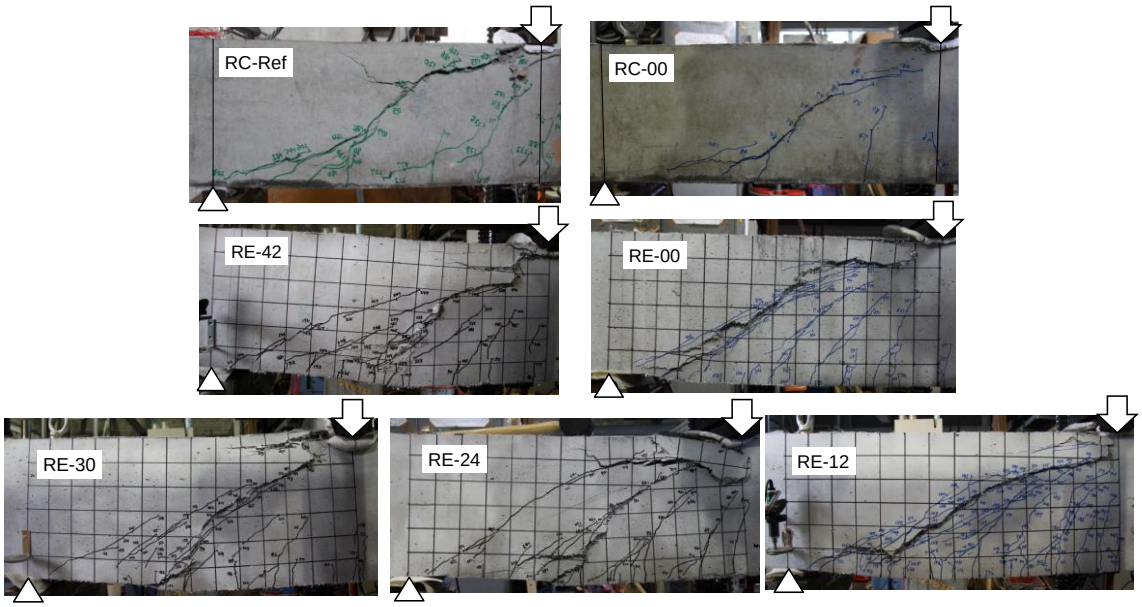

Photo 4.4.1 Crack pattern in failed span after loading tests.

cannot be fully developed, and then the shear capacity dominates the ultimate load-carrying capacity.

RC-00 and RE-00 was another pair of counterpart beams without stirrups. RE-00 exhibited load-displacement behavior similar to that of RC-00 before the diagonal cracking. Compared with commonly known brittle mode of shear failure such as what occurred in RC-00, the shear failure of RE-00 was much gentle and slow. This is due to the bridging effect resulting from the PP fibers. At the beginning, vertical flexural cracks first appeared at the tensile side of the beam. When the principal tensile stress within a shear span exceeded the cracking strength of ECC, a diagonal crack propagated through the beam web. Instead of several wide cracks appearing, numerous fine cracks developed in the ECC beams and they spread throughout the shear span. The shear capacity of RE-00 was significantly increased by the bridging force carried by the fibers. The peak load of RE-00 was 208.76 kN, compared to that of RC-Ref wherein the load and deflection capacity only decreased by 10.8% and 6%, respectively. Moreover, the load and deflection capacity of RE-00 increased by 107.6% and 85.2%, respectively, compared to RC-00.

The load vs. deflection curves for five PP-ECC beams were plotted as shown in **Figure 4.4.1(c)**. With various stirrup ratios from the level of control beam and zero, the peak loads of PP-ECC beams were decreasing as the decrease in stirrup ratios. The stiffness

of these PP-ECC beams was found to be proportional to the stirrup ratios, indicating that the stirrup ratio has positive effect on increasing the stiffness.

The load vs. deflection curves for two RC beams were plotted as shown in **Figure 4.4.1(d)**. The peak load of RC-00 decreased 57% from the level of RC-Ref since the absence of the stirrups, while the peak load of RE-00 just decreased 26% from RE-42. It shows that stirrup ratio plays more important role in enhancing the shear capacities in RC beams than in PP-ECC beams.

The failure mode for all specimens was shear tension failure in spite of the localized crushing of concrete or PP-ECC adjacent to the loading points. This is because even in four-point loading tests of RC beams with $a/d > 2.5$, the concrete was always observed to have crushed near the loading points. Sometimes, it is difficult to judge shear tension or compression failure only by the crushing of concrete at the compression zone. Once stirrups crossed by the critical diagonal crack yielded, the stress along the critical crack will be redistributed to these factors, such as the intact portion in the compression zone and fiber bridging effect, which may result in the crushing of the intact portion of the compression zone near the loading points. In the RE-series of this study, all the peak loads occurred after the yielding of stirrups. Therefore, all RE specimens were considered to have developed shear tension failure.

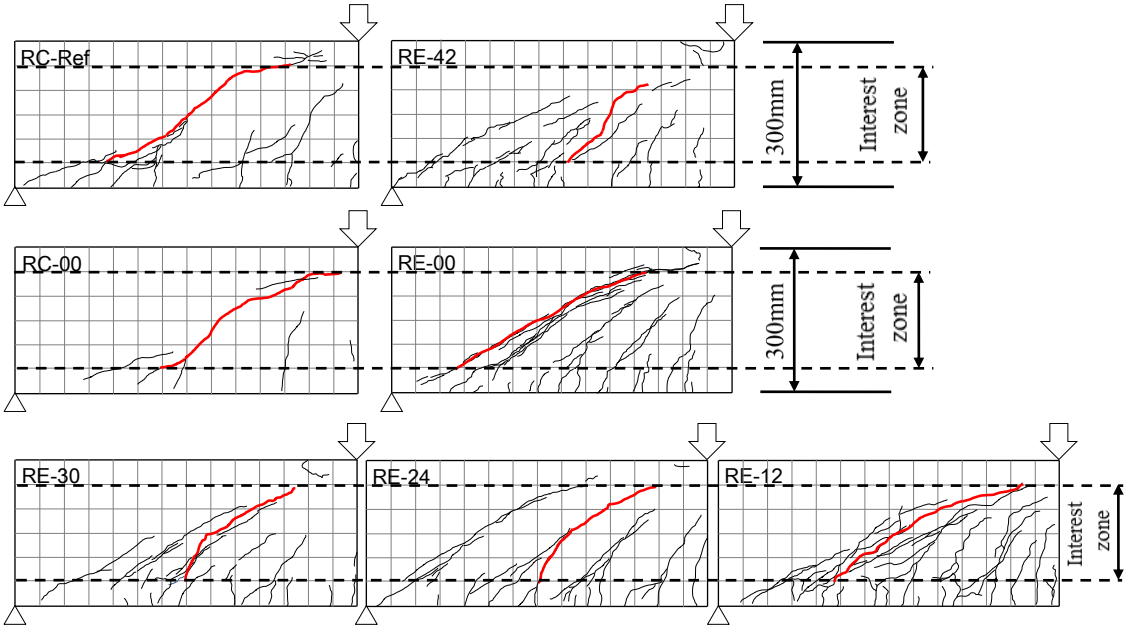

Figure 4.4.3 Crack pattern in failed span at the peak load.

4.4.2 Cracking behavior during loading tests

Figure 4.4.3 shows visible cracks of all specimens at the peak load as well as the critical crack that developed after the peak load in the interest zone as shown in red bold lines. The interest zone for investigation was the zone between the longitudinal tension and compression bars with height from 50 to 250 mm. The portion above the interest zone adjacent to the loading plates was considered as the dominant compression zone where the localized concrete crushed. In addition, since the tip of the diagonal tension crack stopped propagating at the level of the longitudinal tension rebars, therefore the level of tension rebars was considered as the lower boundary of the interest zone.

For the RC beams, only one diagonal crack formed at the peak load. Since four to six predominantly inclined cracks developed at the web of the beam before the load capacity in each PP-ECC beam, the main diagonal crack was difficult to identify. After

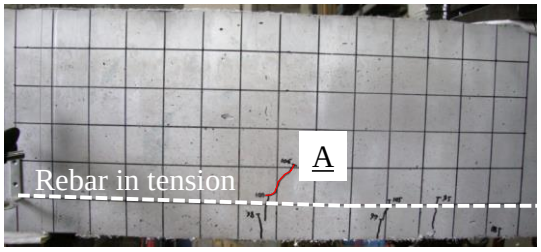

(a) At the load of 110 kN.

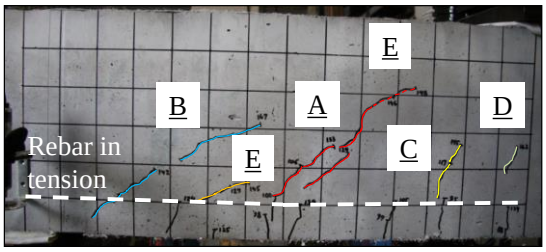

(b) At the load of 170 kN.

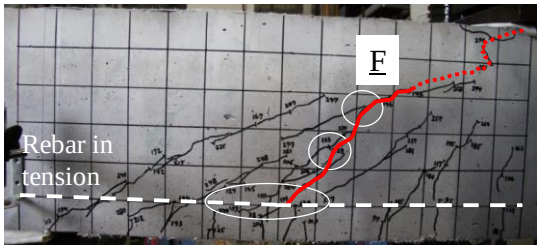

(c) At the peak load.

Figure 4.4.4 Development of visible cracks in RE-42.

the peak load, as the loading further progressed, these inclined cracks propagated to both supporting and loading plates and the main diagonal crack became more and more distinguishable among these inclined cracks. All five PP-ECC beams exhibited cracking behavior in a similar way. **Figure 4.4.4** shows the development of cracking in beam RE-42 in the loading test. Initially, a number of flexural cracks became visible at the edge of beam that was subjected to tension. At the load level of 106 kN, the first inclined crack A (A in **Figure 4.4.4(a)**) appeared. As the loading went up to 170 kN, three more inclined cracks (B, C and D in **Figure 4.4.4 (b)**) had been formed. The inclined cracks that appeared initially had angles ranging from 40° to 50° to the member axis. As the loading progressed, the tip of these cracks began to propagate to the supporting and loading plates (E in **Figure 4.4.4 (b)**) and some inclined cracks merged with the other existing ones (white dashed-line circles in **Figure 4.4.4 (c)**). The peak load of the beam was reached before the full development of cracking propagation. Immediately after the peak load, an inclined crack, as shown in red-dashed, bold line in **Figure 4.4.4 (c)**, propagated into the uncracked compression zone up to the loading plates. Meanwhile, the critical crack began to be localized and propagated to the loading plate earlier than it could come near the supporting plate. Upon investigating the area where the critical crack crossed the tension rebars, a number of cracks due to the dowel force developed parallel to the tension rebars and propagated to merge with the inclined cracks (F area in **Figure 4.4.4 (c)**).

According to the above-mentioned cracking behavior of RC and PP-ECC beams, the failure mechanism of these two types of beams was considered as follows:

For the RC beams, during the propagation of the critical crack, the opening at the critical crack tip simultaneously induced the sliding along the crack surfaces between the crack tip, which in turn developed a significant degree of shear resistance because of the aggregate interlock and rough planes of crack surfaces. The shear resisting factors incorporated stirrups, aggregate interlock along the crack surfaces, dowel action of longitudinal tension rebars and uncracked compression zone. When the critical crack propagated, the maximum shear carrying capacity of RC beam was achieved.

For PP-ECC beams, due to the absence of coarse aggregate, the aggregate interlock effect in PP-ECC beams was significantly weakened. Nevertheless, the fiber bridging contributed substantially to shear transfer resistance. Thus, the shear resisting factors of PP-ECC beams with stirrups during the propagation of shear cracks incorporated

stirrups, weakened interlock along the crack surfaces, fiber bridging, dowel action of longitudinal tension rebars and uncracked compression zone. The maximum shear capacity of PP-ECC beams was achieved when the critical crack propagated into the uncracked zone, which led to a sliding failure through the compressive strut.

4.4.3 Investigation on behavior of the critical crack

In all five PP-ECC beams, three types of crack paths in the critical crack were observed. Therefore, the critical crack was divided into three regions, namely, Regions 1, 2 and 3. For beam RE-42 and RE-12, three regions were divided as shown in **Figure 4.4.5**. In Region 1, the inclination of the crack surface was comparatively flat. The crack surface in this region was smoother than that in Region 3. Compared to Region 2, there are fewer ruptured PP fibers extending out of the crack surface, as shown in **Figure 4.4.6**(a). Some remaining fibers extended out of crack surface oriented to the direction of relative displacement of two surfaces that occurred as shown in **Figure 4.4.6**(a). In Region 2, the angle of crack to the beam axis was about 45°. Compared with Region 1, fibers out of the crack surface increased and they tended to be perpendicular to the crack surface, as shown in **Figure 4.4.6**(b). In Region 3, the critical crack formed at the level of

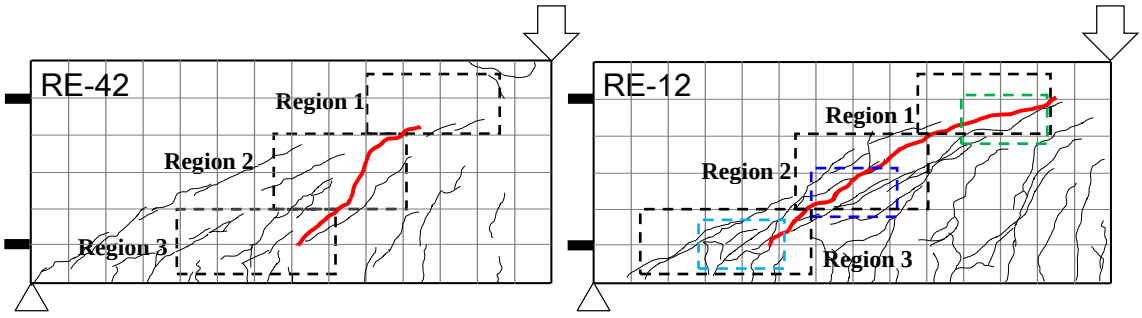

Figure 4.4.5 Regions divided for the critical crack.

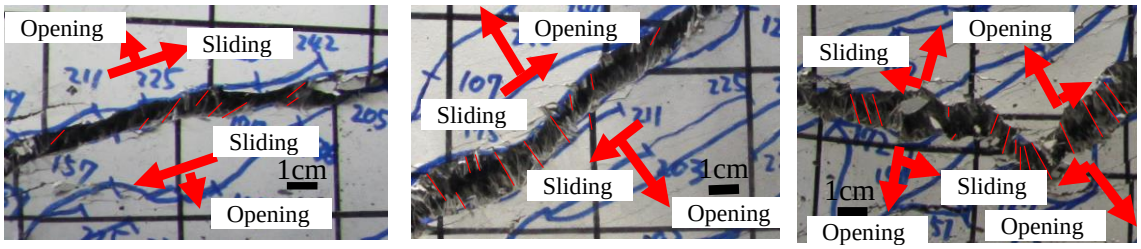

(a) Region 1. (b) Region 2. (c) Region 3.

Figure 4.4.6 Critical crack behavior of RE-12 at 90 kN in the post peak stage.

tension rebar, and the surface of crack was jagged and a number of fine cracks occurred close to the critical crack. The quantity of visible fibers in this region was the highest among these three regions. Most fibers were oriented perpendicular to the crack surface, as shown in **Figure 4.4.6**(c). Since the tension rebars crossed the critical crack, the jagged crack was considered to have formed because of the dowel action of the longitudinal bars, which tended to peel off the cover of the ECC.

It was postulated that the damage induced by the ruptured PP fibers resulting from the sliding on the critical crack surfaces for each PP-ECC beam at the peak load was different. Therefore, more significant sliding on the critical crack surfaces could be observed at the post-peak stage in the PP-ECC beam due to more ruptured fibers at the peak load. Therefore, to further investigate the damage induced by the sliding of the critical crack surfaces in the post-peak stage, the grid with unit square size of 50mm×50mm was marked on the side surface of the beam specimens prior to the loading tests. Those points where the critical crack intersected with the grid lines parallel to the beam axis at different beam heights were selected as sample points for investigating the cracking behavior. Specifically, the digital images, which were taken by the digital cameras per 10 kN from the start of loading tests up to the unloading, were implemented to locate these sample points for further investigation of the opening and sliding. At the load level for investigation, the corresponding images taken at that load level were enlarged to evaluate these sample points manually. However, it should be noted that, because the inevitable error during this process affected significantly by the accuracy of values of opening and sliding when the displacement of critical crack was insignificant, only the images showing the significant displacement of the critical crack in the post peak stage were utilized to investigate the opening and sliding in this study.

The horizontal (Δx) and vertical displacements (Δy) as shown in **Figure 4.4.7** were measured first according to the desired load level. Then the resultant displacement (ΔL) of a sample point and its angle (α) to the horizontal axis can be calculated by Eq. (4.4.1) and Eq. (4.4.2), respectively.

$$\Delta L = \sqrt{\Delta x^2 + \Delta y^2} \tag{4.4.1}$$

$$\alpha = \arctan \frac{\Delta y}{\Delta x} \tag{4.4.2}$$

The resultant displacement consists of two dis-placements resulting from the crack opening (δ_{op}) perpendicular to the critical crack surfaces and crack sliding (δ_{sl}) parallel to the critical crack surfaces. According to **Figure 4.4.7**, the opening and sliding of the critical crack could be calculated by Eq. (4.4.3) and Eq. (4.4.4), respectively.

$$\delta_{op} = \Delta L \cdot \sin\theta \tag{4.4.3}$$

$$\delta_{sl} = \Delta L \cdot \cos\theta \tag{4.4.4}$$

where δ_{op} and δ_{sl} are the opening and sliding of the critical crack, respectively; θ is the angle of resultant displacement to the crack surface and can be obtained by Eq. (4.4.5):

$$\theta = \alpha - \beta \tag{4.4.5}$$

where β is the average angle of the critical surface to the horizontal axis in one grid.

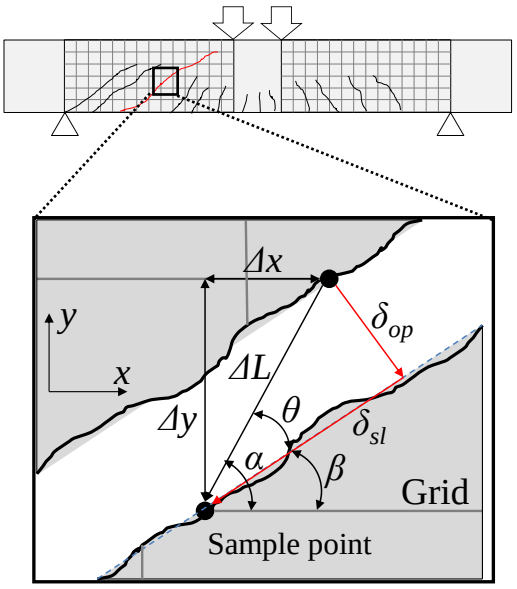

Figure 4.4.7 Displacement of a sample point.

The calculated opening and sliding of the critical cracks along the height of a beam in the interest zone for four PP-ECC beams (RE-42, RE-30, RE-24 and RE-00) at the load level of 160 and 130 kN in the post-peak stage are presented in **Figure 4.4.8**. By comparing the cracking behaviors at the load level of 160 and 130 kN in the post-peak stage, not only the values of the sliding in all specimens but also the opening at the beam height of 50 mm, where the longitudinal reinforcements were arranged, increased significantly as the loading progressed in the post-peak stage. However, the significant increase in the opening at the beam height of 50 mm resulted from the flat critical crack due to the dowel action of longitudinal reinforcements. From the load level of 160 kN to 130 kN in the post-peak stage, the increase in opening was slight while the increase in sliding was significant, which indicates the damage of sliding on the bridge effect is more significant.

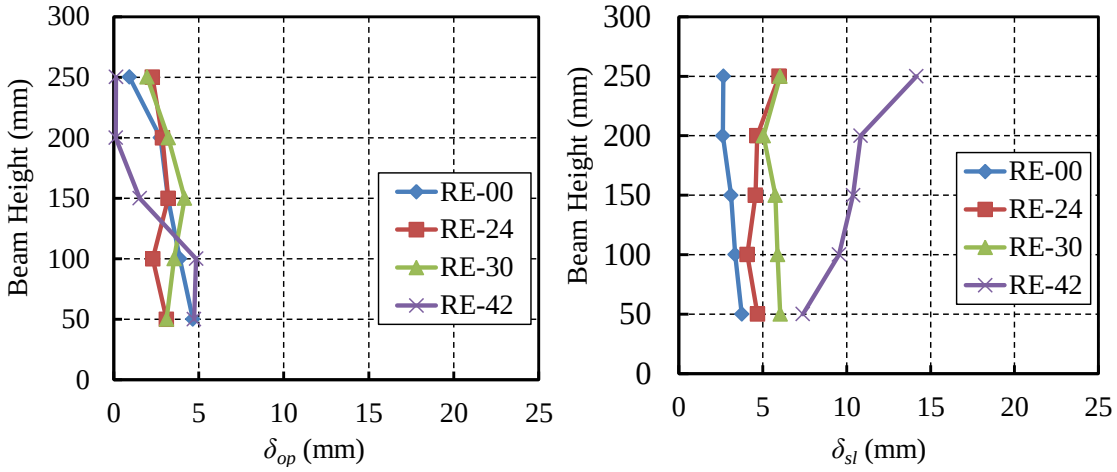

(a) Opening and sliding at the load of 160 kN.

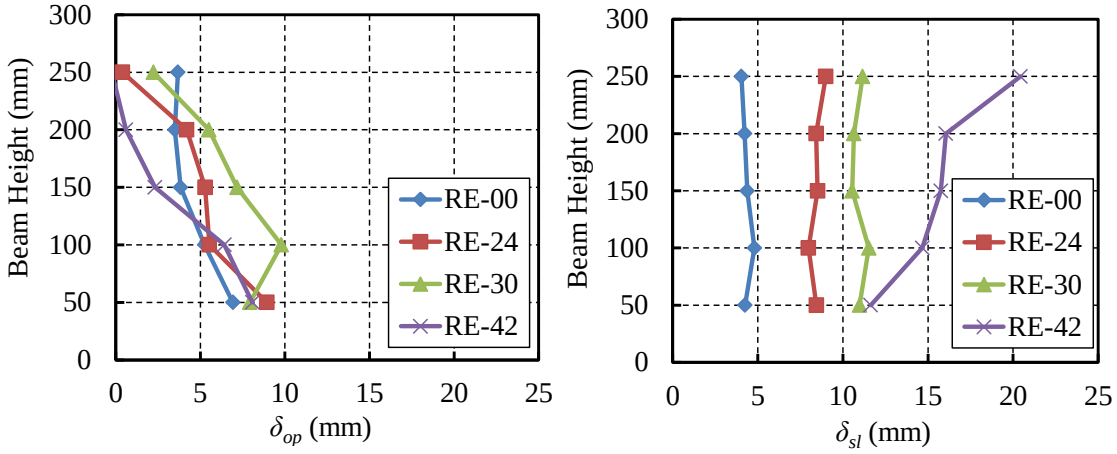

(b) Opening and sliding at the load of 130 kN.

Figure 4.4.8 Opening and sliding of the critical cracks in the post peak stage.

In addition, the significantly increased sliding in PP-ECC beams with varying stirrup ratios also indicates the different damage level in PP-ECC beams. As shown in **Figures 4.4.8**, the sliding on the critical crack surfaces in PP-ECC beams relates to stirrup ratio, and it becomes more significant when the stirrup ratio increases. Meanwhile, it indicates that the damage level in PP-ECC beams at the peak load with higher stirrup ratio is more significant.

4.4.4 Shear cracking angles of PP-ECC beams

As shown in **Figure 4.4.3**, the angles of the critical cracks in the interest zone at peak load for five PP-ECC beams were measured. Each angle was determined as the beam axis to the line that linked the points crossed by the critical cracks in the upper and lower boundary of the interest zone. The angles of critical cracks to the beam axis for five PP-ECC specimens are listed in **Table 4.4.2**. The relationship between the angle of critical crack and stirrup ratio, as shown in **Figure 4.4.9**, reveals that the critical cracks of PP-ECC beams with more stirrups become steeper, which implies that the

Table 4.4.2 Angle of the critical crack in the interest zone.

Beams	RE-42	RE-30	RE-24	RE-12	RE-00
Angle (°)	43.9	40.3	39.3	27.3	26.5

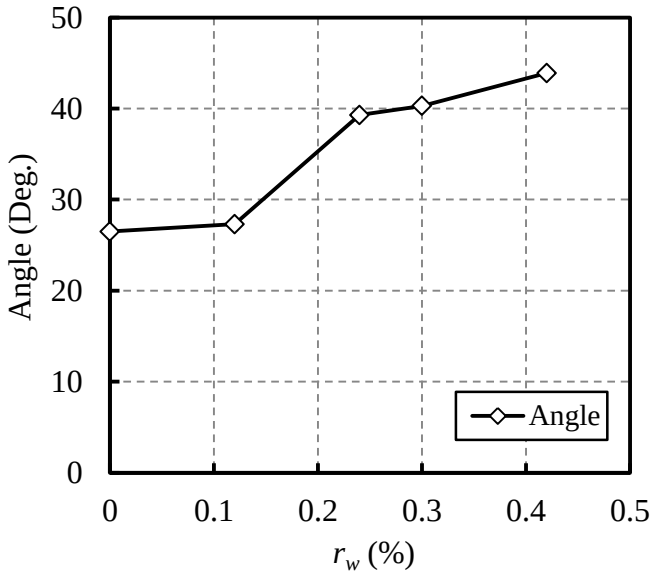

Figure 4.4.9 Angle of the critical cracks in PP-ECC beams.

development of critical cracks was suppressed in PP-ECC beams with increasing stirrup ratio r_w. The steeper critical cracks result in shorter diagonal crack length and thereby reduced the shear carried by PP fibers in ECC.

4.4.5 Effects of stirrup ratio

As confirmed by previous extensive experimental studies (Leonhardt, 1965), for RC beams with stirrups governed by shear failure, the shear capacity will increase significantly with the increase in stirrup ratio. It was assumed that the shear capacity of beams varies proportional to stirrup ratios. The regression analysis between shear capacities of PP-ECC beams and RC beams were performed and the results were indicated in the **Figure 4.4.10**. Steeper slope of regression line represents more effective shear reinforcing effect resulting from stirrups. The shear capacity of PP-ECC beams did not increase significantly as that of RC beams with the increase in stirrup ratio. It appears possibility that the shear capacity of RC beams with high stirrup ratio would exceed that of PP-ECC beams according to the trend shown in **Figure 4.4.10**. However, due to the lack of experimental data, this needs to be confirmed in a future study.

Although the shear capacity of RC beams is proportional to the stirrup ratio, it should be noted that the shear force carried by concrete can be assumed to be almost constant with varying stirrup ratio, which has been experimentally demonstrated and depicted in *JSCE Standard Specifications for Concrete Structures-2007 [Design]* (2010), was defined as

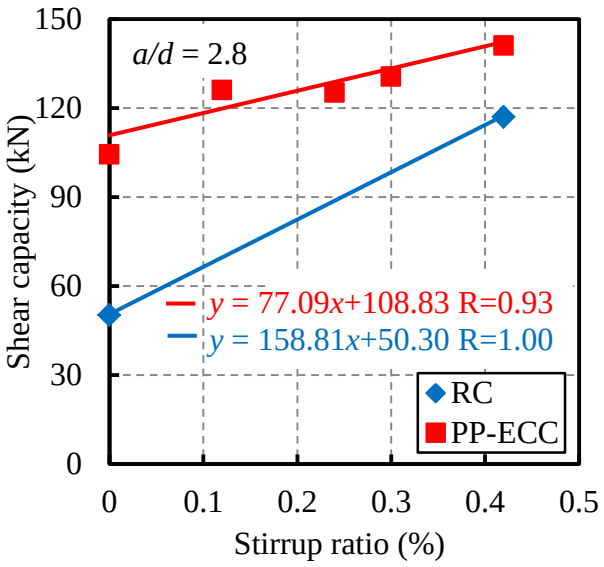

Figure 4.4.10 Shear capacities vs. stirrup ratios.

Eq. (4.2.2) in **Section 4.2.1**.

The experimental shear carried by stirrups (V_{s_exp}) can be obtained from the experimental data of strain in stirrups, which was recorded by data-logger during loading tests. Thus, the shear force carried by stirrups (V_{s_exp}) can be formulated by Eqs. (4.4.6) and (4.4.7).

$$V_s = \sum_{i=1}^{n_s} A_w \sigma_{si} \tag{4.4.6}$$

$$\sigma_{si} = \begin{cases} E_s \varepsilon_{si} \left(\varepsilon_{si} < \varepsilon_y \right) \\ f_{wy} \left(\varepsilon_{si} \geq \varepsilon_y \right) \end{cases} \tag{4.4.7}$$

where n_s is the number of stirrups crossing the critical crack, σ_{si} is the stress of stirrup crossing a critical crack at the peak load, Aw is cross sectional area of a pair of stirrups within s (mm^2), E_s is the elastic modulus of stirrup, ε_s is the stirrup strain recorded during the loading tests, and ε_y is the yielding strain of stirrups listed in **Table 4.2.3**. It should be noted that in all PP-ECC specimens with stirrups, according to experimental data recorded by the data-logger, the values of all strain gauges attached on stirrups in the shear span, which were crossed by the critical cracks, including the strain gauges which were not exactly crossed by the critical diagonal cracks, exceeded the yield strain at their peak load. Therefore, the prediction was not affected significantly by the exact location of the strain gauges. The total shear force carried by PP-ECC and RC beams can be formulated by Eqs. (4.4.8) and (4.4.9), respectively.

$$V_{exp} = V_{ECC\_exp} + V_{s\_exp} \tag{4.4.8}$$

$$V_{exp} = V_{c\_exp} + V_{s\_exp} \tag{4.4.9}$$

where V_{ECC_exp} is the experimental shear carried by ECC for PP-ECC beams, and V_{c_exp} is the experi-mental shear carried by concrete for RC beams. From Eqs. (4.4.6) to (4.4.9), V_{ECC_exp} and V_{c_exp} can be calculated by Eqs. (4.4.10) and (4.4.11), respectively.

$$V_{ECC\_exp} = V_{exp} - V_{s\_exp} \tag{4.4.10}$$

$$V_{c\_exp} = V_{exp} - V_{s\_exp} \tag{4.4.11}$$

The experimental value of shear taken by stirrups and matrix (ECC or concrete) is listed in **Table 4.4.3**. The experimental shear resisting components versus stirrup ratio (r_w) for RC and PP-ECC beams were plotted and are shown in **Figures 4.4.11**. For two RC beams, as shown in **Figures 4.4.11(a)**, the shear taken by concrete was almost constant even with varying stirrup ratios, while the shear taken by stirrups (V_{s_exp}) increased proportionally to the stirrup ratio. For five PP-ECC beams, as shown in **Figures 4.4.11(b)**, the tendency of shear carried by PP-ECC was decreasing with the increase in stirrup ratio while the shear force carried by stirrup increased with the increase in stirrup ratio. Since the increase in shear force carried by stirrups was more significant than the decrease in shear carried by PP-ECC, consequently the reinforcing effect of stirrups in PP-ECC beams is not as significant as that of RC beams.

Table 4.4.3 Shear resisting proportions in PP-ECC and RC beams.

Beam	V_{exp} (kN)	V_{ECC_exp} or V_{c_exp} (kN)	V_{s_exp} (kN)	V_{ECC_exp} or V_{c_exp} (%)	V_{s_exp} (%)
RC-Ref	117.0	45.1	71.9	39	61
RC-00	50.3	50.3	0.0	100	0
RE-42	141.1	59.3	81.8	42	58
RE-30	130.6	69.6	61.0	53	47
RE-24	125.2	84.3	40.9	67	33
RE-12	126.1	105.6	20.5	84	16
RE-00	104.4	104.4	0.0	100	0

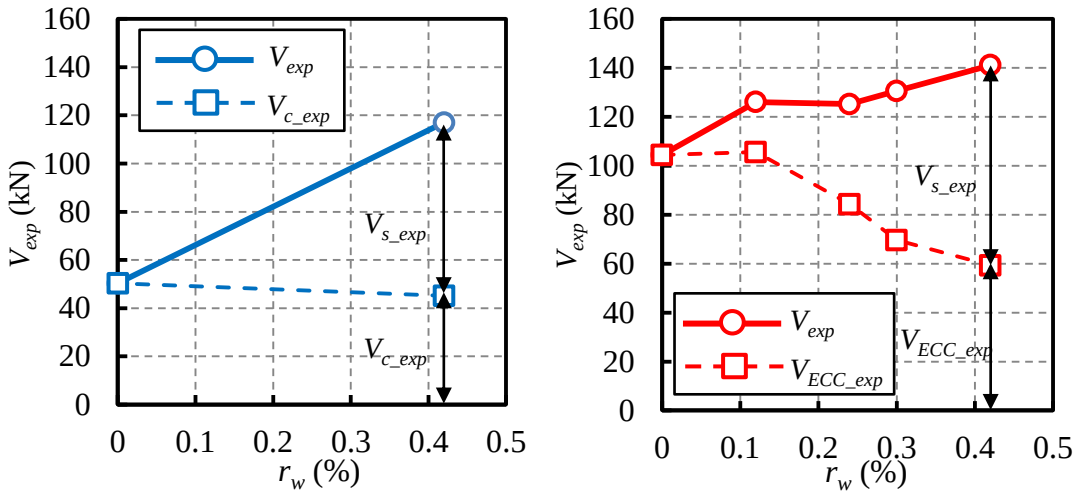

(a) RC beams. **(b)** PP-ECC beams.

Figure 4.4.11 Experimental shear resisting proportions in RC and PP-ECC beams.

In a previous study (Suryanto *et al.*, 2010), five PVA-ECC panels with reinforced steel bars in two orthogonal directions were tested under static pure shear, in which, two panels were isotropically reinforced and the rest of three one were anisotropically reinforced. An anisotropy index was induced to account for the difference in reinforcement amount quantitatively. For two isotropically reinforced panels, it was found that the contribution of the ECC to overall shear capacity decreases when the amount of reinforcement increases. As for three anistropically reinforced ECC panels, the contribution to overall shear capacity increases when the amount of the reinforcement in the two orthogonal directions is different.

The shear capacity of PP-ECC beams observed in this study also agrees with the shear prediction in Suryanto's study (2010). However, further comparison with Suryanto's study (2010) showed that the reduction in the shear capacity carried by PP-ECC with the increase in stirrup ratio in this study is more significant. This significant reduction may result from the more significant variation in the anisotropic level of reinforcements in R/ECC specimens in this study. As Suryanto *et al.* (2010) observed, the stress-carrying mechanisms of ECC rely more on the actions of compression and tension, while the increase in anisotropic level decreases compressive strength. According to this finding, more significant increase in stirrup ratio significantly decreases the compressive strength and therefore decreases the shear capacity carried by PP-ECC.

4.4.6 Comparisons between experimental results and design guidelines

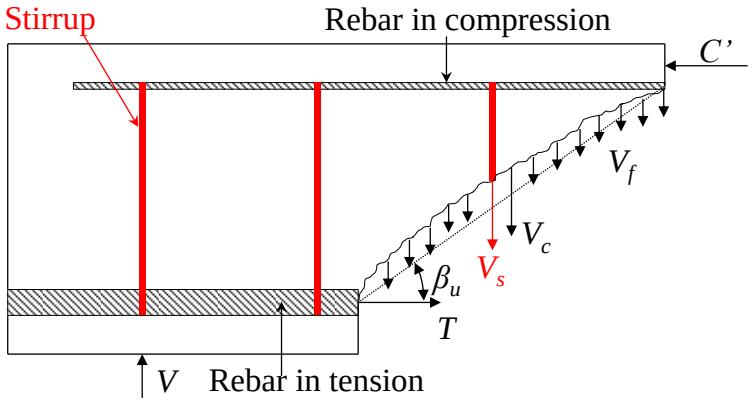

Figure 4.4.12 Free body diagram of PP-ECC beam.

So far, several researchers (Suryanto *et al.*, 2010; Kanakubo *et al.*, 2007) have attempted to develop models to evaluate the shear strength of PP-ECC structural members. The currently available simplified models are the truss-and-arch model based on *AIJ Design Guidelines for Earthquake Resistant Reinforced Concrete Buildings Based on Ultimate Strength Concept* (1990) and the modified truss model recommended by JSCE, which incorporated an equation accounting for the shear carried by fibers (V_f). Both models mentioned above incorporated the shear carried by fibers independently by employing an equation. In this study, the shear carried by PP-ECC structural members followed *JSCE Recommendations for Design and Construction of High Performance Fiber Reinforced Cement Composites with Multiple Fine Cracks (HPFRCC)* to evaluate the shear strength of R/ECC beams by summing up the shear-resisting factors, as shown in **Figure 4.4.12** and expressed by Eq. (4.4.12).

$$V = V_c + V_s + V_f \tag{4.4.12}$$

where *V* represents calculated total shear capacity of ECC structural member; and *Vc*, *Vs* and *Vf* represent shear carried by members without stirrups excluding the fiber effects, stirrups and fibers, respectively. *Vc* is similar to the equation that is defined in the JSCE code for RC structural members, but a reduction factor of 0.7 is incorporated because ECC allows cracks in service, which is expressed by Eq. (4.4.13).

$$V_c = 0.7 \times 0.2 \sqrt[2]{f'_{ECC}} \cdot \sqrt[4]{1/d} \cdot \sqrt[3]{100 p_w} \cdot b_w \cdot d \tag{4.4.13}$$

where V_c is the shear carried by members without stirrups excluding the fiber effects, f'_{ECC} is compressive strength of ECC (MPa), d is effective depth (m), p_w is longitudinal reinforcement ratio and b_w is the web thickness (mm). The experimental and calculation values of shear carried by fibers can be obtained by Eqs. (16) and (17).

$$V_{f\_exp} = V_{exp} - V_c - V_{s\_exp} \tag{4.4.14}$$

$$V_{f\_cal} = (f_{ty} / \tan \beta_u) \cdot b_w \cdot z \tag{4.4.15}$$

where f_{ty} is the yield tensile strength of ECC determined based on the stress-strain relationship immediately after the first cracking based on the testing method described in **Chapter 3** (MPa) and β_u is the angle of critical crack surface to the member axis,

taking the value listed in **Table 4.4.2**. Although tensile ductility is the main characteristic of ECC, it did not affect the shear capacity of PP-ECC beams. Based on the experimental observation, as described in **Chapter 3**, the ultimate tensile strain corresponding to the tensile strength was reached when a localized crack formed among multiple fine cracks. However, the critical crack of a PP-ECC beam could not be distinguished at the peak load even immediately after the peak load. It became a localized crack as the loading progressed in the post peak-stage. Therefore, it was supposed that the shear capacity was reached before the ultimate strain corresponding to the tensile strength.

Table 4.4.4 lists the experimental and calculation results of shear forces. The values of V_c, V_{s_exp}, V_{f_exp} and V_{f_cal} were calculated from Eqs. (4.4.12), (4.4.7), (4.4.13) and

Table 4.4.4 Experimental and calculated results of shear forces.

Beam	V_{exp} (kN)	V_c (kN)	V_{s_exp} (kN)	V_{f_exp} (kN)	V_{f_cal} (kN)	$v = \frac{V_{f\_exp}}{V_{f\_cal}}$
RE-42	141.1	32.3	81.8	27.0	85.1	0.32
RE-30	130.6	33.2	61.0	36.4	88.4	0.41
RE-24	125.2	32.7	40.9	51.6	95.0	0.54
RE-12	126.1	34.0	20.5	71.6	154.7	0.46
RE-00	104.4	33.1	0.0	71.3	163.3	0.44

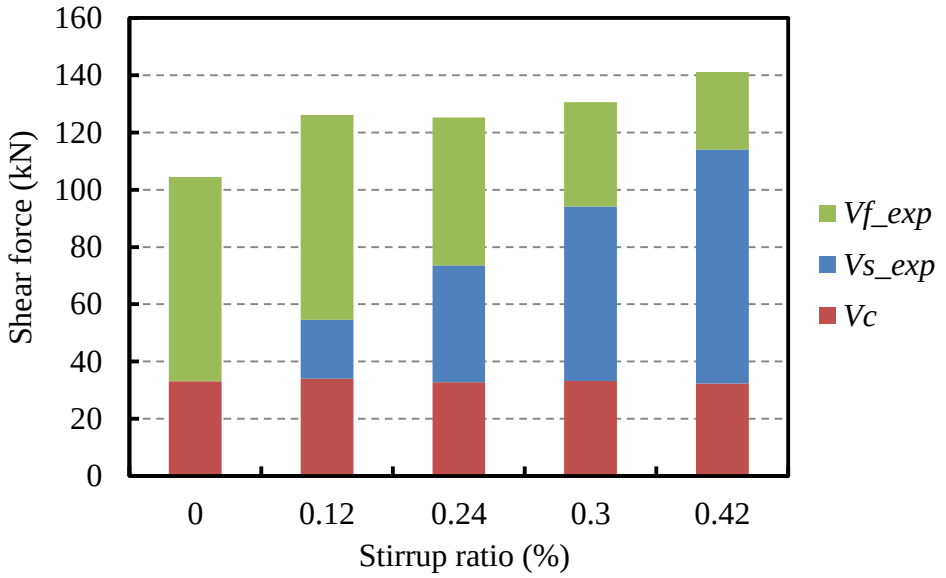

Figure 4.4.13 Shear forces in PP-ECC beams.

(4.4.14), respectively. As shown in **Figure 4.4.13**, unlike the calculated components of shear resistance in the JSCE for HPFRCC (2008), the experimental value of shear carried by fibers decreased with the increase in stirrup ratio in PP-ECC beams. This behavior is supposed to be the result of the shear-resisting component in the JSCE recommendation (2008) being a calculated rather than experimental value based on Eq. (17).

For the shear carried by fibers, a reduction factor, which was defined as the ratio of experimental value to calculation value as expressed by Eq. (4.4.16) and listed in **Table 4.4.4**, was used to account for the reduced shear due to sliding.

$$v = V_{f\_exp} / V_{f\_cal} \tag{4.4.16}$$

As shown in **Figure 4.4.14**, the value of a reduction factor ranges from 0.32 to 0.54 and it trends to decrease with the increase in stirrup ratio, which indicates that the shear carried by fibers in ECC beams with dense stirrups is smaller than that with less stirrups. However, the reduced shear carried by fibers due to the increase in stirrup ratio was not considered in the JSCE code. This is because Eq. (4.4.13) was derived from the predictive Eq. (4.2.2), which is a predictive equation for shear capacity of concrete. As earlier described in **Section 4.2.1**, Eq. (4.2.2) incorporated the interlocking action resulting from coarse aggregate. However, the difference be-tween shear-resisting

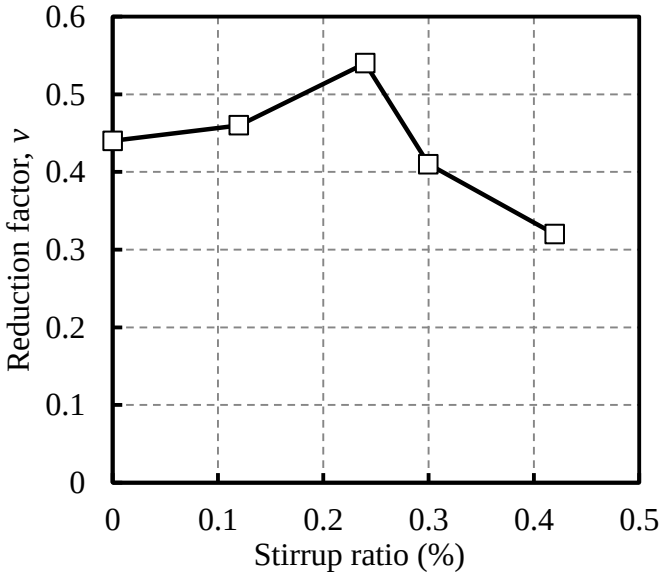

Figure 4.4.14 Reduction factor to V_{f_cal}.

mechanisms in RC and PP-ECC is that, the opening induced sliding along the crack surfaces which, in turn, developed a significant degree of shear resistance because of the aggregate interlock in RC beams, while the opening induced sliding, which resulted in damage to the fiber bridging effect and the decrease in shear capacity in a PP-ECC beam. Consequently, the shear capacity of a PP-ECC beam was reached prior to the full exertion of tensile behavior. To reproduce this phenomenon, as shown in **Figure 4.4.14**, a reduction factor to V_f is necessary to keep a safer prediction.

4.5 Summary

This chapter describes the shear behavior of PP-ECC beam specimens with various stirrup ratios by experimental investigation. A total of seven beams: two normal steel reinforced concrete and five steel reinforced PP-ECC beams, were tested under static monotonic loading condition. The following conclusions could be deduced:

1) Owing to the absence of coarse aggregates in PP-ECC, which affects its fiber bridging effect, the shear carrying capacity of the beam with stirrups and without stirrups increased 20.6% and 107.6%, respectively by replacing concrete with PP-ECC. The shear carrying capacity can be increased by replacing the matrix from concrete to PP-ECC, especially in the case of lower stirrup ratio.

2) The damage to the fiber bridging effect induced by sliding on the critical crack surfaces in PP-ECC beams with higher stirrup ratio at the peak load is more significant compared to those with lower shear reinforcement ratio. This is one of the factors for the decrease in the shear carried by ECC in PP-ECC with the increase in stirrup ratio.

3) The angle of critical crack to the beam axis in PP-ECC beam decreases with the increase in stirrup ratio, which simultaneously triggers a reduction in the shear carried by fibers along the critical crack. Again, this results in a decrease in the shear carried by PP-ECC with the increase in stirrup ratio.

4) Unlike in the shear resisting proportion in RC beams, in which the shear carried by concrete is almost constant even with varying stirrup ratios and the shear carried by stirrup is proportional to the stirrup ratio, the shear carried by ECC in PP-ECC beams decreases with the increase in stirrup ratio. This decrease in shear carried by

fibers results from the combined action of the reduction on shear carried by fibers along the critical crack and the increased damage to fiber bridging induced by sliding along the critical crack surfaces.

5) The current JSCE code does not consider that due to sliding, the shear carried by fibers in ECC decreases with the increase in stirrup ratio. This may result in an overestimation of the shear capacity of PP-ECC structural members.

References

Japan Society of Civil Engineers (JSCE): *Recommendations for Design and Construction of High Performance Fiber Reinforced Cement Composites with Multiple Fine Cracks (HPFRCC)*, Japan Society of Civil Engineers, 2008.

Japan Society of Civil Engineers (JSCE): *Standard Specifications for Concrete Structures-2007* [*Design*], 2010.

Kabele, P. and Kanakubo, T.: Experiential and Numerical Investigation of Shear Behavior of PVA-ECC in Structural Elements, *Proc. of 5th International RILEM Workshop on High Performance Fiber Reinforced Cement Composites* (HPFRCC5), Reinhardt and Naaman, eds., pp. 137-146, 2007.

Leonhardt, F.: Reducing the Shear Reinforcement in Reinforced Concrete Beams and Slabs, *Magazine of Concrete Research*, Vol. 17, No. 53, pp. 187-198, 1965.

Li, V. and Fischer, G.: Effect of Matrix Ductility on Deformation Behavior of Steel Reinforced ECC Flexural Members under Reversed Cyclic Loading Conditions, *ACI Structural Journal*, Vol. 99, No. 6, pp. 781-790, 2002.

Okamura, H. and Higai, T.: Proposed Design Equation for Shear Strength of Reinforced Concrete Beams without Web Reinforcement, *Proceedings of Japan Society of Civil Engineers*, No.300, pp.131-141, 1980.

Macgregor, J.G. and Wight, J.K.: Reinforced Concrete: Mechanics and Design, Sixth Edition, Pearson, 2011.

Niwa, J.: Evaluation of the Equation for Shear Strength of Reinforced Concrete Beams without Web Reinforcement, *Proceedings of Japan Society of Civil Engineers*, No.372/V-5, pp. 167-176, 1986.

Parra-Montesinos, J. G., Peterfreund, W. S. and Chao, S.: Highly Damage-Tolerant Beam-Column Joints Through Use of High-Performance Fiber-Reinforced Cement Composites, *ACI Structural Journal*, Vol. 102, No. 5, 2005.

RILEM: Strain Hardening Cement Composites: Structural Design and Performance, *State of the art report of RILEM technical committee 208-HFC*, SC3, 2012.

Suryanto, B., Nagai, K. and Maekawa, K. : Modeling and Analysis of Shear-critical ECC Members with Anisotropic Stress and Strain Fields, *Journal of Advanced Concrete Technology*, Vol. 8, No. 2, pp. 239-258, 2010.

Suryanto, B., Nagai, K. and Maekawa, K.: Bidirectional multiple cracking tests on High-Performance Fiber-Reinforced Cementitious Composite Plates, *ACI Materials Journal*, Vol. 107, No. 5, pp. 450-460, 2010.

Suryanto, B., Nagai, K. and Maekawa, K.: Smeared-crack Modeling of R/ECC Membranes Incorporating an Explicit Shear Transfer Model, *Journal of Advanced Concrete Technology*, Vol. 8, No. 3, pp. 315-326, 2010.

Szerszen, M., Szwed, A. and Li, V.: Flexural response of reinforced beam with high ductility concrete material, Proceeding of Brittle Matrix Composites 8, A.M. Brandt, V.C. Li and I.H. Marshall, eds., pp. 263-274. Woodhaed Publication, Warsaw, 2006.

Chapter 5

CYCLIC RESPONSE OF BEAM-COLUMN JOINTS WITH REDUCTION OF TRANSVERSE REINFORCEMENTS BY USING PP-ECC

5.1 Introduction

This chapter is going to the investigation of T-joints of rigid-framed railway bridges. With the objective of avoiding the over congestion at the T-joints, shear reinforcements in the joint, the beam and the column are reduced. The strength deficit caused by the reduction of shear reinforcements is maintained by the PP-ECC in the specimens. The feasibility of PP-ECC to maintain the performance ever after the reduction of shear reinforcements are examined through the investigation of crack pattern, load-displacement hysteretic loop, strain in rebar, moment-curvature hysteretic loop, energy dissipation capacity and stiffness degradation.

In rigid-framed railway bridges, intermediate beams tie the columns together. T-shaped beam-column joints are formed at the junction of a column and an intermediate beam. The intermediate beams are provided to enhance the stiffness and stability of bridges in particular the high bridges. In order to meet the design standard to withstand lateral load resulting from seismic events, extensive numbers of transverse reinforcements were provided in columns and intermediate beams are common in Railway Bridge.

Within the range of beam-column joint connections, being non-load bearing structural member, formation of plastic hinges is expected in the end of intermediate beams adjacent to the column face rather than in columns or joint zones. This is because, if the intermediate beam is stronger than column, the column will be damaged and dissipated major energy resulting from a large seismic event while the intermediate beam remained

contact, which probably leads to the whole collapse of the structure. In order to avoid such kind of failure, the principle of "strong column and weak beam" was adopted by many design specifications to ensure the intermediate beam fails firstly to dissipate sufficient energy resulting from a large seismic event prior to failure in the column.

In Japanese railway design standards (Railway Technical Research Institute, 2004), there are no clauses to deal with the shear strength of beam-column joints, clause 14.13.4 of the standards mentions that the beam-column joints should be reinforced such that the joints can exhibit the required loading capacity and ductility. For the other design specifications such as AIJ standards, ACI352-R02, ACI318-08, Eurocode-8 etc. (Architecture Institute of Japan, 1991; Joint ACI-ASCE Committee 352, 2002; ACI Committee 318, 2008; Commission of the European communities, 2004) have included the provisions to design beam-column joints mainly focus on the shear strength of the joint and development anchorage length of rebars. All these standards consider compressive strength of concrete and minimum numbers of transverse rebars in the joints as governing parameter of shear strength of the joints.

Irrespective of design codes, a large amount of steel rebars are required to be provided in the beam-column joint connection to prevent brittle shear failure. To ensure the capacities of the joints higher than the adjacent members such as beams and columns, the joint portions are enlarged and long-sufficient anchorage are provided in longitudinal rebars. For conventional reinforced concrete (RC) rigid-framed bridges, the considerable amount of steel reinforcements are provided in the beam-column joint and the plastic hinge in the beam end adjacent to the column face in beam-column joint connections to confine concrete to realize the formation of ductile inelastic behavior in the plastic hinge. The increased and elaborated reinforcement details bring the difficulties in fabricating this complicated steel reinforcement cage as well as placing and consolidating concrete in it during the construction phase. The contradiction between increased high cost for design and construction due to these complicated reinforcements with accordingly raised requirements on seismic performance becomes more and more apparent.

In previous studies, the T-joints exhibited poor structural performance failing in shear when the hooks in longitudinal beam rebar were bent out of the joint and little transverse rebars were provided in beam-column joint core and adjacent member (Hakuto *et al.*, 2000). However, on bending beam rebar hooks into the joints, the plastic

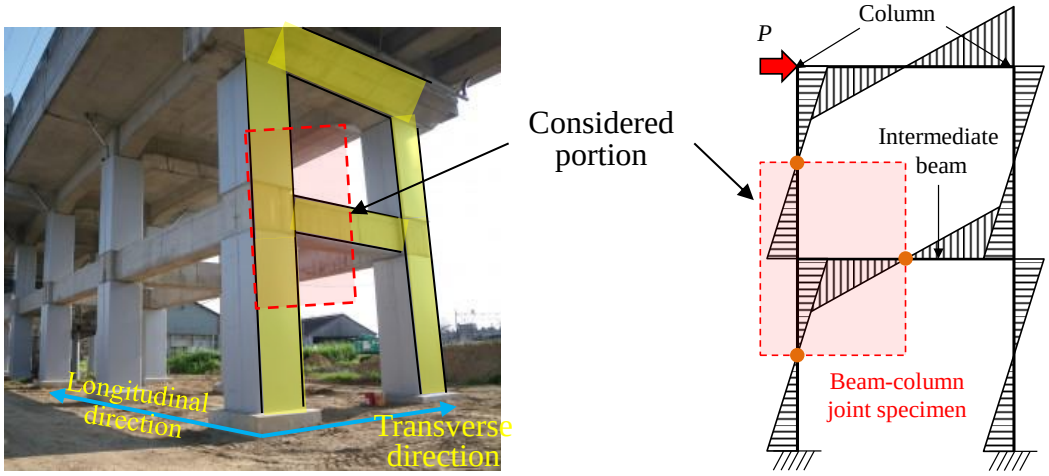

(a) Bridge elevation. (b) Moment diagram.

Figure 5.2.1 Selection of beam-column joint.

hinge was formed in the beams showing the satisfactory performance. As an effort to reduce congestions at the beam-column joints of buildings, numbers of closely spaced ties in the joints were decreased after using steel fibers (Filiatrault *et al.*, 1994). Moreover, Parra-Montesinos *et al.* (2005) totally eliminated the ties in the joint and increased stirrup spacing to half the effective beam depth in the plastic hinge region of the beam by using PE-ECC with volume fraction of 1.5% PE fibers. The experimental results showed excellent structural performance in terms of strength, deformation capacity and damage tolerance. The presented study shows that the congestion at the beam-column joints of rigid-framed bridges can be remarkably reduced after replacing the transverse reinforcements with PP-ECC.

5.2 Design and Construction of Beam-Column Joint Specimens

5.2.1 Specimen design

In the loading tests of beam-column joint specimens, an existing railway bridge designed following the Japanese code, "Design Standard for Railway Structures and Commentary (Concrete Structures)" (Railway Technical Research Institute, 2004), was considered as a prototype structure. Since this type of rigid-framed railway bridge is extended in longitudinal direction for several hundred meters. Its stiffness in longitudinal direction is far larger than that in transverse direction. Hence, in past earthquakes as described in **Chapter 1**, the damage to this kind of bridge was usually

vulnerable in transverse direction (**Figure 5.2.1**(a)) to earthquakes and therefore the frame structure in transverse direction was selected as the study target. Once an earthquake occurred, it was considered that an idealized seismic force would act at the location of the bridge horizontally in transverse direction as shown by red arrow in **Figure 5.2.1**(b). The structural response to this laterally applied force in whole elevation structure would have the bending moment diagram as shown in **Figure 5.2.1**(b). It was noted that two deflection points and one deflection point were formed in the column and intermediate beam, respectively, as indicated by the three dots in brown color. Therefore, The shape of a specimen (T-shape) and the boundary conditions of the test assembly were chosen corresponding to half the height of the column above and below the intermediate beam and half span of the intermediate beam of a rigid-framed bridge as enclosed by dashed box in **Figure 5.2.1**(b). The moment due to the lateral load in the considered portion of the portal frame and test specimen were similar.

Due to the constraints of the testing facility, the scale factor of experiment specimen was selected to be one-sixth. It is worth mentioning that the length of the beam in scaled specimen is longer than that in the exactly scaled one, which results in larger shear force in exactly scaled one than that in present study but still within the shear capacity of PP-ECC beam without stirrups. Moreover, the joint shear stress is almost constant due to the combination of bending moment transferred from the beam. Therefore, the increase of beam length in this study is acceptable. **Figure 5.5.2** shows a sketch of the test setup used in this study and overall specimen details. The height of column was considered as 1500 mm and length of beam from the column face to the end was considered as 900 mm. The column cross section was 250 mm × 250 mm, and the beam was 170 mm wide and 200 mm deep as shown in **Figure 5.2.2**(b). The thickness of cover concrete was 20 mm. The arrangement of longitudinal and transverse reinforcements in columns and beams are shown in **Figure5.2.2**. Totally three beam-column joint specimens were constructed with PP-ECC and concrete. **Figure 5.2.3** shows the layout and reinforcements arrangement in all specimens. In the specimen, TJ-1, which refers to the specimen based on the existing railway bridge designed following the Japanese standards, "*Design Standard for Railway Structures and Commentary (Concrete Structures)*" (Railway Technical Research Institute, 2004), the amount of steel reinforcements was provided according to the existing railway bridge. In the other two specimens, namely TJ-2 and TJ-3, amount of transverse reinforcements in beams and columns were reduced one after another while the amount of longitudinal reinforcements in beams and columns was kept unchanged. For the

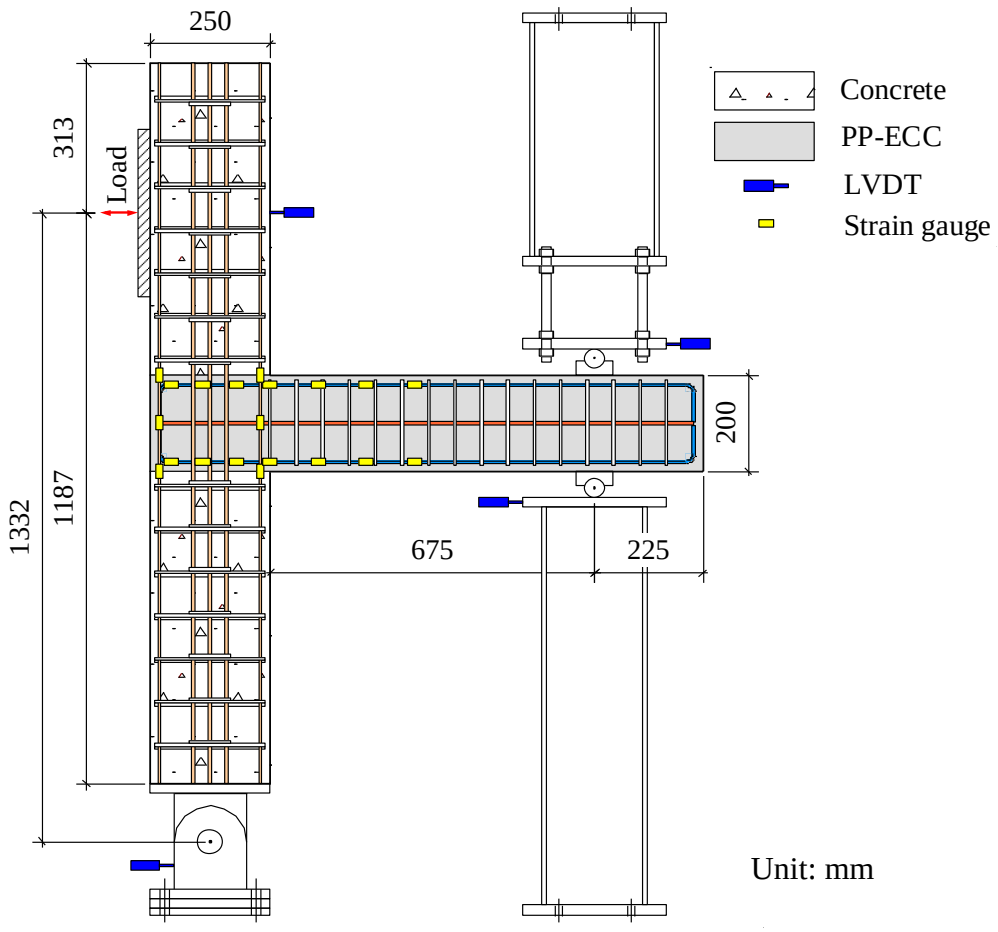

(a) Specimen dimensions.

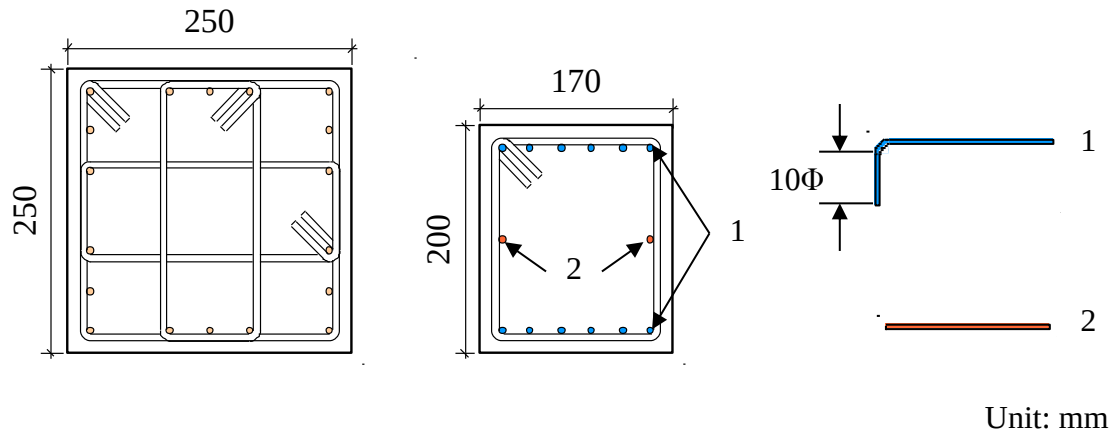

(b) Cross section of columns and beams.

Figure 5.2.2 Specimen details.

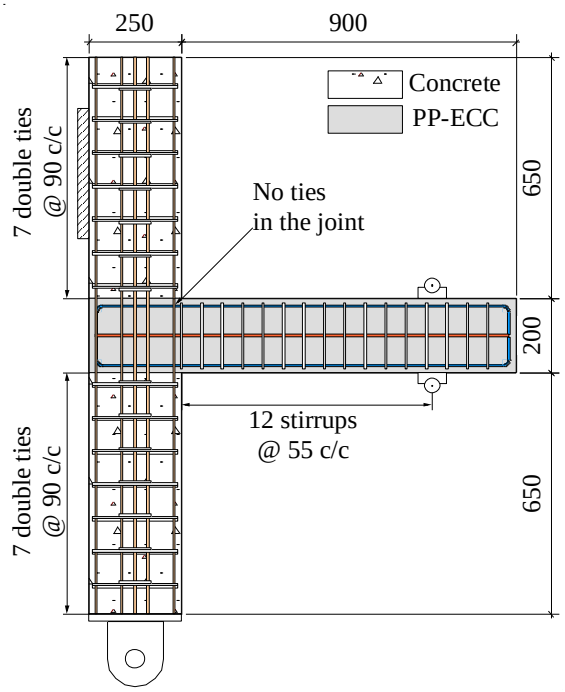

Unit: mm

(a) TJ-1.

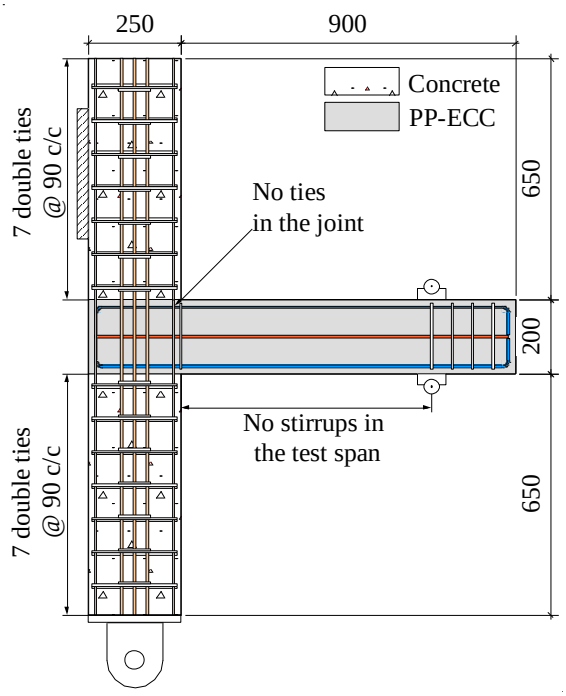

(b) TJ-2.

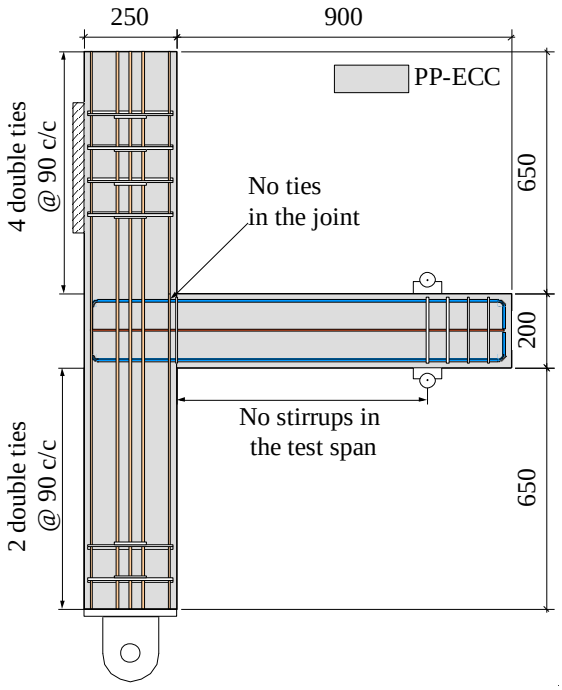

(c) TJ-3.

Figure 5.2.3 Layout of specimens and reinforcement details.

Table 5.2.1 Mechanical properties and amount of steel reinforcements.

Specimen	Bar nominal diameter (mm)	Transverse reinforcement diameter (mm)	Yield strength (N/mm^2)	Tensile strength (N/mm^2)	Reinforcement ratio (%)			
					Beam		Column	
					Longitudinal reinforcement	Transverse reinforcement	Longitudinal reinforcement	Transverse reinforcement
Prototype	31.8	15.9	*	*	1.324	0.636	0.991	0.530
TJ-1	6.35	6.35	325	525	1.304	0.677	1.064	0.563
TJ-2	6.35	6.35	325	525	1.304	0.000	1.064	0.563
TJ-3	6.35	6.35	325	525	1.304	0.000	1.064	0.000

* Data not available.

Table 5.2.2 Summary of transverse reinforcement reduction.

	Transverse reinforcement ratio (%)		
	TJ-1	TJ-2	TJ-3
Joint	0	0	0
Beam	0.68	0	0
Column	0.56	0.56	0

Table 5.2.3 Properties of concrete.

Specimen	f'_c (N/mm^2)	G_{max} (mm)	W/C (%)	Unit weight (kg/m^3)				
				W	C	S	G	Superplasticizer
Prototype	30.0	25	55	160	297	[a]	[a]	[a]
TJ-1	50.0	15	60	169	281	830	896	2.82
TJ-2	45.2	15	60	169	282	830	896	2.82

[a]: Data is not available; f'_c: compressive strength of concrete; G_{max}: maximum aggregate size; W: water; C: cement; S: fine aggregate; G: coarse aggregate.

Table 5.2.4 Properties of PP-ECC.

Specimen	f'_{ECC} (N/mm^2)	Slump Flow (mm)	W/B (%)	FA/B (%)	Unit weight (kg/m^3)			
					W	B	PP Fiber	AE
TJ-1	48.2	Approx. 500	27	33	371	1400	27	7
TJ-2	33.6							
TJ-3	33.6							

f'_{ECC}: compressive strength of PP-ECC; W: water; B: binder; FA: fly ash; AE: air entrainment.

name of these three specimen, “TJ” represents T-joint. The comparison of amount of reinforcements used in prototype structure and test specimens is presented in **Table 5.2.1**.

In TJ-1, all the 18 numbers of longitudinal rebars in column were provided with 60 mm long 180 hooks and ties were spaced at 85 mm center to center. 14 numbers of longitudinal rebars with stirrups spaced at 50 mm center to center were provided in the beams. In top and bottom beam rebars, 90 hook with 60 mm (10Φ, Φ is diameter of rebar) hook extension were provided but not hooks were provided in the side face rebars. The minimum clearance between two adjacent longitudinal rebars of column was 28 mm and that between adjacent longitudinal rebars of beam was 15 mm. Based on the specimen TJ-1, the stirrups in testing span of the beam were eliminated in the specimens TJ-2 as shown in **Figure 5.2.3**(b), while the amount of longitudinal and ties in the column was kept unchanged. In the specimen TJ-3, as shown in **Figure 5.2.3**(c), the amount of transverse reinforcements not only in the beam but also in the column was reduced to the minimum for fabricating a reinforcement cage. PP-ECC was used in the beam-column joint and the beam region in TJ-1 and TJ-2 while the normal concrete would be used in the column region. However, only PP-ECC was only used in TJ-3 specimen. The percentage reduction of transverse reinforcements in the specimens is summarized in **Table 5.2.2**.

The material properties in the test specimens were tried to keep similar to that in the prototype structure. However, due to some constraints, few compromises were made while selecting material properties.

In the prototype bridge, the concrete with compressive strength of 30 N/mm^2 was used. In order to obtain the concrete with compressive strength of 30 N/mm2, the concrete mix design followed the JSCE Guidelines for Concrete, No. 6, “*Standard Specification for Concrete Structure – 2007 (Materials and Construction)*” (JSCE, 2007). The mix proportions used for different specimens along with compressive strength are tabulated in **Table 5.2.3**. The maximum aggregate size of 10 mm was selected to maintain the workability during casting concrete into the steel cage. In each specimen, three cylinders with 100 mm diameter and 200 mm height and two cylinders with 150 mm diameter and 250 mm height were cast in concrete and cured along with beam-column joint specimens for compressive strength and tensile splitting tests, respectively. Uniaxial compression tests and tensile splitting tests were conducted according to JIS A

1108: *Method of test for compressive strength of concrete* and JIS A 1113: *Method of test for splitting tensile strength of concrete*, respectively. 1% of high performance air entrainment water reducing agent by weight of cement was added into TJ-1 and TJ-2 specimens. It should be noted that, because of the constraints, the cement used in the concrete was high early strength cement which usually takes 7 days to reach the compressive strength of 30 N/mm^2. However, the cement in PP-ECC is Ordinary Portland Cement (OPC) which takes 28 days to reach the compressive strength of 30 N/mm^2. Hence, the curing period of concrete was extended to that of PP-ECC and therefore the compressive strength in concrete was higher than that in the prototype structure.

In this study, the target nominal compressive strength of the PP-ECC is 30 MPa. The material components and mixture proportion used in this investigation were based on a study by Hirata *et al.* (2009). Ordinary Portland Cement (OPC), fly ash (maximum grain size of 0.3 mm), water and 3% volume fraction of PP fibers were combined using mix proportion along with compressive strength are tabulated in **Table 5.2.4**. It should be noted that, different from conventional concrete, the compressive strength of ECC is not only affected by water-to-cement ratio, but also other factors, such as tensile strength of fiber, compressive strength of matrix, bonding strength of fiber with matrix, the volume fraction of fibers, air content, etc. (Kawamata et al.). The air content of PP-ECC used in this study is around 10%. The PP fibers are fibrillated fibers having diameter of 36 μm, length of 12 mm, tensile strength of 482 MPa and elastic modulus of 5 GPa, as explained in **Chapter 3**. This fibrillated polypropylene fiber with rugged surface results in improvement of bond properties and exhibits the pseudo strain hardening and multiple fine cracking of ECC under tensile stress. The production process of PP-ECC is earlier described in **Section 3.2**, **Chapter 3**.

In the prototype structure, steel rebars have different yield strengths were used at the different locations. However, the steel rebars with yield strength of 325 N/mm^2 were used for both longitudinal and transverse rebars. The diameter of 6 mm deformed steel bar (D6) was used for longitudinal and transverse rebars in columns and beams of all beam-column joint specimens. The stress-strain curve of D6 rebars as shown in **Figure 5.2.4** was obtained from the tensile test in order to determine the yielding of rebars during loading tests. The yield strength, tensile strength and yield strain are 325 N/mm^2, 525 N/mm^2 and 1750×10^{-6}, respectively. The D6 rebars complies with the standard of JIS G 3112 SD295A. **Table 5.2.5** summarizes the properties of D6 steel bar.

Table 5.2.5 Tensile properties of D6 rebar.

Steel bar	Nominal diameter (mm)	Yield tensile Strength (N/mm^2)	Tensile Strength (N/mm^2)	Yield strain (με)
SD 295A	6.35	325	525	1625

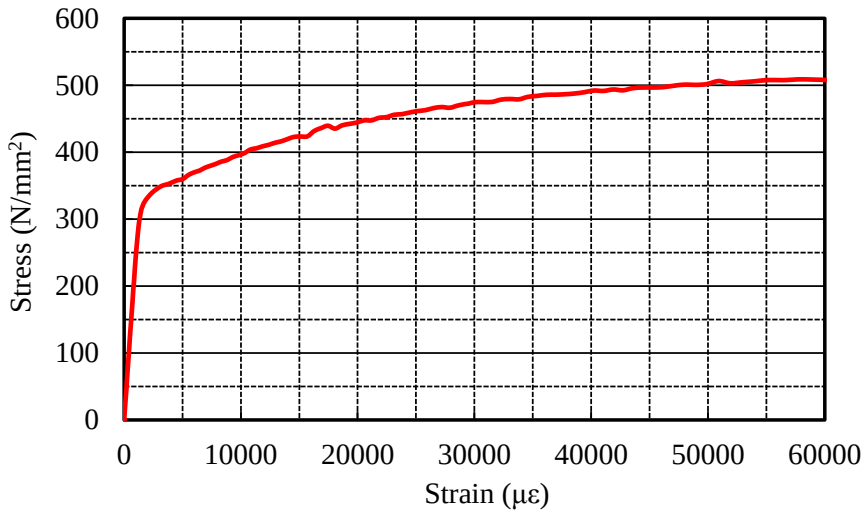

Figure 5.2.4 Stress-strain curve of D6 rebar.

5.2.2 Design verification and reduction of transverse reinforcements

In rigid-framed railway bridges, the intermediate beams tie the columns together to enhance the structural stiffness and stability of the structure under the vertical load. During a large seismic event, the formation of plastic hinges in the intermediate beam rather than in the column is expected. The principle of "strong column and weak beam" is also applicable to rigid-framed railway bridge. The column is designed stronger than beam it means during strong earthquake column member remain elastic so it can provide stability and strength of the whole structure. Meanwhile, the development of plastic hinge forms at the end of beam can dissipate energy by using special reinforcement detailing or confinement to improve ductility, energy absorption capacity and perform inelasticity.

According to ACI 318-08 and ACI 352R-02 (ACI Committee 318, 2008; Joint ACI-ASCE Committee 352, 2002), the strong column and weak beam approach should be followed by using following equation:

$$\frac{M_c}{M_B} \geq 1.2$$

where, M_c is the flexural capacity of a column and M_b is the flexural capacity of a beam. The flexural capacity of beam and column was calculated according to the methods specified in *Standard Specifications for Concrete Structures-2007 [Design]* (JSCE, 2010). For scaled beam-column joint specimens in concrete with concrete compressive strength of 30 N/mm^2 in this study, M_c is 20.7 kN·m for column while M_b is 12.4 kN·m, as a result M_c / M_b = 1.67 > 1.2 indicating that the strong column and weak beam approach can be achieved. Since the PP-ECC can enhance the flexural shear capacity slightly, the ratio of flexural capacities in all specimens is taken greater than 1.2.

5.2.3 Specimen construction

For the specimen TJ-1 and TJ-2, because of two types of materials, concrete and PP-ECC, were used in one specimen, it was important to consider the treatment of interface between these two materials to ensure no failure occurred at that locations. Hence, the casting sequence of concrete and PP-ECC was specially designed. As reported by the other researchers (Kojima *et al.*, 2004), since the ECC exhibits strong bonding effect to the concrete, the concrete in the column portion was determined to be

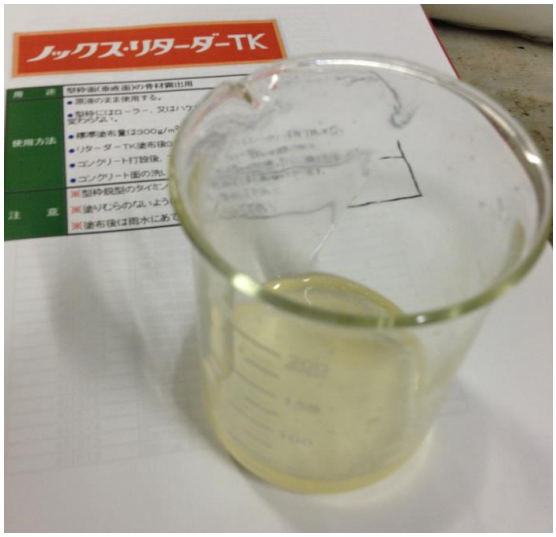

Photo 5.2.1 Concrete retarder.

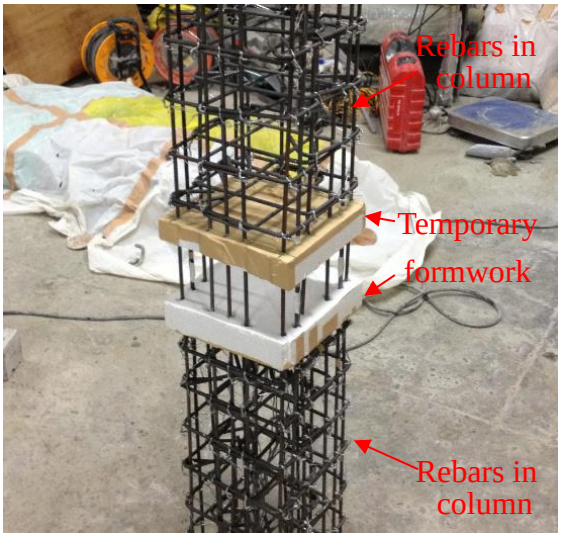

Photo 5.2.2 Temporary formwork for setting retarder.

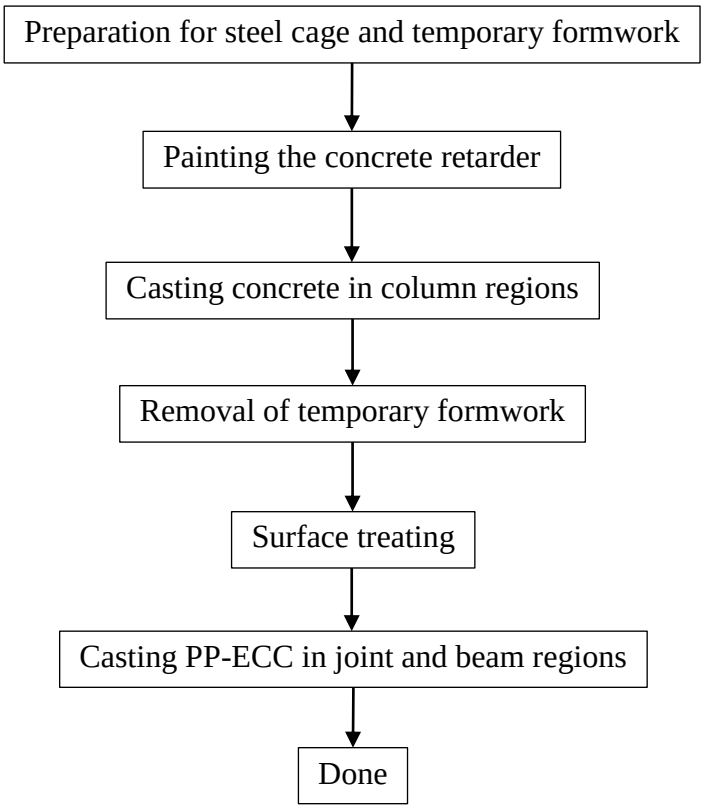

Figure 5.2.5 Construction sequence for TJ-1 and TJ-2.

cast in advance and PP-ECC in joint and beam region was cast afterwards. In addition, in order to increase the bonding at the interface between PP-ECC and concrete, the surface retarder, as shown in **Photo 5.2.1**, a kind of admixtures was utilized to delay the set of the surface cement paste so that the coarse aggregate can be exposed easily. Since the formwork at the interface should be removed for casting PP-ECC after 24-hour curing of concrete, a kind of daily used foamed plastic, which is easy to be tear off, was utilized to be formwork here for temporary use, as shown in **Photo 5.2.2**.

The construction of sequence for TJ-1 and TJ-2 was illustrated by the flow chart **Figure 5.2.5**. After the fabrication of steel cage in the column region along with the temporary formwork, according to the instruction of the concrete retarder, it was painted on the surface of temporary formwork within 24 hours before casting concrete. Then the concrete was cast and placed into the column regions as shown in **Photo 5.2.3**(a). After 24 hours curing, the temporary formwork was tear off to expose the interface with delayed set of cement (**Photo 5.2.3**(b)). The high pressure water was utilized to flush the surface as shown in **Photo 5.2.3**(c) to expose the coarse aggregate. **Photo 5.2.3**(d)

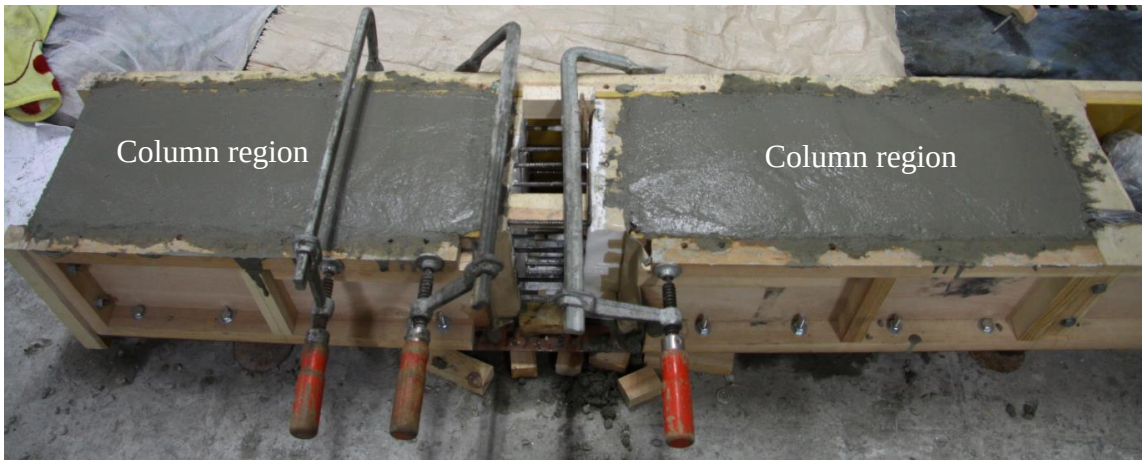

(a) Casting concrete in column regions.

(b) After removal of temporary formwork.

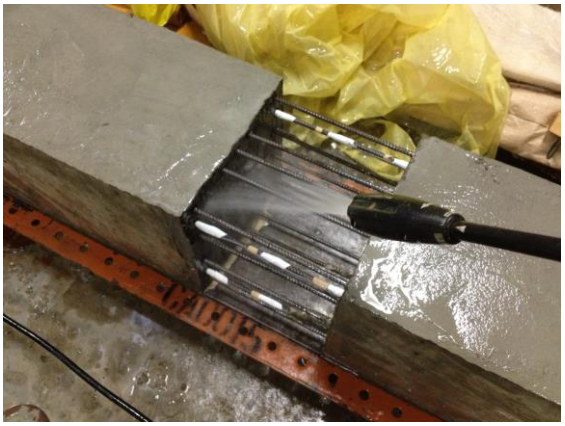

(c) Flushing surface.

(d) Exposure of coarse aggregate.

(e) Setup formwork for PP-ECC.

Photo 5.2.3 Surface treatment and preparation for casting PP-ECC.

(a) After casting the PP-ECC. (b) Before loading tests.

Photo 5.2.4 Casting the PP-ECC region and testing preparation.

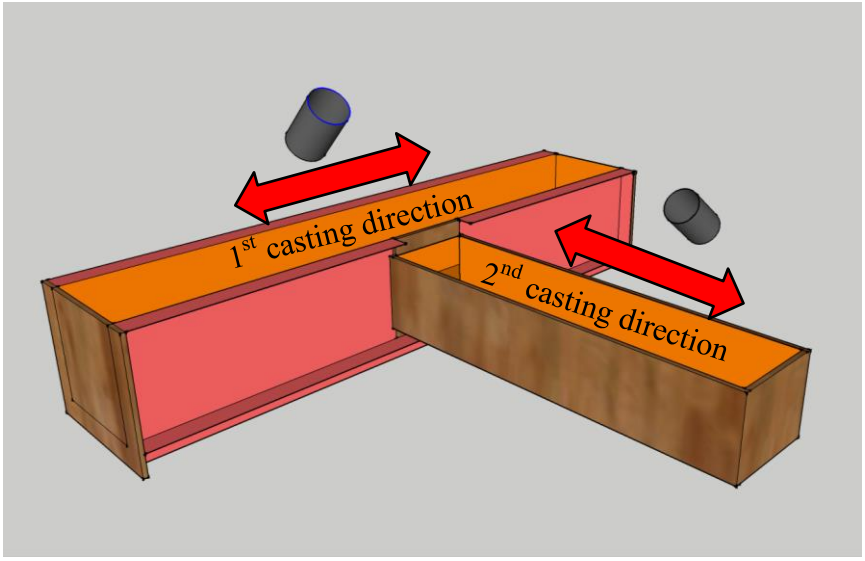

Figure 5.2.6 Casting the PP-ECC in TJ-3.

shows the exposure of coarse aggregate after flushing. As last, the steel cage and formwork in the beam region was setup after surface treatment (**Photo 5.2.3**(e)) and then the PP-ECC was cast and placed into the beam region (**Photo 5.2.4**(a)). **Photo 5.2.4(b)** shows the TJ-1 specimen after curing.

The casting direction of the PP-ECC is important to control the orientation of fibers in some extent. In TJ-1 and TJ-2, the PP-ECC was poured into the formwork along the direction of beam axis. In TJ-3, PP-ECC was firstly cast along the direction of column axis and then cast along the direction of beam axis as shown in **Figure 5.2.6**. Due to some constrains, the TJ-1 was cured in moist environment more than 3 months which

resulted in significant increase in compressive strength of PP-ECC in TJ-1 while TJ-2 and TJ-3 were cured in moist environment for 28 days before testing.

5.3 Experimental Program and Instrumentation

5.3.1 Experiment setup

Uni-lateral cyclic loading experiments were conducted using a digital closed-loop controlled dynamic testing facility at Tokyo Institute of Technology shown in **Photo 5.3.1**. The horizontal actuator has a capacity of 200 kN. The bottom of the column was pinned to the loading frame and the beam was supported by two rollers, which were rested on the steel supporting system firmly connected to the loading frame. The boundary conditions allowed a rotation of the column and a horizontal displacement of the beam. The vertical movement of the beam was constrained by the steel plates above and under roller supports.

5.3.2 Loading protocol

Uni-lateral cyclic loading experiments were conducted under displacement control. The cyclic loading was supplied by a hydraulic actuator and the amplitude was increased at

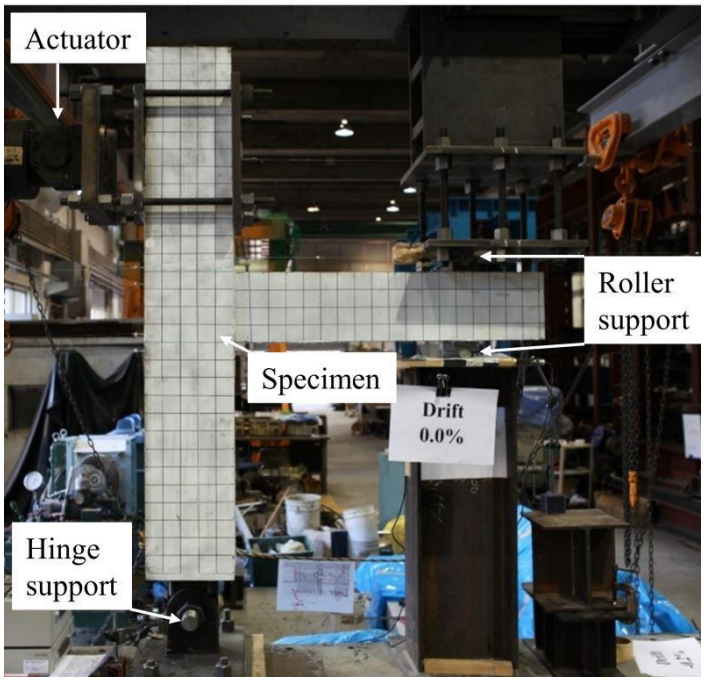

Photo 5.3.1 Test setup.

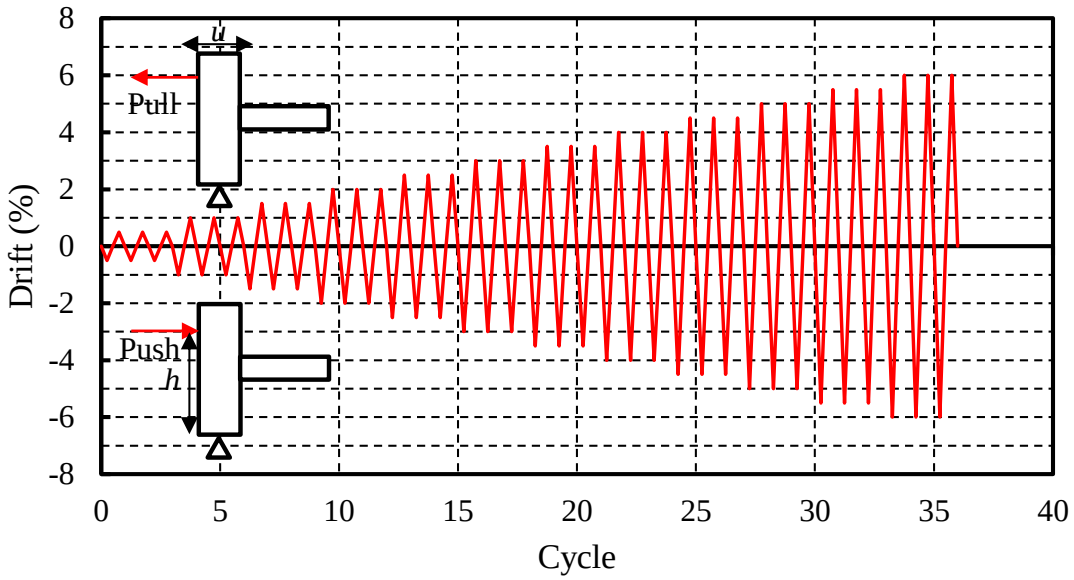

Figure 5.3.1 Lateral displacement history.

one half of the drift ratio at each loading step. Drift ratio (u) is defined as the column lateral displacement at the loading point divided by the distance from the hinge to the loading point, which is given by the following equation:

$$u = \frac{x}{h} \times 100\% \tag{5.3.1}$$

where, x is the applied lateral displacement (mm) and h is the height from the hinge to the level of applying lateral load (mm), which is 1332 mm in this study. Thus, 1% drift ratio corresponds to 13.32 mm. The applied drift ratio was ranged from 0.5% to 6.0% as shown in **Figure 5.3.1**.

When the column was pulled towards the actuator, the displacement was considered as positive displacement and vice versa. The column was first loaded into the negative direction until -0.5% drift ratio, then loaded back to the positive direction until 0.5% drift ratio, then finally unloaded in negative direction to original position. At each drift level, the cycles was repeated for three times. For all specimens, the cyclic loading tests were terminated at 6.0%.

5.3.3 Instrumentation

Various instrumentations were used to measure displacements, longitudinal and tie bar strains. Linear Variable Differential Transformers (LVDTs) and strain gauges were installed at various locations as shown in **Figure 5.2.2**(a) to record and analyzing structural behavior such as deformations and strains. The strain gauges were attached in series on both horizontal and vertical rebars at the beam-column joint. In addition, the longitudinal rebars in column and beam were attached by strain gauges. All strain gauges were stuck on the external face of rebars. For the measurement of displacement, the wire type displacement transducers were used. Several typical LVDTs were used to measure the horizontal displacement in the base steel of the hinge and steel supporting column so that these lateral displacements in the supports can be corrected by incorporating them into the displacements at the other locations if there were any displacements in supports.

5.4 Experimental Results and Discussions

5.4.1 Crack pattern and failure process

The crack patterns observed in the specimens by the end of the tests are shown in **Photo 5.4.1**. The first fine flexural cracks initiated from the bottom edge of beams for all specimens were observed at the first cycle in drift of 0.5%. As the cyclic loading progressed up to 2.0% drift for TJ-1 while 2.5% drift for TJ-1, more and more flexural fine cracks were developed from the top and bottom edge of beam. At the drift of 2.0%, the inflation of cover PP-ECC on the external face of the column due to the pull out effect of beam longitudinal reinforcements was observed. Because of the bridging effect of fiber, the inflated PP-ECC did not spall off until the loading test finished. However, this pull out of beam longitudinal reinforcements was not observed in the loading tests of TJ-1 and TJ-3.

In the specimen of TJ-1, the flexural cracks were initiated from the bottom edge of beam at the first cycle of 0.5% drift in terms of fine cracks, which is one of the most notable characteristics of ECC. At the same drift level, the inclined shear cracks were also developed in the joint region in terms of fine cracks. As the loading progressed up to 2.0% drift, more and more flexural cracks were developed along the beam in the test span. At the first cycle of 2.0% drift, a localized crack occurred at the interface between

the column face and beam end was observed. After the localization of cracks at the interface, fewer cracks were developed while the opening of localized cracks became more and more significant. After the loading test, the cover of PP-ECC at the region of plastic hinge was cut off to investigate the damage situation of beam longitudinal rebars. As summarized in **Table 5.4.1**, all top layer of beam rebars and 2 out 6 bottom layer of beam rebars were buckled and finally, 5 out of 6 top longitudinal rebars in beam were ruptured while just buckle of bottom rebars was observed. As a result, the TJ-1 failed in flexure. Compared to TJ-2 and TJ-3, the number of cracks developed was the least and the concentration of cracks was not so significant as TJ-2 and TJ-3.

In the specimen TJ-2, the first flexural fine crack was also observed to be initiated from

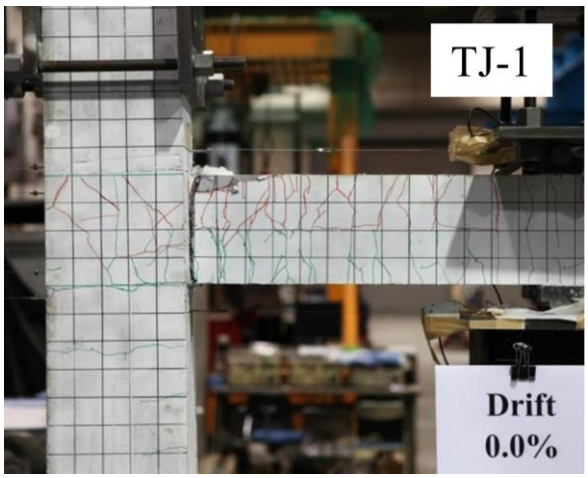

(a) TJ-1.

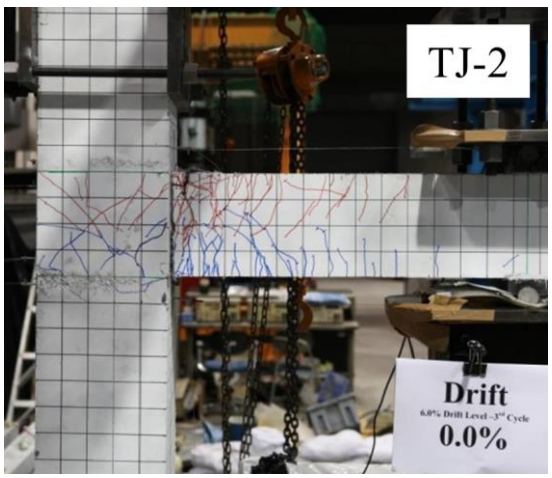

(b) TJ-2.

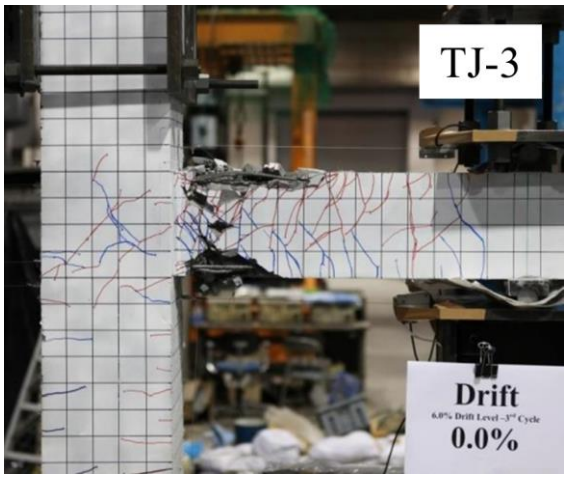

(c) TJ-3.

Photo 5.4.1 Crack pattern by the end of the test.

Table 5.4.1 Summary of the beam-column joint tests.

		TJ-1	TJ-2	TJ-3
First cracking drift cycle		0.5% - 1st	0.5% - 1st	0.5% - 1st
Peak load during positive loading		23.4 kN	21.1 kN	19.6 kN
Peak load during negative loading		18.0 kN	17.2 kN	18.6 kN
Pull out of longitudinal rebars		Top rebars	Bottom rebars	None
Beam rebar buckling	Top rebars	All	4 out of 6	All
	Bottom rebars	2 out of 6	3 out of 6	All
Beam rebar rupture	Top rebars	5 out of 6	2 out of 6	2 out of 6
	Bottom rebars	None	1 out of 6	4 out of 6
Failure mode		Flexure	Flexure	Flexure

the bottom edge of beam at the first cycle of 0.5% drift while the first shear crack in the joint region was observed at the second cycle of 1.5% drift. As applied displacement increased, more and more cracks were developed up to 2.5% drift, when the localized crack at the interface between the column face and beam end initiated from bottom edge was observed. However, the opening of this firstly developed localized crack did not increase as significant as that of TJ-1 when the drift amplitude was increased. It was noted that the cover of PP-ECC, at the location where bottom longitudinal rebars of the beam projected on the external face of the column opposite to beam side, was inflated at the drift of 2.0%. As a result, 4 out of 6 top layer of beam rebars buckled with 2 ruptures and 3 out 6 bottom layer of beam rebars buckled and with 1 ruptured were observed in TJ-2, indicating that TJ-2 was also failed in flexure. It is worth mentioning that the external face of joint began to be spalled from 4.5% drift, which results from the pull out of bottom layer of beam rebars. Compared to TJ-1, apparently more cracks were developed and most of them were concentrated in the beam length of 200 mm from the column face.

In the specimen TJ-3, the first flexural fine crack was observed to be started from the bottom edge of beam at the first cycle of 0.5% drift while the first shear crack in the joint region was observed at the second cycle of 1.0% drift. In addition, different from no flexural cracks in columns of TJ-1 and TJ-2, several flexural fine cracks in the

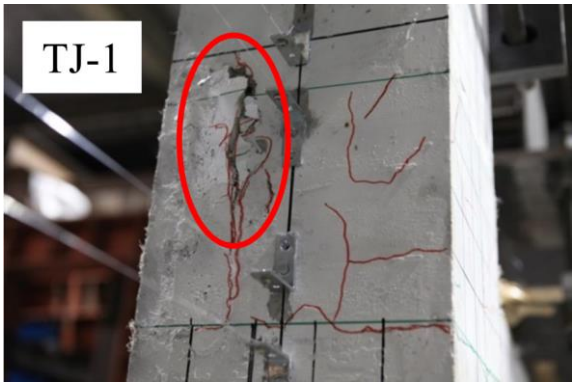

(a) TJ-1.

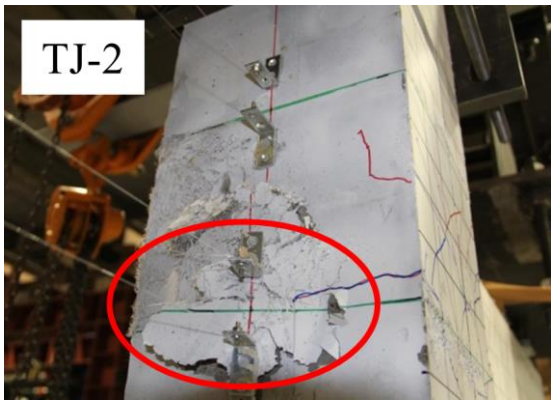

(b) TJ-2.

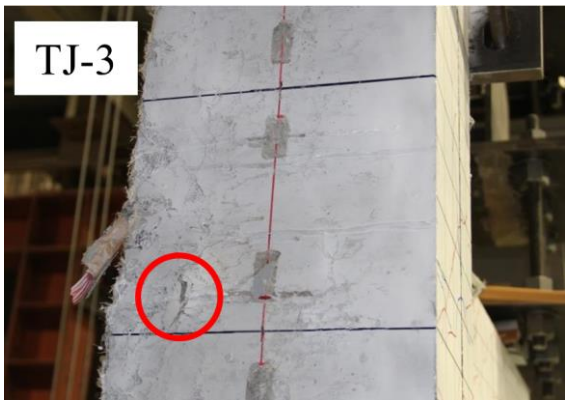

(c) TJ-3.

Photo 5.4.2 Pull out of beam longitudinal rebars after loading tests.

column of TJ-3 was observed to be started from the left edge under the beam level at the second cycle of 1.0% drift. Because of the effect of ‘strong column and weak beam’, compared to the number of the flexural cracks in the beam, quite limited number of flexural fine cracks were developed before crack localization. More and more flexural fine cracks were developed up to 2.0% as drift increased, when the crushing of PP-ECC at the bottom edge of the beam adjacent to column face occurred. Accordingly, the cover of PP-ECC at the top edge of the beam opposite to damage portion below was crushed in the second cycle of 3.0% drift. As a result, all top and bottom layer of beam rebars buckled with 2 ruptures in top layer while 4 ruptures in bottom layer. The significant rupture of beam rebars leads to the final flexural failure. The number of cracks developed in TJ-3 was the most among these three specimens.

Photo 5.4.2 shows the pull out of beam longitudinal reinforcements on the external face of a column in all specimens after the loading test due to the slipping between beam

longitudinal reinforcements and the PP-ECC in the joints. Different extents of pull out of reinforcements in all specimens were observed. There were pulling out of top beam reinforcements in TJ-1 as shown in **Photo 5.4.2**(a), but all beam reinforcements buckled and five out of six top beam reinforcements ruptured by the end of the loading test. The similar damage that the pull out of bottom beam reinforcements as shown in **Photo 5.4.2**(b) in TJ-2 was also observed, but all top beam reinforcements buckled and only two out of six top reinforcements ruptured. The pull out of beam reinforcements in TJ-3 as shown in **Photo 5.4.2**(c) was quite insignificant compared to the specimens TJ-1 and TJ-2, manifesting that the bonding between beam reinforcements and the PP-ECC in the joint of TJ-3 was the best and finally two out of six top beam reinforcements and four out of six bottom beam reinforcements ruptured. As for the pulling out of rebars, it could be prevented by increasing the anchorage length of rebar. Moreover, modifications of the rebar detailings in the joints were also proposed by the provision of inclined rebars in joints along with hoops showed the increase in the strength and energy dissipation capacity and no appreciable strength deterioration even after attainment of maximum capacity (Tsonos et al. (1992), Chalioris et al. (2008)).

Photos 5.4.3 and **5.4.4** show damage at the top and bottom of beams adjacent to the

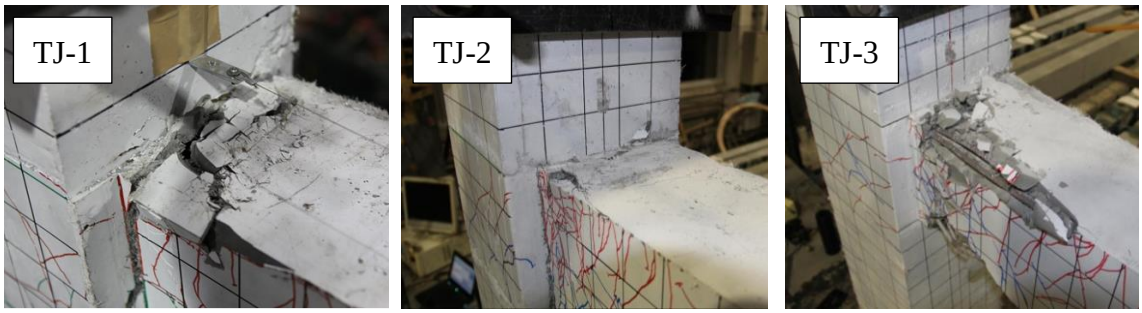

Photo 5.4.3 Damage at the top of the beam by the end of tests.

Photo 5.4.4 Damage at the bottom of the beam by the end of tests.

column by the end of the tests. The PP-ECC at the top fiber of the beam was crushed when the specimen was pushed away from the actuator. As earlier described, the localized poor distribution of fibers resulted in the crushing and spalling of PP-ECC near joint region on the view side in TJ-3, while the in the opposite side, due to the good condition of fiber distribution, this kind of crushing and spalling off did not occur.

Hence, based on the observation of the crack patterns in all specimens, it became clear that the pull out of beam longitudinal rebars in specimens (TJ-1 and TJ-2) using two types of materials was more severe. This is because the limited space between beam reinforcements and the interface in the column impaired the bonding between reinforcements and the PP-ECC.

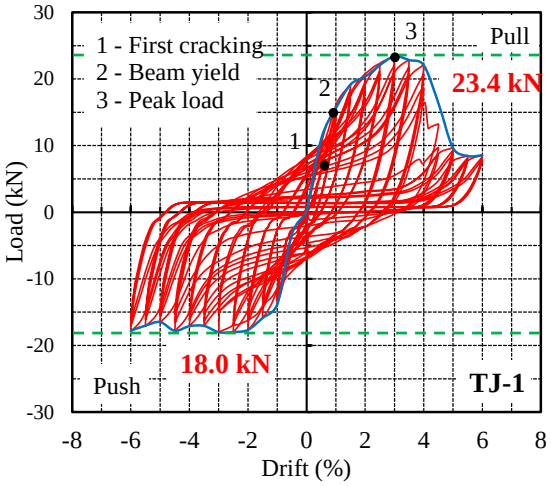

(a) TJ-1.

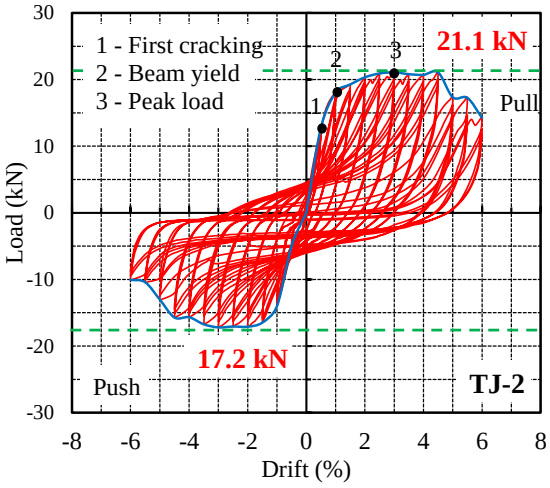

(b) TJ-2.

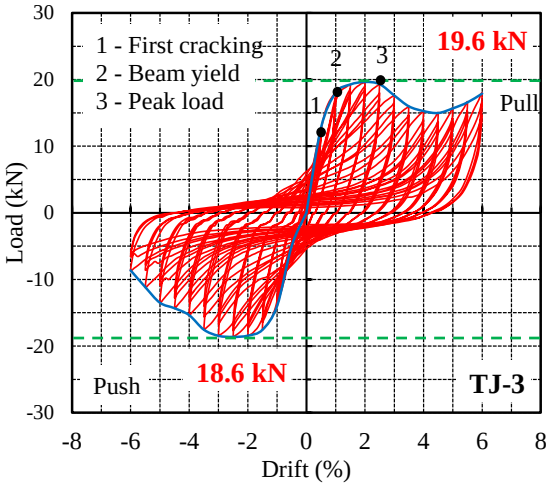

(c) TJ-3.

Figure 5.4.1 Load-displacement hysteretic loops.

5.4.2 Load-displacement hysteretic loops

The load-displacement hysteretic loops obtained from the cyclic loading tests are shown in **Figure 5.4.1**. The hysteretic envelop curves for all specimens are also shown by connecting the peak loads at each drift level in blue lines. **Table 5.4.1** summarizes the experimental results of each specimen. The hysteretic loops of all specimens were pinched to an equivalent level. The maximum loads in both positive and negative directions occurred in the first cycles during each drift level. However, the peak load of TJ-1 in positive loading cycles was the highest among all specimens, which was mainly attributed by its higher compressive strength of PP-ECC among all specimens. As shown in **Figure 5.4.1**(a), on applying the cyclic load in TJ-1 after the peak load at 3.0% drift, the load dropped drastically when TJ-1 was loaded towards 4.5% drift in the first cycle due to the ruptures of beam top longitudinal reinforcements. On reversing the load, only the beam bottom longitudinal reinforcements participated to carry the load. However, after the peak load, the strength marginally decreased in subsequent cycles up to 4.5% drift forming a plateau in load-displacement envelope curve of TJ-2 and slightly decreased from 2.5% to 4.5% but increased from 4.5% to 6.0% forming a flat basin in the load-displacement envelope curve of TJ-3 due to inelastic behavior of plastic hinge adjacent to the column face and the bond deterioration in the joint region.

5.4.3 Moment-curvature relationship

Ductility is one of the major parameters for earthquake-resistant structure to make it have better nonlinear response under a seismic event. The induced shear stress and the rotation in the beam-column joints during application of reversal load significantly affect the ductility. The moment-curvature relationship can be a suitable criterion to understand the ductile behavior of a beam-column joint involves the formation of a plastic hinge at the beam end adjacent to the column face.

The formation of plastic hinges is the way to undergo nonlinear and ductile behavior in structures. The curvature exists in the plastic hinge or nearby portion where the nonlinear response is exhibited while the curvatures in the remained portion are still elastic. The moment-curvature relationships at various sections were obtained by analyzing the strains on the rebars. Various beam sections of the top and bottom longitudinal rebars were attached with strain gauges as shown in **Figure 5.4.2**. The strain gauges reading at a section can be converted to a curvature ϕ, which was

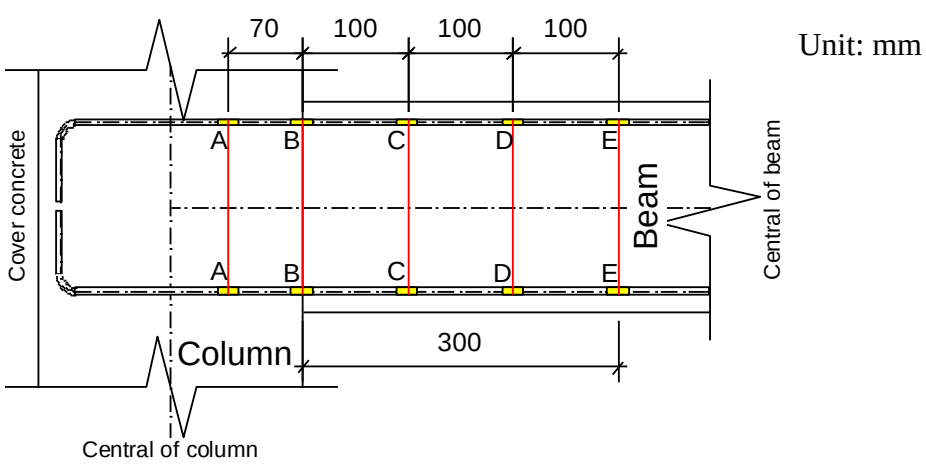

Figure 5.4.2 Location of sections in beams instrumented with strain gauges.

calculated by using the measured strains in the top/outer and bottom/inner rebars:

$$\phi = \frac{\varepsilon_t - \varepsilon_b}{d_0} \tag{5.4.1}$$

where, ε_t is strain gauge reading at top/outer rebar, ε_b a is strain gauge reading at bottom/inner rebar and d_0 is the distance between top/outer and bottom/inner rebars.

The locations of the five sections (A-A, B-B, C-C, D-D and E-E) in the beams instrumented with strain gauges are shown through **Figure 5.4.3** to **5.4.5**. The moment-curvature hysteretic loops at these sections were checked to locate the plastic hinge. The beam rebars at the section A-A, B-B and C-C endured inelastic response in all specimens (**Figure 5.4.3**(a–c), **Figure 5.4.4**(a–c) and **Figure 5.4.5**(a–c)). Moreover, D-D section in TJ-2 remained elastic while in TJ-1 and TJ-3 exhibits slightly nonlinear response. Highly nonlinear response exhibited by TJ-3 implied the high ductility of the specimen which can be attributed to strong anchorage in the joint. In TJ-2, the bottom rebars were pulled out while the top rebars remain in good bonding condition; as a result, most of the curvature was observed in the positive direction (**Figure 5.4.4**(c)).

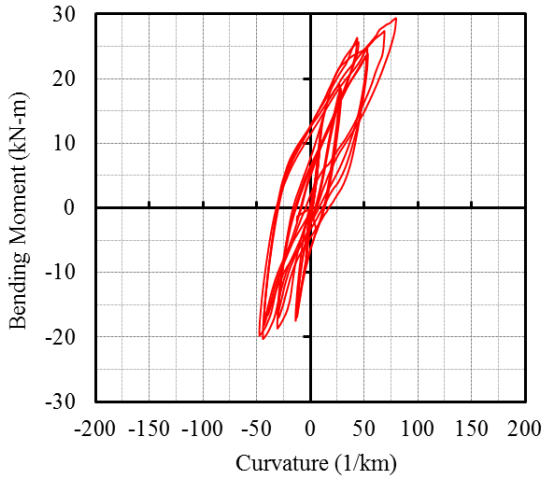

(a) A-A section.

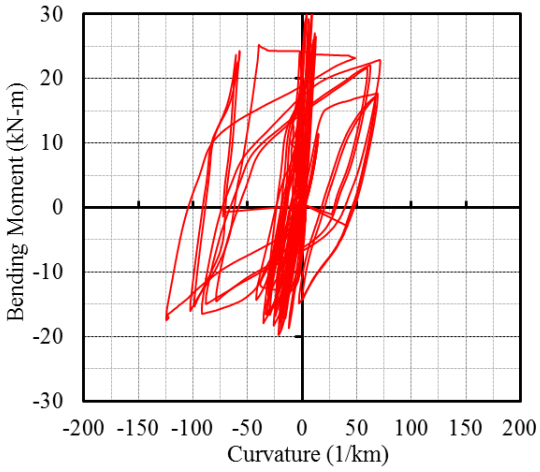

(b) B-B section.

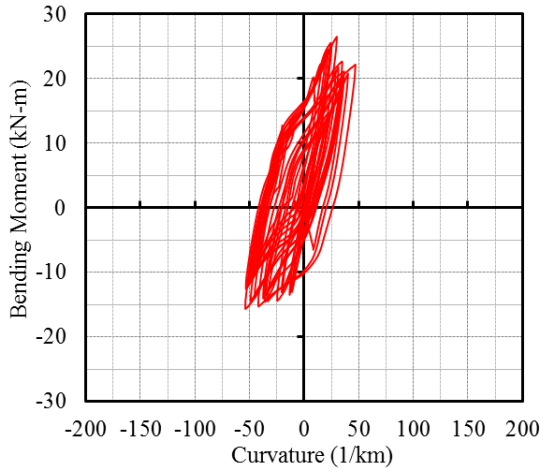

(c) C-C section.

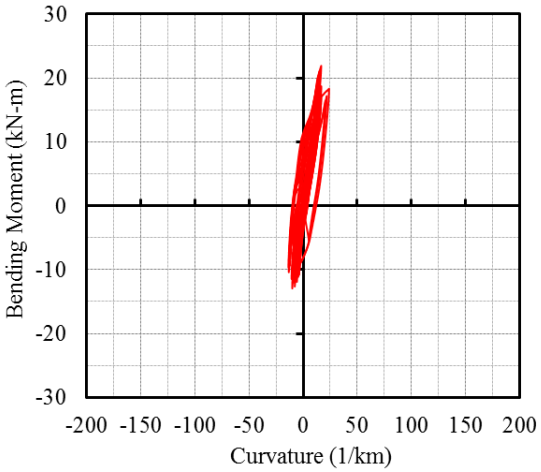

(d) D-D section.

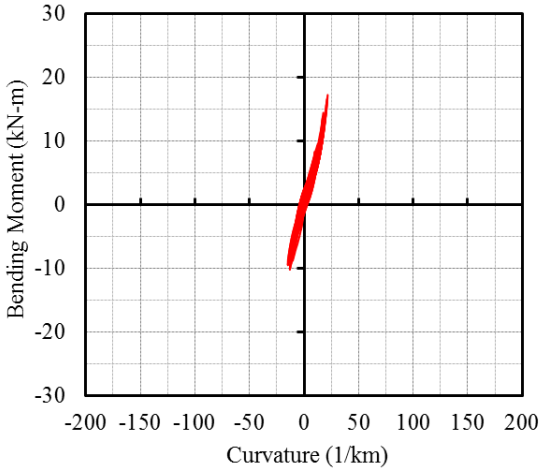

(e) E-E section.

Figure 5.4.3 Moment-curvature relationship at the sections in the TJ-1.

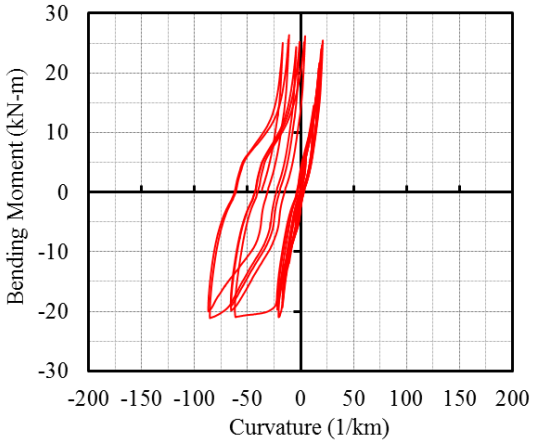

(a) A-A section.

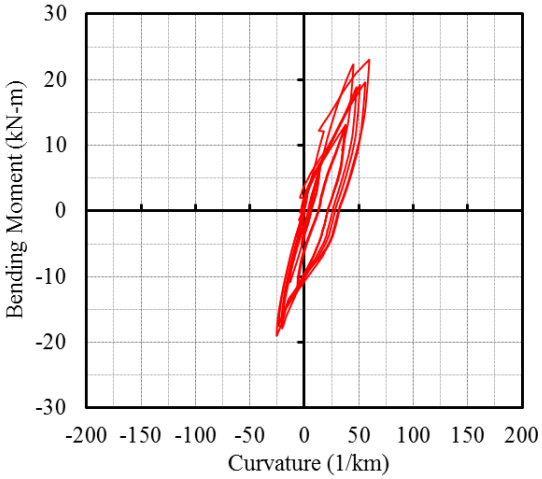

(b) B-B section.

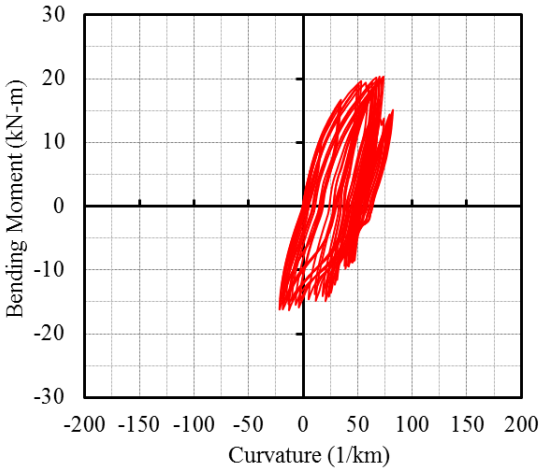

(c) C-C section.

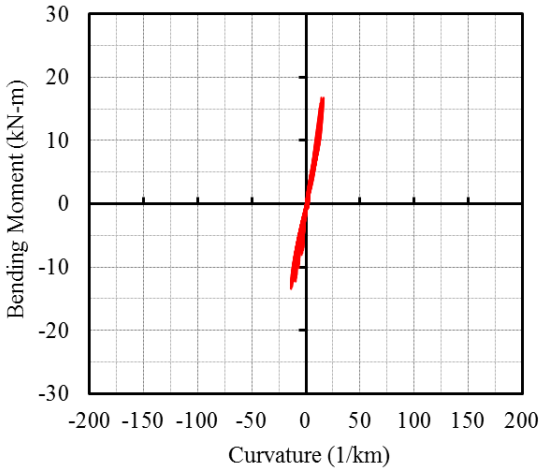

(d) D-D section.

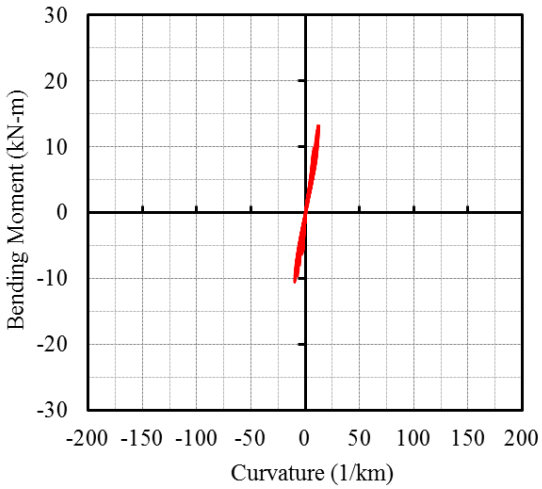

(e) E-E section.

Figure 5.4.4 Moment-curvature relationship at the sections in the TJ-2.

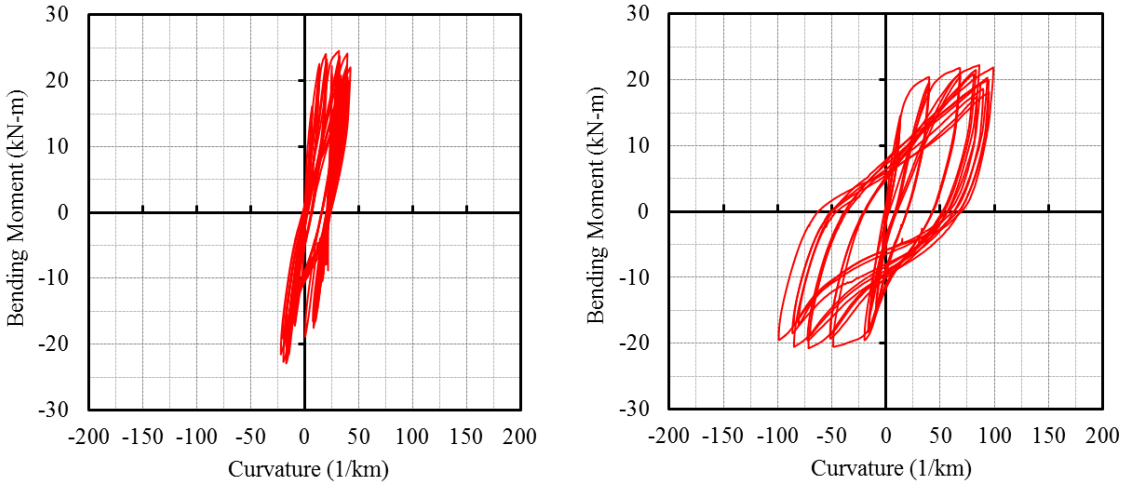

(a) A-A section.

(b) B-B section.

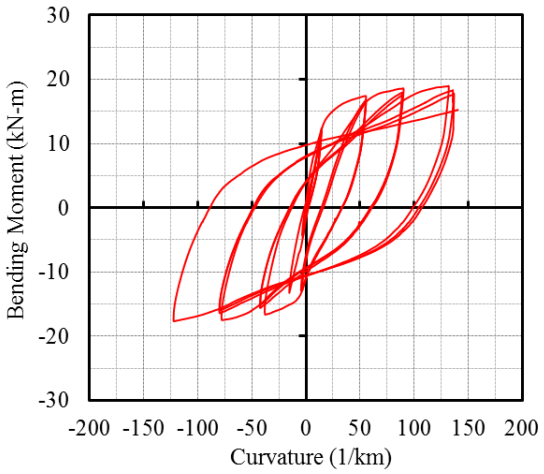

(c) C-C section.

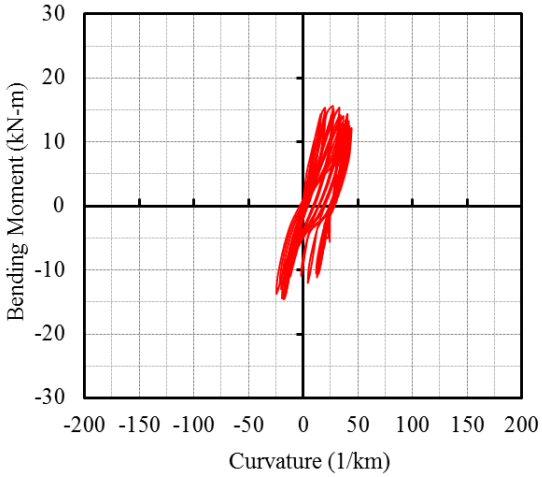

(d) D-D section.

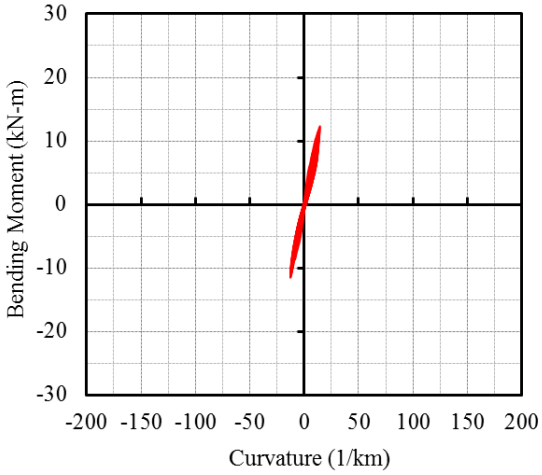

(e) E-E section.

Figure 5.4.5 Moment-curvature relationship at the sections in the TJ-3.

5.4.4 Energy dissipation and stiffness degradation

Energy dissipation indicates the capability of structures to dissipate energy through yield mechanism with satisfactory performance in the inelastic range, which occurs due to induced damages in the specimens in terms of cracking of concrete or ECC, yielding and buckling of steel reinforcements and debonding of steel rebars from concrete or PP-ECC and PP fibers from PP-ECC. Energy dissipation was assessed by computing the cumulative energy dissipation W_e at each load cycle, namely, the area enclosed by the corresponding load-displacement loop and is illustrated by **Figure 5.4.6**(a) and given by:

$$W_e = \int P dx \tag{5.4.2}$$

where, P is the applied load and dx is the increment of the applied displacement. Due to the pinching and strength degradation in all specimens, the energy was not proportionally increased to the increase in the applied drift. **Figure 5.4.6**(b) shows energy dissipation capacity of each specimen. Up to the drift of 3.0%, all specimens dissipated almost the same amount of energy. At the drift level of 4.5%, TJ-1 dissipated 15.7% more energy than the specimen without transverse reinforcements TJ-3. The

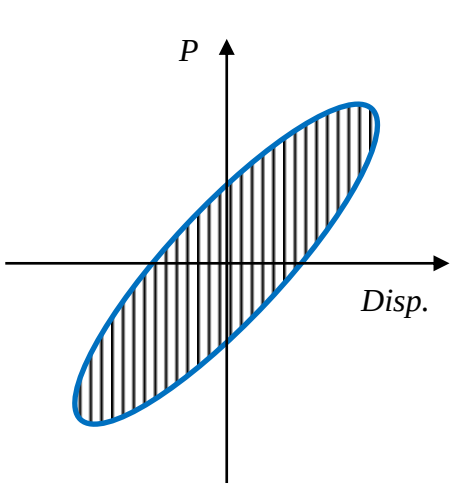

(a) Definition.

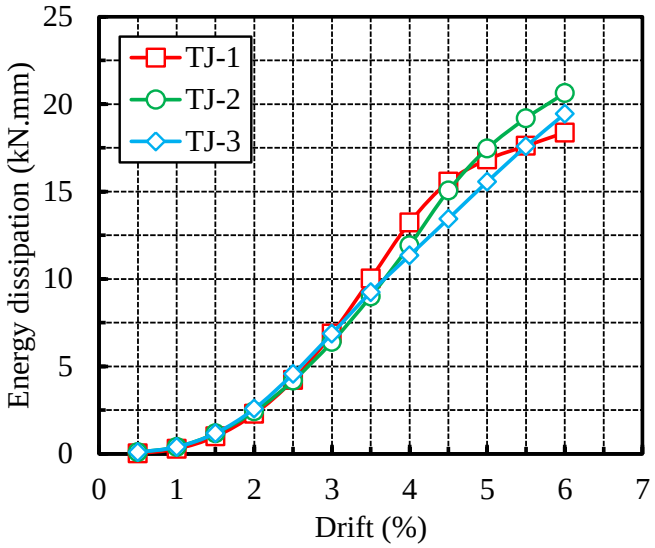

(b) Results.

Figure 5.4.6 Energy dissipation.

growth of energy dissipation in TJ-1 slowed down markedly due to the rupture of top beam reinforcements in TJ-1 at the drift level of 4.5% while fewer ruptures of beam reinforcement in of TJ-2 and TJ-3 at this drift. As a result, the TJ-2 and TJ-3 dissipated more energy than that of TJ-1. Among all specimens, the energy dissipated by TJ-2 and TJ-3 was almost equivalent to that dissipated by TJ-1. The comparable energy dissipation even after reducing the amount of transverse reinforcements in the specimens TJ-2 and TJ-3 also highlighted the shear reinforcing effectiveness of PP-ECC.

The stiffness degradation was evaluated by calculating the stiffness of beam-column joints during each cycle of the loading based on the load-displacement hysteretic loops. Specifically, it was assessed by computing the slope of the line connecting the peak load and zero load at half cycle of each drift level as illustrated by **Figure 5.4.7**. **Figure 5.4.8** shows the stiffness degradation of all specimens during the cyclic loading. At the firstly applied 0.5% drift, even with higher compressive strength in TJ-1, at the initial 0.5% drift, the stiffness of TJ-1 at 0.5% drift increased by 11.4% and 7.0%, respectively, while at -0.5% drift, it increased by -2.7% and 4.5% , respectively, compared to that of TJ-2 and TJ-3. Even with the elimination of transverse reinforcements in TJ-2 and TJ-3, TJ-2 and TJ-3 exhibited the comparable performance of TJ-1, indicating that the little effect on the stiffness degradation due to the reduction of transverse reinforcements by using PP-ECC. In addition, it was noted that although the crushing of the defective

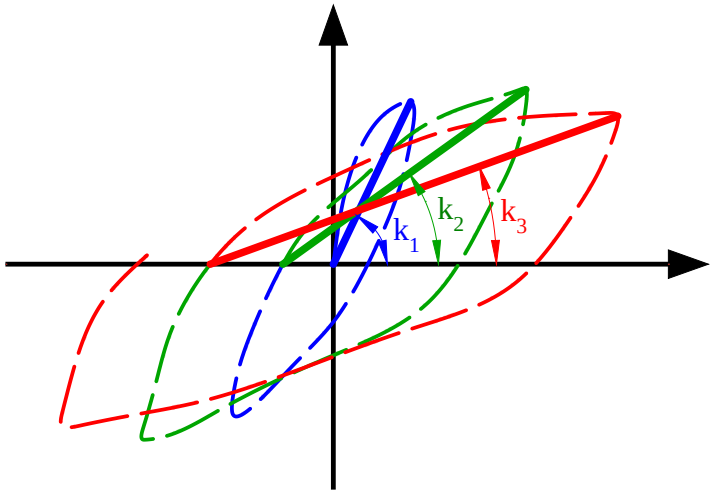

Figure 5.4.7 Definition of stiffness degradation.

PP-ECC on the view side in TJ-3 was observed during the loading tests, the comparable energy dissipation and stiffness degradation exhibited by TJ-3 indicates that the effect resulting from this defective PP-ECC was ignorable.

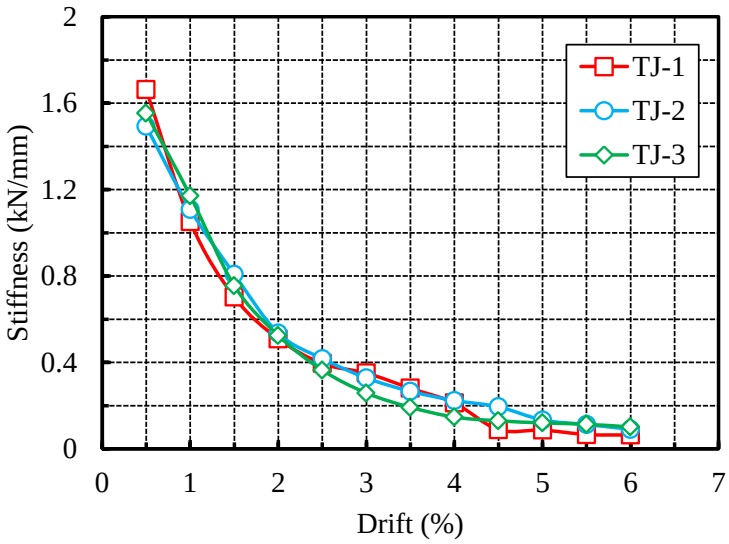

(a) Positive loading.

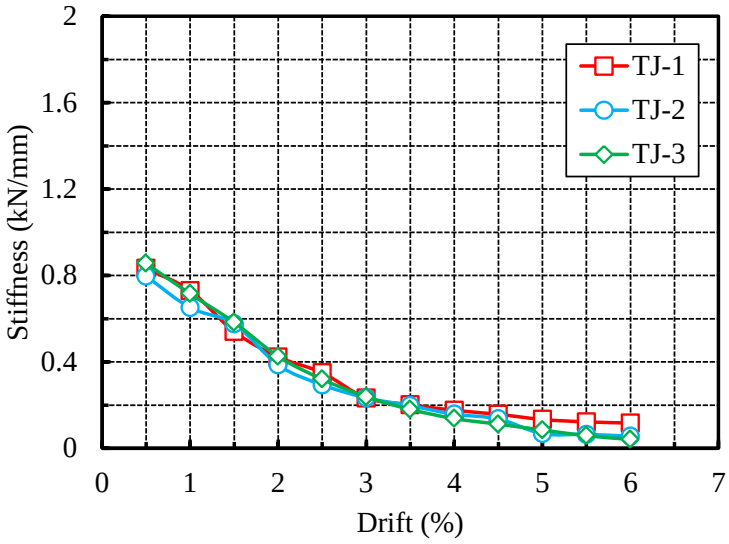

(b) Negative loading.

Figure 5.4.7 Stiffness degradation.

5.5 Summary

The experimental results of quasi-static cyclic loading on 1/6 scaled T-shape beam-column joint specimens have been presented in this chapter. An effort was made to reduce the amount of transverse reinforcements in the joint, the beam and the column of the beam-column joints which were designed following the Japanese railway design standards. The result of this study can provide an option to reduced shear rebars and thereby avoiding the congestion of steel rebars in the joints. Based on the experimental results, the following conclusions can be drawn:

1) After the reduction of transverse reinforcements in the joint, the beam and the column in the beam-column joint specimens, the fabrication of steel cage became easier. Further, more time for fabrication and cost was reduced.

2) The concrete retarder useful to treat interface between conventional concrete and PP-ECC to prevent the interface failure and increase the integrity of composite structure.

3) The failure mode of the specimens even with elimination of transverse reinforcements was still flexural failure, which was the same as that of the specimen without elimination of transverse reinforcements indicating that the PP-ECC can be the replacement of transverse reinforcements to provide sufficient shear strength.

4) The peak loads of PP-ECC joint specimens with elimination of transverse reinforcements remained comparable to the specimen without elimination of stirrups in the beam without shear failure, indicating that the PP-ECC can act as transverse reinforcements to carry the applied load.

5) Sufficient ductile behavior could be achieved even with reduction of the transverse reinforcements by using PP-ECC.

6) The specimens with the reduction of transverse reinforcements by using PP-ECC dissipated analogous amount of energy with that without reduction of transverse reinforcements.

7) Reduction of transverse reinforcements by using PP-ECC had little effect on

stiffness degradation under cyclic loading.

Reference

American Concrete Institute (ACI) Committee 318: ACI 318-08, *Building Code Requirements for Structural Concrete and Commentary*, 2008.

American Concrete Institute (ACI) Committee 544: ACI 544.1R-96 (Reapproved 2002), *State-of-the-Art Report on Fiber Reinforced Concrete*, 2002.

Architectural Institute of Japan: *AIJ Standards for Structural Calculation of Steel Reinforced Concrete Structures*, 1991.

Chalioris, C. E., Favvata, M. J. and Karayannis, C. G.: Reinforced Concrete Beam-Column Joints with Crossed Inclined Bars under Deformations, *Earthquake Engineering and Structural Dynamics*, Vol. 37, No. 6, pp. 881-897.

Commission of the European Communities: Eurocode 8: *Design of Structures for Earthquake Resistance – Part 1: General Rules, Seismic Actions and Rules for Buildings*, 2004.

Japan Society of Civil Engineers (JSCE): *Standard Specifications for Concrete Structures (Material and Construction)*, 2007.

Japan Society of Civil Engineers (JSCE): *Standard Specification for Concrete Structures-2007* [Structural Performance and Verification], 2010.

Joint ACI-ASCE Committee 352: ACI 352R-02, *Recommendations for Design of Beam-Column Connections in Monolithic Reinforced Concrete Structures*, 2002.

Kojima, S., Sakata, N., Kanda, T. and Hiraishi, T.: Retrofitting Application of Spraying High Ductile Cementitious Composites, *JCI Concrete Journal*, Vol. 42, No. 5, pp. 135-139, 2004. (in Japanese)

Railway Technical Research Institute: *Design Standards for Railway Structures and*

Commentary (Concrete Structure), 2004.

Railway Technical Research Institute: *Design Standards for Railway Structures and Commentary (Concrete Structure) – Verification Examples – RC Rigid-Framed Elevated Bridges*, No. 421, 2005.

Tsonos, A. G., Tegos, I. A. and Penelis, G. G.: Seismic Resistance of Type 2 Exterior Beam-Column Joints Reinforced with Inclined Bars, *ACI Structural Journal*, Vol. 89, No. 1, pp. 3-12.

Chapter 6

CONCLUSIONS AND RECOMMENDATIONS

6.1 General Conclusions

Polypropylene fiber reinforced engineered cementitious composites (PP-ECC), as a kind of newly developed construction material exhibits strain hardening and multiple cracking upon loading in tension which leads to improvement in ductility, toughness, fatigue resistance and performance capacity, were utilized in this study to reducing shear reinforcement in beam and beam-column joints. Through the monotonic compression and uniaxial tensile tests, it was found that PP-ECC has similar compressive strength to the normal strength concrete while its elastic modulus is lower than normal strength concrete. PP-ECC also has a higher compressive strain than that of normal strength concrete. PP-ECC exhibits the strain hardening behavior and its yield and ultimate tensile strength is greater than 2.5 N/mm^2 and 3.0 N/mm^2, respectively. The tensile strain capacity of PP-ECC is greater than 2.5%. All above described mechanical properties of PP-ECC makes PP-ECC an ideal material for enhancing the shear capacity of structural members.

Setting the goal to avoid congestions at the beam-column joints caused by the use of extensive amount of shear reinforcements in the beam-column joints, the first step is to confirm the effect of stirrup ratio in PP-ECC structural member. A total of seven beams designed to be failed in shear, including two RC beams with stirrup ratio of 0.42% and 0.00%, respectively, and five PP-ECC beams with various stirrup ratios ranging from 0.42% to 0.00%., were tested under four point loading tests. The effect of stirrup ratio on shear capacities in PP-ECC beams was investigated, and then the current Japan Society of Civil Engineers (JSCE) design code for ECC was correlated with experimental results.

It was found that owing to the fiber bridging effect in PP-ECC, the shear capacities of

the beams with stirrups and without stirrups increased 20.6% and 107.6%, respectively, by replacing concrete with PP-ECC. The shear capacity can be increased by replacing the matrix from concrete to PP-ECC, especially in the case of lower stirrup ratio.

Crack surface displacement, which is the total displacement of crack surface describing the direction of the cracking moment, was measured. The critical crack surface displacements along the critical crack in the area below compression rebars and above tension rebars were measured in the post peak stage since the critical crack in PP-ECC beams before the peak load are still ambiguous. It was found that the damage to the fiber bridging effect induced by sliding on the critical crack surfaces in PP-ECC beams with higher stirrup ratio at the peak load is more significant compared to those with lower stirrup ratio. This is one of the factors for the decrease in the shear carried by ECC in PP-ECC with the increase in stirrup ratio. All PP-ECC beams failed in shear sliding in the post peak stage.

The angle of critical crack to the beam axis in PP-ECC beam decreases with the increase in stirrup ratio, which simultaneously triggers a reduction in the shear carried by fibers along the critical crack. Again, this results in a decrease in the shear carried by PP-ECC with the increase in stirrup ratio.

Unlike in the shear resisting proportion in RC beams, in which the shear carried by concrete is almost constant even with varying stirrup ratios and the shear carried by shear reinforcement is proportional to the stirrup ratio, the shear carried by ECC in PP-ECC beams decreases with the increase in stirrup ratio. This decrease in shear carried by fibers results from the combined action of the reduction on shear carried by fibers along the critical crack and the increased damage to fiber bridging induced by sliding along the critical crack surfaces.

The current JSCE design code for ECC does not take into account that due to sliding, the shear carried by fibers in ECC decreases with the increase in stirrup ratio. This may result in an over-estimation of the shear capacity of PP-ECC structural members.

Based on the confirmation of shear reinforcing effect from PP-ECC, the transverse reinforcements in the beam-column joint tests were reduced. After the reduction of transverse reinforcements in the joint, the beam and the column in the beam-column joint specimens, the fabrication of steel cage became easier. Further, more time for

fabrication and cost was reduced.

The concrete retarder is useful to treat interface between conventional concrete and PP-ECC to prevent the interface failure and increase the integrity of composite structure. The use of concrete retarder provides a way to utilize the ductility of PP-ECC into concrete structure.

The failure mode of the beam-column joint specimens even with reduction of transverse reinforcements were still flexural failure, which was the same as that of the specimen without reduction of transverse reinforcements indicating that the PP-ECC can be the replacement of transverse reinforcements to provide sufficient shear strength. The peak loads of PP-ECC joint specimens with reduction of transverse reinforcements remained comparable to the specimen without elimination of stirrups in the beam without shear failure, indicating that the PP-ECC can act as transverse reinforcements to carry the applied load. Sufficient ductile behavior could be achieved even with reduction of the transverse reinforcements by using PP-ECC.

The specimens with the reduction of transverse reinforcements by using PP-ECC dissipated analogous amount of energy with that without reduction of transverse reinforcements. Reduction of transverse reinforcements by using PP-ECC had little effect on stiffness degradation under cyclic loading.

Based on these findings, this research provides some ideas regarding to effect of stirrup ratio on shear capacities of PP-ECC structural members. Also, these findings may provide some useful suggestions for applying PP-ECC on structural member to reduce the shear reinforcements.

6.2 Recommendations for Future Research

Since the PP-ECC beams with only one shear span-effective depth ratio of 2.8 were tested in this study, it is quite interesting to investigate the shear capacities of PP-ECC at the other shear span-effective depth ratio. In addition, at the current shear span-effective depth ratio, if the stirrup ratio was further increased, whether the shear capacity of PP-ECC beam would be equal to that of concrete beam or not.

The conducted research only deal with one part of the whole frame, before varying the

amount of transverse steel rebars along the columns of the whole frame, for verification, it is better to conduct experiments on the whole rigid-framed specimens. Since it was observed that the casting direction of PP-ECC has close connection with structural performance, how to cast PP-ECC so that the best structural performance could be achieved needs to be further studied in the future research.

Whatever the beam tests or beam-column joint tests, due to the constrain of the time and testing facility, the size effect of structural member using PP-ECC was not conducted in this research. Therefore, as an important factor before putting into application, it is necessary to be clarified in the future research.